

BOSTON UNIVERSITY
GRADUATE SCHOOL OF ARTS AND SCIENCES

Dissertation

**RECOVERY PROCESSES AND DYNAMICS IN SINGLE AND
INTERDEPENDENT NETWORKS**

by

ANTONIO MAJDANDZIC

M.Sci., Zagreb University, 2011

Submitted in partial fulfillment of the
requirements for the degree of
Doctor of Philosophy

2016

Approved by

First Reader

H. Eugene Stanley, Ph.D.
Professor of Physics,
William Fairfield Warren Distinguished Professor

Second Reader

Plamen Ivanov, Ph.D.
Research Professor

To my family and good friends, both scattered around the World.

Acknowledgments

I would like to thank my mentor and thesis advisor, H.E. Stanley. Gene is an institution himself. A great scientist, a perfect advisor and a great friend. In the final version of this draft I will write a luxurious paragraph on him and the five years I spent at BU. I enjoyed so much in his research group. Unfortunately, good things do not always last forever, but hopefully are replaced by other good things in life.

I would like to thank my best friend Berislav, for being a person I could call at 3AM in the morning and talk about life, science, or any other topic. I thank him for reading all my papers and this thesis manuscript. He's also a physicist.

I would like to thank my other best friend, Boris Podobnik, the funniest guy I know, for doing a great work with research. I miss our dinners at restaurants around Kenmore and BU campus.

I thank Shlomo Havlin for being a huge motivator and inspiration, both as a scientist and as a wonderful person. Working with him, I was never afraid of my ideas.

I thank my research collaborators, with whom I enjoyed both work and a company: Lidia Braunstein, Chester Curme, Irena Vodenska, Dror Kenett, Sary Levy, and others.

I am grateful to my thesis Committee; Gene, Shlomo Havlin, Lawrence Sulak, William Skocpol and Plamen Ivanov, for their advices and help with my thesis.

I thank Tomislav Lipic for discussing my research with me, and teaching me how to code.

I thank Mirtha Cabello for helping me so many times at BU. When I remember Boston University, a few things come to my mind first, and Mirtha is one of them.

I would like to thank the whole Room 101, present and past: Nima, Chester, Asher, Duan, Shuai, Xin, Adam... Room 101 will long stay in my memory as "home".

I thank my sister and parents for supporting me in everything, in particular, in pursuing things that I like and enjoy.

RECOVERY PROCESSES AND DYNAMICS IN SINGLE AND INTERDEPENDENT NETWORKS

(Order No.)

ANTONIO MAJDANDZIC

Boston University Graduate School of Arts and Sciences, 2016

Major Professor: H. Eugene Stanley, William Fairfield Warren Distinguished
Professor, Professor of Physics

ABSTRACT

Systems composed of dynamical networks - such as the human body with its biological networks or the global economic network consisting of regional clusters – often exhibit complicated collective dynamics. Three fundamental processes that are typically present are failure, damage spread, and recovery. Here we develop a model for such systems and find phase diagrams for single and interacting networks. By investigating networks with a small number of nodes, where finite-size effects are pronounced, we describe the spontaneous recovery phenomenon present in these systems. In the case of interacting networks the phase diagram is very rich and becomes increasingly more complex as the number of interacting networks increases. In the simplest example of two interacting networks we find two critical points, four triple points, ten allowed transitions, and two “forbidden” transitions, as well as complex hysteresis loops. Remarkably, we find that triple points play the dominant role in constructing the optimal repairing strategy in damaged interacting systems. To test our model, we analyze an example of real interacting financial networks and find evidence of rapid dynamical transitions between well-defined states, in agreement with the predictions of our model.

Contents

1	Introduction	1
1.1	Networks around us	2
1.2	Basic terminology	3
1.3	Modern research in networks	4
1.4	Interacting networks	5
1.5	Processes with failures, recoveries and spread of damage (FRS)	6
2	Processes with failure, recovery and damage spread in single networks	7
2.1	Introduction	7
2.2	Model definition	8
2.3	Numerical simulations	9
2.4	Analytical solution	11
2.5	Critical exponents and comparison with other models	18
3	Phase flipping in single networks with FRS	20
3.1	Finite size phenomena: Phase Flipping	20
3.2	Dynamics of Phase flipping	24
3.2.1	State lifetimes	27
3.3	Phase flipping in real networks	28
3.4	Flash crashes	31

4	Phase diagrams of FRS processes in interdependent networks	35
4.1	Interdependent networks	35
4.2	FRS process in interdependent networks	35
4.3	Model	36
4.3.1	Model rules	37
4.4	Mean field theory	39
4.4.1	Additional phase diagrams	52
4.4.2	Forbidden transitions	53
5	Optimal repairing strategies in interdependent networks	54
5.1	The problem of optimal repair	54
5.2	Solution	55
5.3	Optimizing the Manhattan distance	58
5.4	Maintaining the functionality	58
5.5	Conclusion	60
6	Dynamics of real interdependent networks	62
6.1	Finite size phenomena	62
6.2	Empirical example: Credit default swap networks	65
6.3	Applying the model to the CDS network: Outline	69
6.4	Building the CDS network	69
6.5	Measuring and estimating model parameters	70
6.5.1	Estimating internal parameters (p_{EU}^* , p_{LA}^*): observing high activity states	71
6.5.2	Alternative measurement of the internal parameters: microdynamics	71
6.5.3	Estimating the external parameters r_{EU} and r_{LA} : observing low activity states	74
6.5.4	Estimating the thresholds $m_{\text{frac,EU}}$ and $m_{\text{frac,LA}}$: visiting times	75

6.5.5	Estimating r_d : correlation between networks EU and LA . . .	76
6.6	Similarity in fluctuation size structure	79
Appendices		82
A	Mean field theory solution for the FRS process in interacting networks	83
B	Credit default swaps (CDS)	86
Curriculum Vitae		96

List of Tables

- 6.1 **Numerical estimates for the model parameters.** Using the "isolation method" we find limits on the numerical values of the model parameters. These observation experiments allow us to gauge the strength of various effects in real world systems. Here we confirm experimental accessibility of all of the model parameters. Note that values for r_d are rather small - this is expected as discussed in the text. 78

List of Figures

- 2.1 **Critical behavior of the system with first order phase transition and hysteresis.** Equilibrium average fraction of active nodes, $\langle z \rangle$, simulation results (symbols) and the MFT prediction (solid lines of corresponding colors). The calculations were performed along the $r = \text{const.}$ lines for three different values of r . Parameters for RR networks, $N = 10^7$, $k = 10$ and $m = 4$ are used in this example. . . . 12
- 2.2 **Phase diagram of the network system.** The phase diagram in model parameters (r, p^*) exhibits two phases. Phase I (green region) represents a high-activity collective network mode where high values of $\langle z \rangle$ are present, while Phase II (orange) represents a low-activity network mode. For $p^* < 0.386$ (subcritical region), there is a hysteresis region (purple) bounded with spinodals, which are denoted by red and blue lines. The lines merge at a “critical point” located at $(r = 0.637, p^* = 0.386)$. Colors in the diagram are for illustration purpose to highlight regions of different phases. Analytical MFT results for spinodals are denoted by black dashed lines. Point A (yellow) shows the parameters used in Fig. 3.1. 13
- 2.3 **Transition lines for different average node degrees.** Comparison of analytical MFT result (dashed lines) with numerical results (dots), for the spinodals in the (r, p^*) phase diagram. For larger k the agreement between theory and simulations is increasingly better. . . 14

2.4	Transition lines for ER network. Comparison of analytical MTF result with simulation results, for ER network with $\langle k \rangle = 10$ and $m = 4$	15
3.1	Two network modes characterized by high and low network activity. Switching between collective network modes in our dynamical network. Dynamic switching (flipping) between two phases in the subcritical region, an example for $p^* = 0.28$, $r = 0.80$ (point A , in yellow, Fig. 2.2), with $k = 10$, $m = 4$ and $N = 100$. The figure shows a fraction of active nodes z , as a function of time, flipping back and forth from one phase to another. Marked with green circles are sharp drops that might be related to "flash crashes", discussed later. . . .	21
3.2	Effective potentials. Outside the hysteresis region, where pure phases exist, there is only one local minimum in the effective potential (effective single-well "potential"). In the hysteresis region, free energy landscape resembles a "double-well potential." In a small system the fluctuations are very pronounced, and after long enough time the system can jump over the barrier from one potential well to another, resulting in a dramatic change of the collective network state.	22
3.3	Probability density function of z values for free evolution of the system. The pdf of z shows a bimodal form, revealing states corresponding to high and low network activity.	23

3.4	Mapping the phase flipping. White line represents trajectory $(r_\lambda(t), p_\lambda^*(t))$ of the system in the phase diagram, from $t=0$ to the moment of the first transition (point “1” Fig. 3.1), in the same numerical simulation where $z(t)$ in Fig. 3.1 was simulated. The system was in low active phase until the trajectory crossed the ”left” spinodal, resulting in a global recovery event. Analogously, when the system is in the high active state the right spinodal becomes relevant (points “2” and “4”). Transitions between the macroscopic states are essentially first passage processes on interchangeable spinodals.	26
3.5	Average lifetimes VS system size. Expected lifetime of the system in a certain state measured in simulations, increases exponentially with the system size N , confirming our theoretical results, Eqs. (3.1) and (3.2). Black lines represent linear regressions in $(N, \log T)$ diagram.	29
3.6	Properties of phase flipping phenomenon in financial data for an undeveloped market. (a) For the constituents of financial index, the Indian index (BSE200), the fraction of stocks z with positive return as a function of time switches back and forth between the two network modes characterized by high and low network activity. (b) Bimodal form in the pdf of financial data during the last decade.	32
3.7	Properties of phase flipping phenomenon in financial data for a developed market. The same as in Fig 3.6 but for the S&P500 financial index. Ashman’s D test validates the significance of bimodality ($D > 2$).	33
3.8	Flash crash. (a) The infamous flash crash of the US financial market on 6 May 2010. The market index value dropped rapidly, followed by an equally rapid recovery. Source: CNBC. (b) Isolated sharp drop associated with an avoided transition, in our model.	34

4.1	Graphical representations of the mean field equations. The blue and brown curves represent Eq. (4.1) and Eq. (4.2), respectively, for $p_A^* = p_B^* = 0.16$, $r_A = r_B = 0.60$ and $r_d = 0.15$, in a system with two interdependent networks ($k = 16$, $m = 8$). There are nine intersections, representing mathematical solutions for network activities a_A and a_B . Four of them are stable solutions (green circles) representing physical states that we also observe in our simulations, and five are unstable solutions (red crosses).	40
4.2	Graphical representations of the mean field equations. Example for $p_A^* = 0.20$, $p_B^* = 0.24$, $r_A = r_B = 0.60$ and $r_d = 0.15$. Here we obtain two stable solutions and one unstable solution. The two stable solutions correspond to 11 state (both networks are at high activity) and 22 state (both networks are at low activity).	41
4.3	First layer of the phase diagram with corresponding transitions. Region of 11 state, in green. Possible transitions are $11 \rightarrow 12$ (orange line), $11 \rightarrow 22$ (blue line) and $11 \rightarrow 21$ (purple line). This layer of the phase diagram has two triple points, marked as black points.	45
4.4	Second layer of the phase diagram with corresponding transitions. Region of 22 state (blue), with two triple points and three transitions.	46
4.5	Third layer of the phase diagram with corresponding transitions. Region of 21 state (purple), with two transition lines (to 11 and 22 state) that merge in a critical point.	47
4.6	Fourth layer of the phase diagram with corresponding transitions. Region of 12 state (orange), with two transition lines (to 11 and 22 state) that merge in a critical point.	48
4.7	Illustration showing states (11, 12, 21 and 22) with allowed (blue arrows) and “forbidden” (red line) transitions.	49

4.8	Total phase diagram, with all four layers. Solid lines represent the borders of region 11 (green), 22 (blue), 12 (orange) and 21 (purple). Dashed lines represent cross-sections where we calculate the activity profile, shown in Figure 4.9. Note that there is a small central “window” where all four states are possible.	50
4.9	States, transitions and hysteresis loops for two activity profiles. a) Activity z_A of network A, as measured in simulations (dots) and predicted by mean field theory (solid lines), along the cross section defined by the black dashed line in Fig 4.8. Parameters p_A^* and p_B^* are changed, preserving the relation $p_B^* = 0.1 + 4/3p_A^*$. Transitions are denoted by arrows. b) Same for the cross section defined by $p_B^* = 0.4 - p_A^*$ (red dashed line in Fig. 4.8). Here we obtain 4 states and 6 different transitions, giving rise to more complex hysteresis loops. Network parameters in all cases are ($k=16, m=8$).	51
4.10	Activity of network A versus internal failure rate. a) Activity $z_A = 1 - a_A$ obtained by solving Eq. (4.1) and (4.2), for a range of p_A^* values, in a system of two interdependent networks ($k = 16, m = 8$). Blue lines correspond to stable physical states and red dotted lines represent unstable solutions. In Fig. 4.10a the same parameters as in Fig. 4.1 are used, except p_A^* which is not fixed but varied. When $p_A^* = 0.16$ (vertical black line) the corresponding values on the blue solid lines (green circles) match the graphical solutions in Fig 4.1 (also green circles). b) An analogous relationship holds between figures 4.2 and 4.10b, in which case two stable states exist.	52

5.1 **Optimal repairing strategies.** The optimal repairing procedure (least expensive in terms of the number of individual node repairs) depends on the initial condition of the collapsed system. The total cost of repair is $|\Delta p_A^*| + |\Delta p_B^*|$ and the problem of optimal repairing translates into finding the minimal Manhattan distance from the point (in the phase diagram) where the collapsed system is initially situated (S_i) to the nearest border of the green region where it becomes fully functional. For a system having the initial condition within the red section (e.g. point S_1), there are two solutions: it is equally optimal to reach any of the two triple points R1 and R2 by decreasing p_A^* and p_B^* . For the systems starting in the yellow regions, it is optimal to reach only one triple point, R1, for the sector containing point S_2 , or R2 for the sector containing point S_3 . Starting in the dark blue regions it is optimal to decrease p_B^* only, i.e., repairing *only* network B. Similarly, in the light blue regions it is optimal to decrease p_A^* only. Triple points play a crucial role when both networks are initially significantly damaged (red and yellow regions). 56

5.2 **Minimum Manhattan distance problem, in two examples.** **a** Finding the minimum Manhattan distance between point S_1 in the red sector and the green region where the system is fully functional. Equidistant curves are plotted in gray and form a “diamond” shape. The largest “diamond” barely touching the green region and having its center at point S_1 , suggests there are two equally optimal solutions to the minimization problem - points R1 and R2. **b** The same geometrical construction for point S_6 in the light blue region, suggests a unique solution: decreasing p_A^* 59

5.3	Subsequent maintenance. Depending on the the initial state, additional repairing support should be provided to the system to be functional after it has beed awaked with a positive shock discused in Figure 5.1. Optimal strategy for the red region is bringing the system to point T, and for blue regions it is decreasing p_A^* only (for the "right" blue region) or p_B^* only (for the "upper" blue region).	61
6.1	Collective dynamics in simulated interacting networks. Simulation of the networks' dynamics, activity versus time, for $N = 100$ and failure parameters $p_A^* = p_B^* = 0.21$, $r_A = r_B = 0.60$, $r_d = 0.15$, shows the switching of the system between four different states. We can easily identify four collective states - 11, 22, 12, and 21.	63
6.2	Collective dynamics in real interacting networks. Dynamics of two CDS geographical networks consisting of 17 European and 8 Latin American countries, showing very similar behavior: individual networks switching between well defined high activity and low activity states, as well as correlated collective behavior of the two networks in interaction. We identify collective states 11, 22, 12 and 21 and mark them with connected black ovals. Note that since the CDS value grows with risk, a higher activity in a CDS network corresponds to bad economic news.	64
6.3	Density plots for the activity of real networks. a Activity density plot for the EU network reveals bimodality, an indication of the existence of two states. b Same for the LA network.	67
6.4	Correlation between individual CDS signals. Correlation matrix of binary CDS signals with the EU (1-8) and LA (9-25) block. Separation into blocks reinforces our initial decision to sort the countries by geographic location.	68

6.5	Quantifying the CDS network and estimating model parameters. Estimating p_A^* and p_B^* by observing intervals in which both networks have high activity ($z \geq \frac{1}{2}$). The region of interest (above $z = \frac{1}{2}$, yellow line) is colored in green, with an example interval in red.	72
6.6	Alternative method of estimation of the internal failure rate. Dynamics of an individual binary signal (Columbia), when the LA network is in the high activity state ($z_{LA} \geq \frac{1}{2}$).	73
6.7	Estimating the numerical value of interdependency parameter. Matching the value of r_d for $Corr = 0.61$: correlation between the signals of two artificial networks with $N_A = N_{EU} = 17$ and $N_B = N_{LA} = 8$ nodes, for different values of r_d , with other parameters fixed to the values from $\langle k \rangle = 5$ row in Table 6.1.	77
6.8	Analysis of network dynamics. a Two model (artificial) networks: Typical time evolution of activity. b–c Activity density plot for two model networks reveals bimodality.	80
6.9	Correlation structure. a–b Fluctuation size peaks around $z \approx 0.5$ for model networks A (d) and B (e). A very similar pattern is found in real networks, EU (c) and LA (d).	81
A.1	Inclusion-exclusion principle.	84

List of Abbreviations

CDS	Credit Default Swap
ER	Erdős – Rényi
FRS	Process with a <i>failure, recovery and spread</i> of damage
MFT	Mean Field Theory
PDF	Probability Density Function

Chapter 1

Introduction

The study of networks has its beginnings in graph theory, a mathematical discipline describing graphs, which are representations of relationships between discrete objects. Leonhard Euler's paper *Seven Bridges of Königsberg* from 1736 is considered the first published work on graph theory. In the 20th century, Erdős and Rényi introduced the probabilistic approach to the graph theory [1]. At the end of nineties, the explosion of data collection and the growth of technological networks led to much scientific attention for network systems outside of discrete mathematics and computer science, especially in physics where the tools of statistical physics are naturally applied to complex networks.

A graph is a set of vertices, or nodes, connected by links. A simple example is a network of friendships, where people are represented by nodes and their friendships by links. Massive study of real networks began relatively recently, with the emergence of the Internet and storing huge amounts of data describing different systems structured as networks. This interdisciplinary field is known as the study of *complex networks* or *networks science*, raging across many disciplines and using tools developed within those disciplines; from physics, math, biology and medicine to sociology, computer science, economy and finance. In all these disciplines we find systems consisting of many discrete object that influence each other, and they can be viewed as networks.

1.1 Networks around us

In the world around us there are many examples of networks [2]. In chemistry, there are metabolic networks where nodes are molecules and the links are chemical reactions between the molecules. Polymer gels can be described using the concepts from the percolation theory and network theory. In biology and ecology, there is a significant research, from the perspective of networks science, of human brain (network of neurons [3, 4]) and biological network system such as food webs (“what-eats-what” networks in ecological communities) [5]. Facebook, LinkedIn, Twitter and Instagram are examples of social networks [6]. In finance, banks borrow money to each other, forming a network of banks. Various types of shock processes and damage spreading processes within the networks of banks have been researched recently [7]. Perhaps the most famous technical network is the World Wide Web, with web pages as nodes and URLs as links [8–10]. Networks of airports and flight connections between them is an example of infrastructure networks.

Networks differ in their shape, structure and size [11, 12], but even more by processes that are “running” on them [13]. Typical processes that take place on networks are epidemic processes, searches, diffusion processes, synchronization, and spread of information, damage or diseases. Presently, epidemic processes are one of the most important applications of the research in complex networks, with significant contributions to understanding of the disease spread and immunization strategies [14]. Searching algorithms on the Internet can often be described as variant diffusion processes. Synchronization networks are networks of coupled oscillators that are capable of emitting and receiving periodic signals. The *synchronization* is a self organizing phenomena when the network as a whole starts oscillating at the same frequency. Examples range from neurons, heart cells to fireflies. Network theory provides results that suggest how to build more resilient infrastructure with respect to both massive

external attack (nuclear weapons, chemical and biological warfare agents, epidemic spread) or more targeted attack (attack on computer hubs) [15].

1.2 Basic terminology

As networks are systems comprising discrete objects and the connections between them, *nodes* and *links* are most fundamental building blocks of complex networks. Nodes can usually have *states*, for example binary states *active* or *failed*. Percolation phenomena has been deeply researched on networks and the related *giant component*, a cluster with a finite size spanning across the whole network, is an important concept used to describe functionality of network systems. Formation of the giant component is a typical percolation-style critical phenomena often arising in network models [13]. When describing structural properties of networks, important concepts are a *node degree* (or *connectivity*, the number of links by which a specific node is connected to other nodes) and the node's *neighborhood* (a collection of nodes connected to the observed node). Node degree is usually denoted by letter k . *Clustering coefficient* C is a parameter describing the occurrence of connection loops and space correlations in connectivity of nodes, usually defined as a probability that two neighbors of a node also have a mutual connection (note also that there are many clustering coefficients defined in the literature, with many possible variations).

By degree distributions, real networks can usually be sorted into two groups: a) networks with a finite second moment of the degree distribution (for example networks with an exponential tail) and b) scale free networks. Erdős - Rényi network model, one of the most famous models for generating random networks, produces a randomly connected network with binomial distribution of degrees, which in the thermodynamic limit becomes Poisson distribution and thus it falls into the first class of network degree distributions. Preferential attachment model generate networks with long-

tailed, power-law distributions asymptotically behaving as $P(k) \propto k^{-\gamma}$, where γ is the exponent of the tail of the degree distribution. Networks with the power law asymptotic distributions are usually denoted as scale-free networks [27].

1.3 Modern research in networks

Within physics, study of complex networks is considered a part of statistical physics. Many networks systems exhibit phase transitions, critical and fluctuation phenomena equivalent to other physical systems. However research in networks recently tends to be interdisciplinary, connecting both theoretical concepts and real systems across different disciplines, ranging from physics to biology and finance.

Modern cycle of massive research in networks, fueled by the explosion of data being observed and stored during the end of 90s, jumped with the research of Barabasi and Albert from 1999 [27]. In their model, today known as Barabasi-Albert model, evolution of networks is described as a dynamical process in which networks grow by adding nodes and links, in a way that new links added have higher probability to be attached to nodes already having large number of links. This leads to the scale-free distribution (power law) of node degrees. Considering examples of real networks, Barabasi and Albert showed that the Internet is a scale-free network.

Researching epidemic spread of viruses is one of the most important applications of the networks science. Network theory methodologies can be used to describe the spread of biological or computer viruses within abstract (network of people) or physical (network of computers) network structures, with results suggesting strategies to improve the herd immunity [14]. *Robustness of networks* as a topic has attracted a particular attention. Network systems can be damaged, intentionally (by attack) or unintentionally (by spontaneous processes). In this sense, significant research has been conducted by studying how networks react to attack/damage. Following the attack there is a cascading process where failed nodes can cause other nodes to fail.

A good and natural measure of the network functionality is the size of the giant component left after the cascade is finished. Bigger giant component corresponds to a higher level of system functionality. If there is no giant component left at all, a network system is considered completely unfunctional. When removing links from the network, giant component size experiences a phase transition [13]. This phase transition can be second order or first order, depending on the process and the correlated behavior of the nodes. Simply removing links from the network with no additional damage spread leads to second order transition in the size of the giant component. If nodes influence each other through links, then damage can spread from failed nodes to active nodes, which sometimes (for strong enough dependences) can lead to first order phase transitions.

1.4 Interacting networks

Networks of the world around us do not usually appear as isolated structures. Interacting networks are systems consisting of many (at least two) networks that are dependent on each other or interact in some specific way [16]. Human body is a typical example of a system consisting of strongly coupled networks, with interacting neurological and physiological networks. Power grid and communication networks are examples of interacting infrastructure networks. Rules of interaction between interacting networks can be different, as well as types of links and the structure of underlying graphs, leading to different physical phenomena. For some processes, interacting networks may have very different behavior from their single network counterparts [17–20]. For instance, it has been shown that for certain types of cascading processes (damage spread through the system), interdependent networks are much less robust than single networks and more susceptible to collapse, sometimes even if a tiny initial damage is done to the system [21].

1.5 Processes with failures, recoveries and spread of damage (FRS)

In networks where nodes are described by binary states (*active* or *failed*), most fundamental events are individual node failures, recoveries of individual nodes and interactions between the nodes. Without any intention to introduce new terminology, I will refer to these processes as FRS processes. These systems show rich critical phenomena and can be well described by the methods of standard statistical physics. This dissertation is mainly based on my research of FRS processes in the domain of complex networks, which was published as a series of papers [22–25]. The results are presented in the chapters that follow. Chapter 2 concerns phase diagrams of FRS processes in single networks, and Chapter 3 deals with rich dynamics in the case of finite size single networks, suggesting that the mechanism of spontaneous recovery might be present in certain real systems. Chapter 4 studies similar processes in interacting networks and the corresponding phase diagrams, which turn out to be much more complicated than in the single network case. Chapter 5 solves the optimal repairing problem for interacting network systems and shows that triple points play a prominent role in the construction of optimal repairing strategies. Chapter 6 concludes with finite size effects in real interacting networks, comparing simulated networks with the real network of credit default swaps and providing a methodology to measure model parameters.

Chapter 2

Processes with failure, recovery and damage spread in single networks

2.1 Introduction

Many network models have been developed to examine (i) a network's static properties, e.g., structural characteristics or percolation, (ii) relaxation processes after abrupt network disruption, mainly concerning epidemics or attacks, and (iii) special topics in dynamics, including dynamical growth and synchronization networks [2, 5, 6, 8–11, 15–18, 20, 26–33]. The response of a network system to an external attack, in particular, has received intensive study [2, 10, 11, 15, 16, 28, 29]. Some research has focused on the details of transient dynamics. For example, in Ref. [31] the failure propagation in the engineering networks was studied, especially the influence of the network topology on the speed of the cascades. Phenomena such as spreading epidemics and attacks on the Internet have been thoroughly described using models of type (ii), describing essentially irreversible processes of failures. However, this is not the case in many real-world examples. The Internet can initially fail after a severe

attack and then, after a period of time, recover. A human brain can spontaneously recover after an epileptic attack. A traffic network returns to its normal state after a period of gridlock. A financial network may, after a period of time, recover after having large fraction its constituents fail. There is an entire class of real-world dynamic complex systems in which networks can spontaneously recover after their collapse, but the mechanism for this network recovery has not yet been modeled nor is it adequately understood. In this paper we develop a framework for understanding the class of dynamic networks that demonstrate an ability to spontaneously recover.

2.2 Model definition

We start with three fundamental assumptions: (i) that nodes in a network can fail due to internal failures, (ii) that they can fail due to external failures, and (iii) that individual nodes have a recovery process.

- (i) We assume that any node can fail randomly and independently of other nodes due to internal causes. We model internal failure using a parameter p . Each node has a probability of internal failure $p dt$ during a time interval dt . Internal reasons for failure can be related to any process essential to node integrity.
- (ii) We assume that any node can fail due to external causes. For example, if the neighborhood surrounding node j (i.e., a collection of nodes directly connected to j) is substantially damaged, it can negatively impact node j . We use a simple threshold rule (similar to that proposed by Watts [37]) to define a *substantially damaged* neighborhood, i.e., a neighborhood containing fewer than or equal to m active nodes, where m is a fixed integer. For externally-induced failures we assume the following: If node j has more than m active neighbors during the time interval dt , its neighborhood is “healthy” and node j is not at risk of externally-induced failure, but if node j has fewer than or equal to m active

neighbors during the interval dt , there is a probability $r dt$ that node j will experience externally-induced failure.

- (iii) We assume that there is a reversal process, a recovery from failures. We use a parameter $\tau \neq 0$ to model the recovery from internal failures. Node j recovers from an *internal* failure after a time period τ . If a node has already failed internally and, before it has recovered, a new internal failure hits this node at t , then the opportunity for recovery will occur at $t + \tau$. A node recovers from an *external* failure after time τ' , which generally is not equal to τ . In our simulations we measure time in units of τ' and, for the sake of simplicity, we use $\tau' = 1$. Instead of introducing recovery times, recovery process could alternatively be described by recovery-rates, as in engineering networks with a “wear-out” process [31] or in forest fire models [38, 39] where vegetation can re-grow after it has been burned.

The parameters p and τ control the internal failures and r controls external failures. A “damage conductivity” parameter r describes how easily damage spreads through the network. When $r = 1$ and there are no recoveries ($\tau = \tau' = \infty$) the system reduces to the Watts model [37] generalized and rigorously solved in Ref. [40]. Introducing (a) dynamic recovery and (b) “damage conductivity” leads to spontaneous network collapse and recovery, i.e., the phase switching phenomena found in this study. Specifically, we find that global recovery is possible only when $r \neq 1$ (i.e., when $r < 1$).

2.3 Numerical simulations

To explore the possible existence of collective network modes and their dynamics we perform numerical simulations and study the system analytically.

We study separately networks with large number of nodes (representing the thermodynamic limit) and more realistic small networks (representing a finite system).

The latter is particularly interesting when studying such real-world networks as those in neuroscience [3, 4] and finance [46].

Numerical simulations for the "thermodynamic limit" are done for regular networks (in which all nodes have the same degree) and for Erdős-Renyi (ER) networks [1, 41]. Figures 2.1 and 2.2 show results of numerical simulations for regular networks with $k = 10$, recovery time $\tau = 100$, the external failure threshold $m = 4$, and $N = 10^7$ nodes, approximating the thermodynamic limit. Parameters p and r are varied and they define a two-parameter phase diagram. Since most numerical results depend only on the product $p\tau$, instead of using p and $\tau \neq 0$, we define a more convenient single parameter $p^* \equiv 1 - \exp(-p\tau)$, later to be shown to have physical meaning; it reveals the average fraction of internally failed nodes in the network.

The network global state is best characterized by the fraction of active nodes in the network z , which is the order parameter of the problem. The most interesting question is how p^* (which controls internal failures) and r (which controls external failures) affect the entire network. For a set of different values of p^* and r , we numerically calculate a time average fraction $\langle z \rangle = \langle z(p^*, r) \rangle$ of active nodes in the network. For a selected value of r , we gradually change the p^* value, starting with small p^* value and increasing it towards $p^* = 1$, while the states of the nodes are dynamically evolving.

We also calculate the $\langle z \rangle$ values in the inverse direction, decreasing p^* from $p^* = 1$ to $p^* = 0$. Figure 2.1 shows the results for $\langle z \rangle$ as a function of p^* , for three different values of r . For some values of r we encounter a discontinuity in $\langle z \rangle$ while slowly changing the p^* value, for the increasing or decreasing direction of p^* , or sometimes both. The hysteresis we find in Fig. 2.1 is the characteristic feature of a first-order phase transition.

Repeating this procedure for many values of r , we obtain the two-parameter (r, p^*) phase diagram presented in Fig. 2.2. It is characterized by a regime of hysteresis behavior: in one part of the phase diagram between the two discontinuity lines, the

equilibrium value of $\langle z \rangle$ is found to depend not only on the values of r and p^* , but also on the initial condition, or the system's past. In the (r, p^*) space, discontinuities define two lines, called spinodals. They separate two collective phases corresponding to high network activity (Phase I - large values of $\langle z \rangle$) and low network activity (Phase II - low values of $\langle z \rangle$). Between the spinodals is the hysteresis region (the purple region in Fig. 2.2), in which either of the two network phases can exist. Spinodals merge at the critical point located at $(r = 0.637, p^* = 0.386)$, followed by a region in which there is no distinction between the two phases (a supercritical region). For the set of parameters used, we find that the *giant component* of active nodes in the network is existent (non-zero) in the entire region presented in Fig. 2.2.

2.4 Analytical solution

We now describe the network system in our model by a set of equations. Let $0 < u(t) < 1$ be the fraction of nodes that are in the internally failed state, where t is a discrete time step. Imagine that on each internally failed node a small clock is activated to measure the time l passed since the last internal failure of the node. At any moment t , each node has a probability $p \ll 1$ to experience a new internal failure, and the clock in the node is then reset to 0. When l reaches the value $\ell = \tau$, the node recovers from the internal failure. Let $c_\ell(t)$ denotes the fraction of nodes that experienced their last internal failure at moment $t - l$. The evolution of $c_\ell(t)$ and $u(t)$ is given by equations

$$c_\ell(t + 1) = (1 - p)c_{\ell-1}(t), \quad (2.1)$$

and

$$u(t + 1) - u(t) = p(1 - u(t)) - c_\tau(t). \quad (2.2)$$

The right hand side of Eq. (2.1) accounts for the process of aging of time ℓ (nodes in $c_{\ell-1}$ transfer to c_ℓ after one time step) and the factor $(1 - p)$ accounts for internal

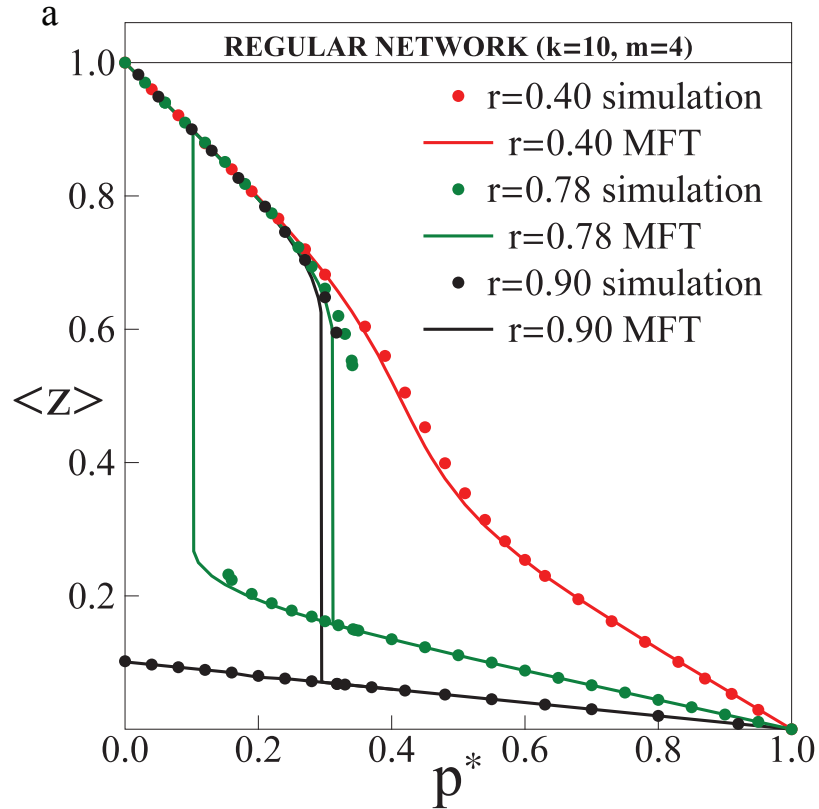


Figure 2.1: **Critical behavior of the system with first order phase transition and hysteresis.** Equilibrium average fraction of active nodes, $\langle z \rangle$, simulation results (symbols) and the MFT prediction (solid lines of corresponding colors). The calculations were performed along the $r = const.$ lines for three different values of r . Parameters for RR networks, $N = 10^7$, $k = 10$ and $m = 4$ are used in this example.

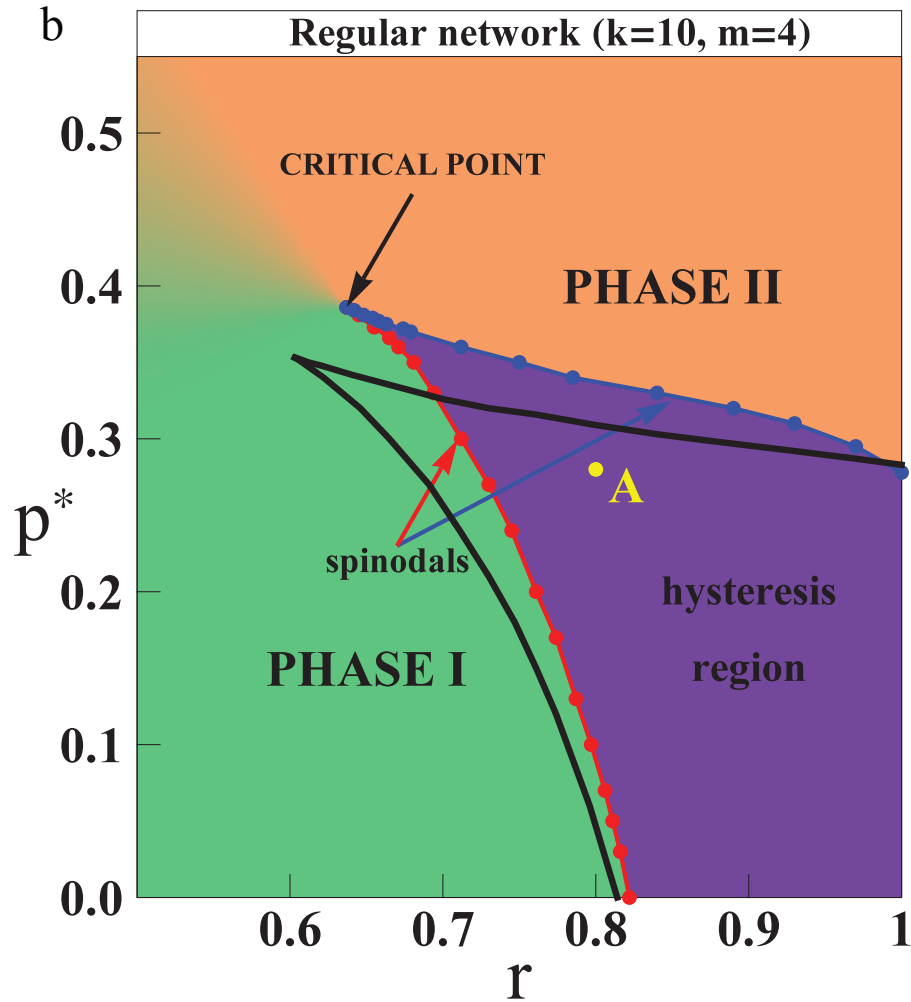


Figure 2.2: **Phase diagram of the network system.** The phase diagram in model parameters (r, p^*) exhibits two phases. Phase I (green region) represents a high-activity collective network mode where high values of $\langle z \rangle$ are present, while Phase II (orange) represents a low-activity network mode. For $p^* < 0.386$ (subcritical region), there is a hysteresis region (purple) bounded with spinodals, which are denoted by red and blue lines. The lines merge at a “critical point” located at $(r = 0.637, p^* = 0.386)$. Colors in the diagram are for illustration purpose to highlight regions of different phases. Analytical MFT results for spinodals are denoted by black dashed lines. Point A (yellow) shows the parameters used in Fig. 3.1.

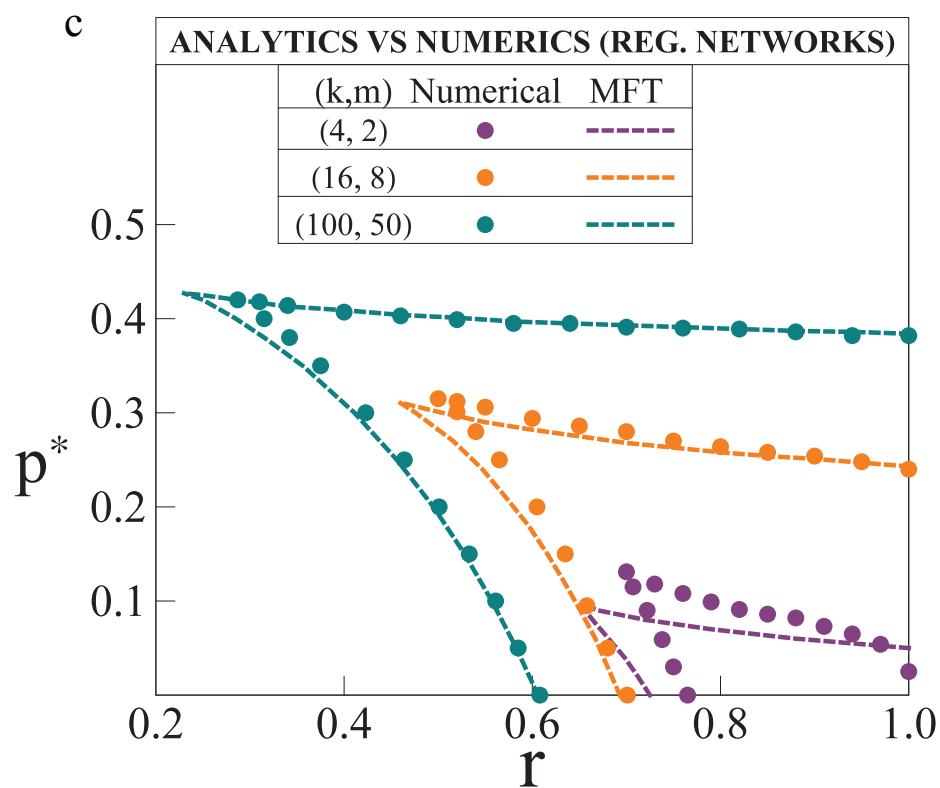


Figure 2.3: **Transition lines for different average node degrees.** Comparison of analytical MFT result (dashed lines) with numerical results (dots), for the spinodals in the (r, p^*) phase diagram. For larger k the agreement between theory and simulations is increasingly better.

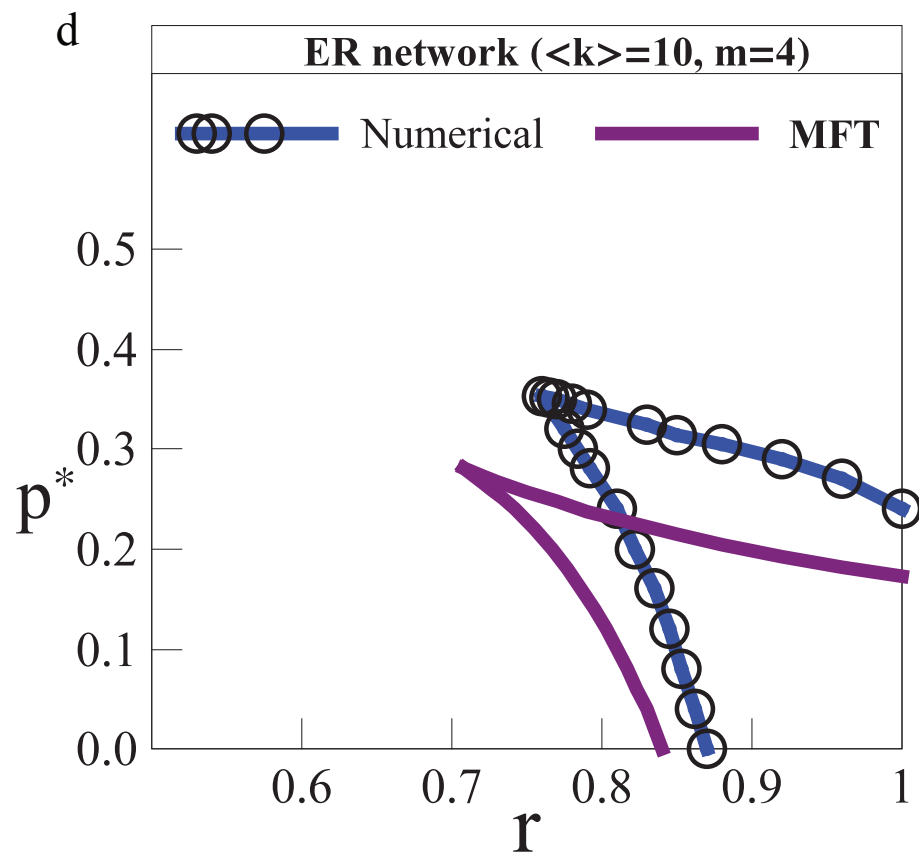


Figure 2.4: **Transition lines for ER network.** Comparison of analytical MFT result with simulation results, for ER network with $\langle k \rangle = 10$ and $m = 4$.

failures during the time step. The boundary condition for $\ell = 0$ is $c_0(t) = p$. In Eq. (2.2), the first term on the right hand side describes the rate of failures of internally active nodes that contributes to the growth of u , while the second term accounts for the decrease in u due to recoveries of nodes with $\ell = \tau$. When the system reaches the steady state, the equation for c_ℓ is $c_\ell = (1 - p)c_{\ell-1}$, with solution $c_\ell = c_0(1 - p)^\ell \approx pe^{-p\ell}$, while the steady state equation for u , $p(1 - u) - c_\tau = 0$, gives the solution $u = 1 - e^{-p\tau} \equiv p^*$.

Next we analytically study the external failures in nodes caused by failed neighboring nodes. Let E_k be the probability that a node of degree k will have a critically damaged neighborhood (fewer than $m + 1$ nodes are active) in the steady state. E_k can be calculated using a mean-field approximation. Assume that the time-averaged fraction of failed nodes in the network (either internally failed or externally failed) is $0 < a < 1$, where a serves as a “mean-field.” Next we calculate E_k , assuming that every node has k neighbors, each with probability a to be failed and probability $1 - a$ to be active. Using combinatorics it is easy to find that $E_k = \sum_{j=0}^m \binom{k}{k-j} a^{k-j} (1 - a)^j$. The probability that a node with a degree k will fail externally is then rE_k . If we denote the events of failures as $A = \{\text{internal failure}\}$ and $B = \{\text{external failure}\}$, the probability that a randomly-chosen node of degree k has failed is

$$a_k = P(A) + P(B) - P(A \cap B), \quad (2.3)$$

where $P(A)$ and $P(B)$ are probabilities of events A and B . We next assume that internal and external failures are independent events, thus $a_k \approx P(A) + P(B) - P(A)P(B)$. For an arbitrarily network with degree distribution f_k , the fraction of failed nodes, $a = \sum_k f_k a_k$, finally becomes

$$a(r, p^*) = p^* + r(1 - p^*) \sum_k f_k \sum_{j=0}^m \binom{k}{k-j} a^{k-j} (1 - a)^j. \quad (2.4)$$

Equation (2.4) is a self-consistent equation of a single variable $a \equiv a(r, p^*)$, recalling that $\langle z \rangle = 1 - a$. Depending on the choice of the values of r and p^* , there is either

a single mathematical solution for $\langle z \rangle$ (corresponding to a single, pure phase), or three solutions (two physical solutions corresponding to the two stable phases, which we observe in the simulations and the third solution which is dynamically unstable). When $r = 1$, the expression for $\langle z \rangle = 1 - a$ resembles the result of the Watts model for irreversible cascades (there is no recovery) with deterministic rules [40], in which case the physical system relaxes to the unique value of z for a fixed choice of the problem parameters. In that model it is assumed that during the cascade of failures, failed nodes cannot become active again, while in our model externally failed nodes failed at the previous stage of the cascade may become active again at the next stage of the cascade since we assume $\tau' = 1$. Our network model also resembles forest-fire models. In a lattice forest-fire model [38], trees grow with probability p from empty sites at each time step, and the fire on a site (node) will spread deterministically to trees at its neighbor sites at the next time step, thus with probability $r = 1$ in our terms. Including the immunity to a certain fraction of trees [39] leads to a continuous phase transition from a steady state with fire to a steady state without fire.

Here we introduce recovery processes and stochastic failures, described by the parameters τ and r , and obtain two physically possible equilibrium values (two physical solutions) for $\langle z \rangle$ for certain choices of (r, p^*) and the emergence of the hysteresis behavior, which enables the dynamical phase switching phenomena in finite-size systems, as we show later. The crucial ability of the system - the spontaneous recovery - will turn out to be possible only for $r \neq 1$. The solution of Eq. (2.4) gives a discontinuity in $\langle z \rangle$ for certain values of r and p^* . Figure 2.1 shows analytical results for $\langle z(p^*) \rangle$ for three different values of r (red, green and black solid lines) for regular network with $k = 10$, $m = 4$, compared to the simulation results (symbols). Mean field theory (MFT) is in good agreement with simulations, but the error becomes larger close to discontinuities. Figure 2.2 shows the MFT prediction for the position of spinodals (black dashed lines), for the same network. The deviation of the MFT approximation from simulations becomes smaller with connectivity k increasing (see

Fig. 2.3) which is the characteristic mean field effect, and for very small k MFT is very crude. Nevertheless, the theory gives qualitatively excellent results. Figure 2.4 shows numerical and analytical results for the case of Poisson degree distribution (ER network [1]), for $\langle k \rangle = 10$ and $m = 4$. In this case there is less agreement between MFT and simulation results compared to the case of regular network (Fig 2.2), due to a substantial fraction of nodes having k close to the value of m .

2.5 Critical exponents and comparison with other models

To further characterize the network system, we measure the standard critical exponents β , δ , and γ around the critical point (for definitions see Ref. [42]). Large random networks can be regarded infinite dimensional systems. For our prototypical regular ($k = 10$, $m = 4$) network we find $\beta = 0.5 \pm 0.1$, $\delta = 2.7 \pm 0.6$, and $\gamma = 1.2 \pm 0.3$, indicating that our model is in the mean field Ising universality class in $d \geq 4$ dimensions, i.e., in systems in which $\beta = 1/2$, $\delta = 3$, and $\gamma = 1$. In contrast to magnetic systems and fluids, the critical exponent α , related to the heat capacity, is not defined for our dynamic network because there is no proper equivalence for heat or energy in our system. Figure 2.2 shows that our phase diagram is similar to the phase diagram found in fluids [43,44] and ferromagnets [42]. Note that the pattern of internal failures in our model is analogous to the external magnetic field in lattice-magnetic models (e.g., the Ising model) or the chemical potential in lattice-gas models. The *external* failures correspond to the interaction between neighboring sites in lattice-gas models or neighboring spins in lattice-magnetic models. The phase diagram of our system is rotated when compared to the phase diagram of the Ising model, similarly to the phase diagram of lattice gas models.

It is interesting to consider "vertical paths" in our phase diagram ($r = \text{const}$ paths) because they correspond to changing p^* only. Since the process of internal

failures that p^* is responsible for, is independent for all the nodes, we might expect p^* to behave like an external field in the magnetic analogy. However, some of the *vertical* paths cross only a *single* spinodal (in the Phase diagram in Fig. 2.1, this occurs for $0.980 > r > 0.877$), and for such paths we got an interesting property: if the system is initially put in Phase II it is stuck in that phase forever when only p^* is allowed to change. This is because the second spinodal is never crossed and we cannot reach Phase I, although it exists on the path. This is like having a magnet the polarization of which is "locked" and cannot be changed from the "south" (Phase II) to the "north" (Phase I) by changing only the external field.

In the case of noninteracting nodes, $p^* = 0$ simply means that *all* nodes in a network are active (that there is maximum "magnetization"). In a 1/2-spin magnetic analogy, this is associated with the magnetic field $H \rightarrow +\infty$ pointing "up," which aligns all spins in the up direction irrespective of temperature. Similarly, $p^* = 1$ corresponds to the internal failure of all nodes, i.e, the effective field $H \rightarrow -\infty$. Local interactions in our model differ greatly from those in magnetic materials, however. Consider a node located in a substantially damaged neighborhood. The magnetic analogy would be a down-spin in a local field. In our model this node has a probability of external failure r , irrespective of the value of p^* . Even if we apply an infinitely strong external field directed up ($p^* \rightarrow 0$, which corresponds to $H \rightarrow +\infty$), the probability that a node will be in the active state is still < 1 . This phenomenon is also reflected in in network behavior at the collective level.

This shows that for an interval of lower values of r , the system behaves similar to a magnet, while for a higher values of r , it shows an anomalous 'plastic' behavior. In a way, this anomaly defines two different regimes with respect to a value of r : the magnetic and 'plastic' regime.

Chapter 3

Phase flipping in single networks with FRS

3.1 Finite size phenomena: Phase Flipping

Most real-world networks are either small or medium-sized. This increases the importance of fluctuations. Sometimes in a large network only a very small number of its constituents play a major role, making the network “effectively” small, e.g., the financial network system is composed of a relatively small number of important banks. To explore the role of fluctuations, we perform numerical simulations for small networks with N nodes in which dynamic fluctuations are very pronounced. For small networks we find a dramatic collective dynamics in the hysteresis region. Figure 3.1 shows the fraction of active nodes $z(t)$ as a function of time t for a network with $N = 100$ when $r = 0.8$ and $p^* = 0.28$ is an arbitrary point in the hysteresis region, again using a regular network ($k = 10, m = 4$) as an example. We find that z flips back-and-forth from one phase to another. In this example the average fraction of active nodes is $\langle z_{\text{high}} \rangle \approx 0.67$ in the high activity phase, and $\langle z_{\text{low}} \rangle \approx 0.14$ in the low activity phase. The probability distribution function (pdf) of z exhibits a bimodal shape (Fig. 3.3).

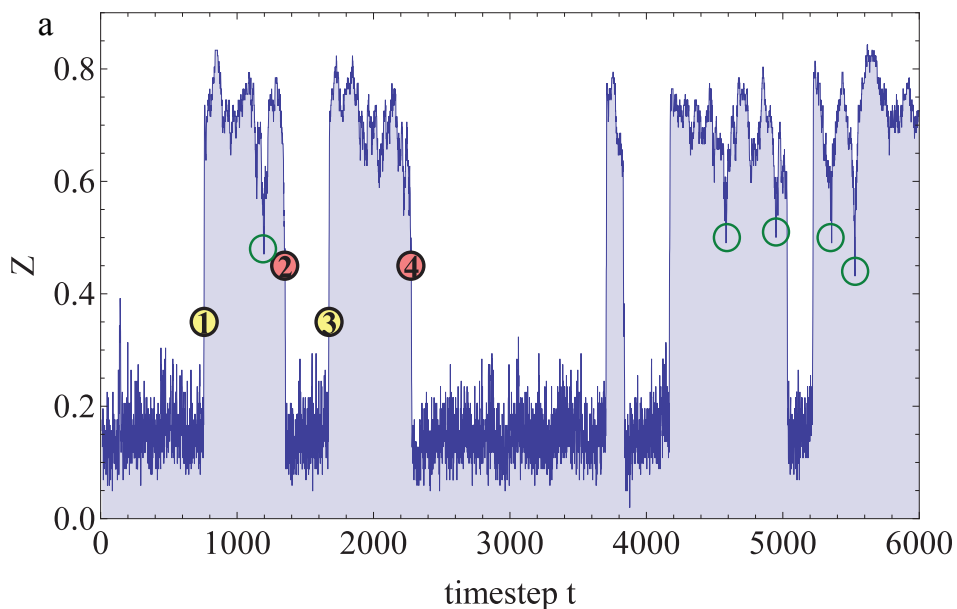


Figure 3.1: **Two network modes characterized by high and low network activity.** Switching between collective network modes in our dynamical network. Dynamic switching (flipping) between two phases in the subcritical region, an example for $p^* = 0.28$, $r = 0.80$ (point A, in yellow, Fig. 2.2), with $k = 10$, $m = 4$ and $N = 100$. The figure shows a fraction of active nodes z , as a function of time, flipping back and forth from one phase to another. Marked with green circles are sharp drops that might be related to "flash crashes", discussed later.

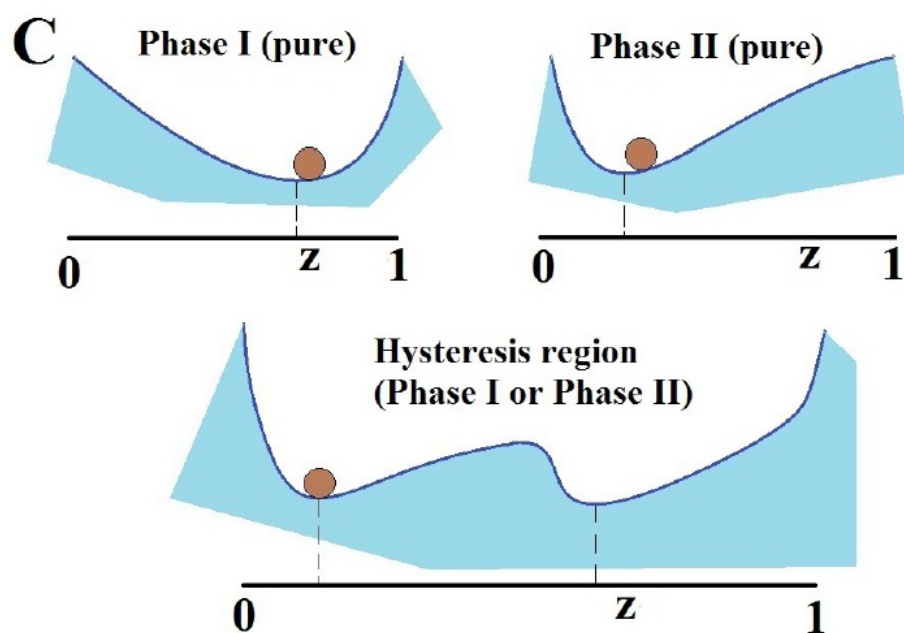


Figure 3.2: **Effective potentials.** Outside the hysteresis region, where pure phases exist, there is only one local minimum in the effective potential (effective single-well “potential”). In the hysteresis region, free energy landscape resembles a “double-well potential.” In a small system the fluctuations are very pronounced, and after long enough time the system can jump over the barrier from one potential well to another, resulting in a dramatic change of the collective network state.

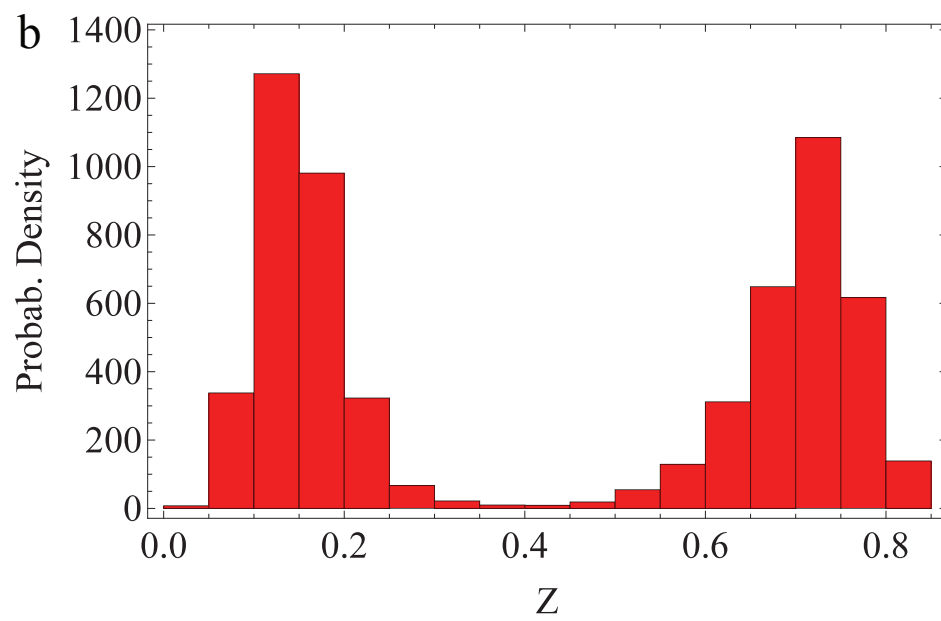


Figure 3.3: **Probability density function of z values for free evolution of the system.** The pdf of z shows a bimodal form, revealing states corresponding to high and low network activity.

The network activity represented by $z(t)$ exhibits behavior similar to a random walker attracted by a potential of asymmetric double-well shape, with minima at $\langle z_{\text{high}} \rangle$ (Phase I) and $\langle z_{\text{low}} \rangle$ (Phase II). In parts of the phase diagram outside the hysteresis region where pure phases exist, there is only one effective minimum (one single-well “potential”) with a single, time averaged equilibrium value of z , and a unimodal pdf $P(z)$. Effective potentials are illustrated in Figure 3.2. System stability and behavior can be described utilizing a recently-introduced concept of *basin stability* [45]. Note that when we initially put the system in one of the two “wells” of the effective double-well potential, the system “rolls” to the bottom of the well and stays in the same well if there are no fluctuations. When a dynamic network is small, the relative fluctuations in z become important and, after a sufficient span of time, the system can jump over the “potential barrier” from one potential well to another (and vice versa) causing a phase flipping.

3.2 Dynamics of Phase flipping

To further understand the violent dynamics of the network system—for example, to explain the average time spent in each phase—we need to determine the mechanism of network global recovery/collapse. Observe a system with a small number of nodes N . Consider the fraction of externally failed nodes among the nodes that have critically damaged neighborhood. This fraction is not exactly r at random time t , but actually fluctuates around r , due to probabilistic nature of external failures. Therefore, for every short time-interval $[t - \lambda, t]$, where λ is its duration, we can define the *local-time realization* of r , the quantity $r_\lambda(t)$, as the time-averaged fraction of externally failed nodes among the nodes having critically damaged neighborhood during that interval. If for λ , which is a time-resolution parameter, we choose a typical relaxation time of the system, we expect that during short intervals the system will behave as the “true” value of the damage conductivity is not r , but $r_\lambda(t)$. As a simple estimate for

λ , we use a typical duration of cascades. For the $N = 100$ network that we examine, $\lambda \approx 5$. In an analogous way, we can define the local-time realisation of p^* as $p_\lambda^*(t)$, the average fraction of internally failed nodes in the interval $[t - \lambda, t]$.

The evolution of the system can then be described as a trajectory $(r_\lambda(t), p_\lambda^*(t))$ in the phase diagram. Our crucial hypothesis is this: The global recovery event of the network in the low activity phase occurs when the trajectory $(r_\lambda(t), p_\lambda^*(t))$ crosses the “left” spinodal (red line in Fig. 2.2), triggering a cascade and resulting in the transition to the high activity phase. A similar explanation is for the spontaneous transition from the high activity phase to the low activity phase. In that case, only the “right” spinodal (blue line in Fig. 2.2) must be crossed by the trajectory. Phase-flipping phenomenon is then simply explained as the interchangeable crossing of the two spinodals by the trajectory $(r_\lambda(t), p_\lambda^*(t))$ in the phase diagram. Numerical simulations confirm our hypothesis. For $z(t)$ in Fig. 3.1, we measure the corresponding $(r_\lambda(t), p_\lambda^*(t))$ trajectory. Point “1” in Fig. 3.1 denotes the moment when the first jump from the down state to the upper state is registered. The position of the point $(r_\lambda(t), p_\lambda^*(t))$ at that moment is marked in the phase diagram shown in Fig. 3.4 using the same symbol, and it is very close to the “left” spinodal. Similarly, the first registered jump from the upper state to the lower state (point “2” in Fig. 3.1) is plotted in Fig. 3.4. As expected, the system at that moment is close to the “right” spinodal. Another few transitions are also presented, confirming our hypothesis for the mechanism of jumps. In Fig. 3.4, the white curve represents the trajectory $(r_\lambda(t), p_\lambda^*(t))$ from $t = 0$ to the moment of the first transition at “1.”

Sometimes the system can cross the spinodal and leave the hysteresis region for a very short time (shorter than the relaxation time) and then quickly go back to the hysteresis region without triggering a cascade and the corresponding transition. Exceptionally large spikes in Figure 3.1, denoted by green circles, correspond to such “untriggered cascades.” These spikes are thus not huge ordinary fluctuations, but a distinctive phenomena associated with the subtle dynamics of the trajectory $(r_\lambda(t),$

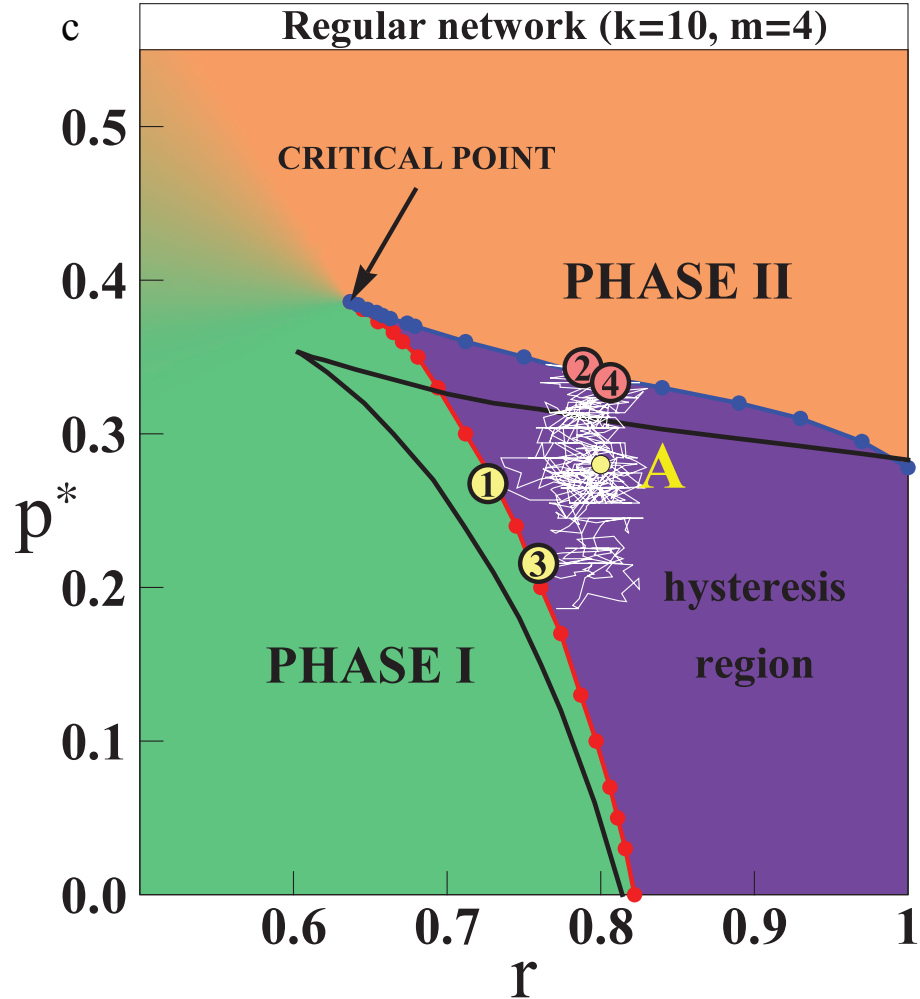


Figure 3.4: **Mapping the phase flipping.** White line represents trajectory $(r_\lambda(t), p_\lambda^*(t))$ of the system in the phase diagram, from $t=0$ to the moment of the first transition (point “1” Fig. 3.1), in the same numerical simulation where $z(t)$ in Fig. 3.1 was simulated. The system was in low active phase until the trajectory crossed the “left” spinodal, resulting in a global recovery event. Analogously, when the system is in the high active state the right spinodal becomes relevant (points “2” and “4”). Transitions between the macroscopic states are essentially first passage processes on interchangeable spinodals.

$p_\lambda^*(t)$.

Our initial choice for λ is supported by simulations. If for λ we take a much larger value than the relaxation time (which is the natural choice), the fluctuations of $r_\lambda(t)$ and $p_\lambda^*(t)$ become too small and the trajectory $(r_\lambda(t), p_\lambda^*(t))$ shrinks to a small region around Point A, and it does not cross the spinodals when it is supposed to. If λ is too small (for example $\lambda = 1$), the system cannot follow rapid changes in $r_\lambda(t)$ and $p_\lambda^*(t)$.

Note that when $r = 1$ the global recovery process is not possible. The fluctuations of r_λ vanish, $r_\lambda(t) = 1$, and the system cannot cross the “left” spinodal, which is necessary for global recovery.

3.2.1 State lifetimes

Two important observables are the average lifetimes of the system in the two states, $T_{\text{down}}(N)$ and $T_{\text{up}}(N)$. These lifetimes can be estimated using a simple model (solved below), with results

$$T_{\text{down}}(N) \sim \exp\left[\frac{N\lambda E[a(r, p^*)](r - r_s)^2}{2r(1 - r)}\right] \quad (3.1)$$

and

$$T_{\text{up}}(N) \sim \exp\left[\frac{N\lambda(p^* - p_s^*)^2}{2p^*(1 - p^*)}\right], \quad (3.2)$$

where r_s and p_s^* are distances from Point A to the left and the right spinodal, respectively. Thus the average lifetime of the system in a certain state exponentially increases with the system size N . This result is confirmed in simulations (see Fig. 3.5).

Now we provide a derivation for formulas (3.1) and (3.2), the crude estimates for the average lifetimes $T_{\text{down}}(N)$ and $T_{\text{up}}(N)$ of the system in each of the two states. The dependence of $T_{\text{down}}(N)$ and $T_{\text{up}}(N)$ on the system size N can be found using a very simple model. For $T_{\text{down}}(N)$, the system is in the low active state, and we suppose that the transition to the high active state occurs when r_λ reaches some

value $r_s < r$; where r_s is a typical r -position on the left spinodal where most cascades to the high active state occur. This is essentially a first passage process. There are $NE(a(r, p^*), k, m)$ nodes in the network having critically damaged neighborhood, and each has a probability r to be externally failed and $1 - r$ not to be externally failed. Since we defined r_λ as the average fraction of externally failed nodes among the nodes with critically damaged neighborhood during interval of length λ , the probability distribution of r_λ values is binomial, and it can be approximated with the normal distribution with mean $\mu = r$ and variance $\sigma^2 = r(1 - r)/n$:

$$f(r_\lambda) \sim \exp\left[-\frac{n(r_\lambda - r)^2}{2r(1 - r)}\right], \quad (3.3)$$

where n is the sample size. Knowing that $n = NE(a(r, p^*), k, m)\lambda$, for the probability that $r_\lambda = r_s$ we get

$$f(r_s) \sim \exp\left[-\frac{N\lambda E(a(r, p^*), k, m)(r_s - r)^2}{2r(1 - r)}\right] \quad (3.4)$$

If there is $f(r_s)$ chance that at random moment t the trajectory $(r_\lambda(t), p_\lambda^*(t))$ is crossing the "left" spinodal, then the rough estimate for $T_{\text{down}}(N)$ is $T_{\text{down}}(N) \sim 1/f_{r_s}$ and we arrive at Eq. (3.1).

Equation (3.2) for $T_{\text{up}}(N)$ can be obtained in an analogous way.

3.3 Phase flipping in real networks

To obtain plausible empirical support for our dynamic network model, we study economic networks in both developed and developing countries. We picture an economic network to be a network of companies linked to each another by economic connections (mostly buyer-supplier dependencies). An aluminum smelter, for example, can be approximated as a node connected by links to its major suppliers (companies that produce or deliver bauxite ore and electricity, necessary in the production of aluminum) and buyers (companies that trade with aluminum or need aluminum in their own production). Disturbances in some of these nodes (companies) can effect

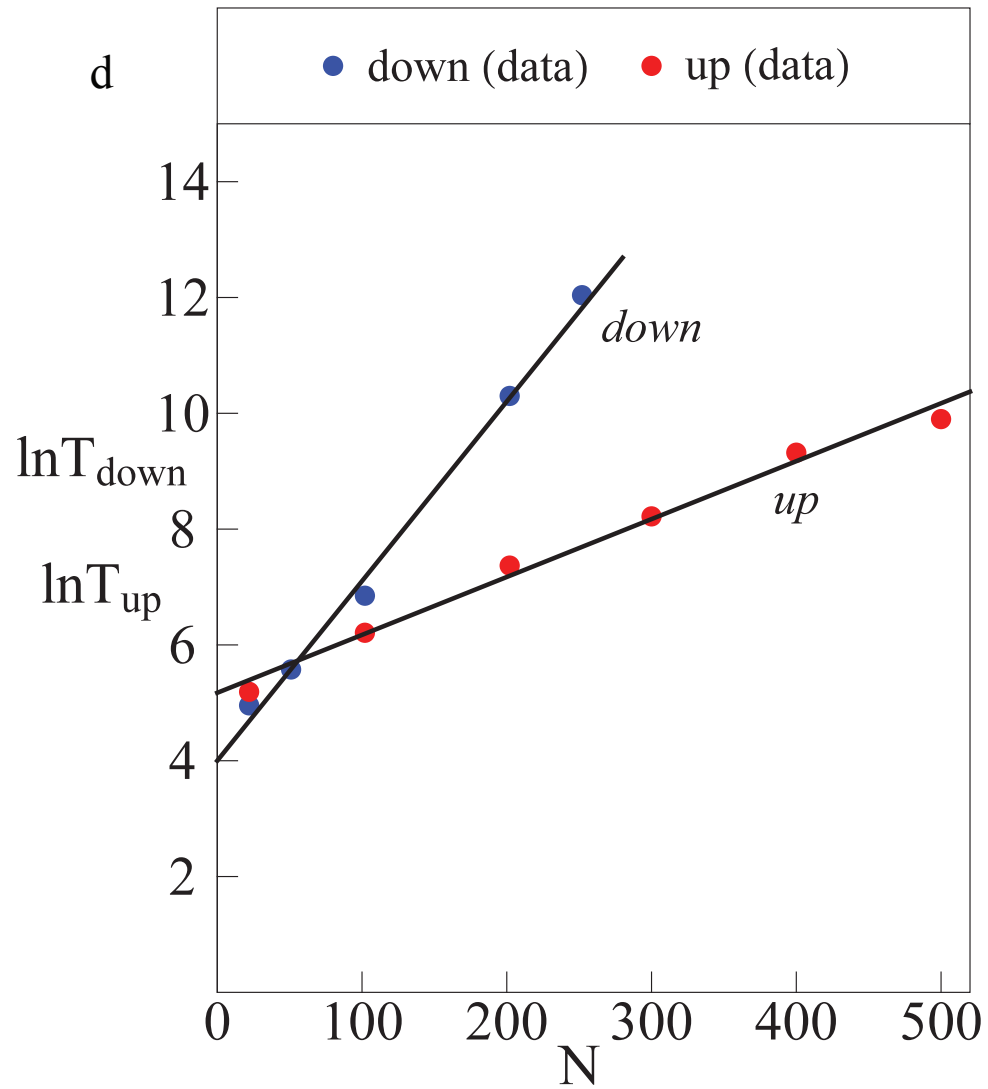


Figure 3.5: **Average lifetimes VS system size.** Expected lifetime of the system in a certain state measured in simulations, increases exponentially with the system size N , confirming our theoretical results, Eqs. (3.1) and (3.2). Black lines represent linear regressions in $(N, \log T)$ diagram.

the functionality of neighboring nodes. Our network model is simple and consists of nodes that can have only two states: *active* or *failed*. To map a real economic network to our dynamic network model, we define an appropriate variable that has two states indicating whether a company is operating well or poorly. We construct this *binary* state variable using market returns, which can be positive or negative. Since market returns on a daily basis are more a result of speculation than fundamental changes in the companies, we chose a reasonably long period of 100 days when we measure the company's net return. The state of company i at moment t we define as “good” if, during the period $[t - 100, t]$, the company has a net market value increase and “bad” if, during the same period, it has a net market value decrease. Much information is lost in this mapping, but essential information, such as whether a company is performing well or badly, is retained. We define the measurable variable $z(t)$ to be the fraction of companies in the economic network that have positive total returns during the period $[t - 100, t]$.

Figures 3.6 and 3.7 show results for $z(t)$ and its pdf $P(z)$ for two real markets over a ten-year period that includes the recent severe recession and market crash. Figure 3.6 shows the Indian financial index as an example of a developing financial market. There are indications that values of $z(t)$ switch back and forth between high and low values, resembling the phase flipping phenomena that our model predicts for the “hysteresis regime.” The pdf $P(z)$ exhibits an asymmetric bimodal shape and indicates that the network mode positions are less than $\langle z_{\text{low}} \rangle \approx 0.2$ and greater than $\langle z_{\text{high}} \rangle \approx 0.5$. From these findings we assume the Indian market is in the hysteresis regime.

We also study the constituents of a widely used US financial index, the S&P500 index, as an example of a developed market. Figure 3.7 shows the evolution of $z(t)$ for the S&P500 during the same ten-year period, and the corresponding frequency distribution. The behavior of $z(t)$ is similar to the Indian market, and $P(z)$ again exhibits a bimodal shape; the system spends more time around *two* values of z ,

$z \approx 0.25$ and $z \approx 0.6$, suggesting two possible modes.

For both the Indian index and the S&P500 index data we find that z exhibits bimodal pdf behavior during the last ten years, the decade that includes the severe economic crisis, but not during previous decades. This finding suggests the intriguing possibility that model parameters of the economic network can change from year to year or from decade to decade, and that the system can enter and exit the hysteresis region. The comparison with real data indicates that our model is a plausible qualitative explanation for the behavior we observe in real economic networks. Our prototypical network model supports the concept of *economic states* [46, 47]. Possible hysteresis was reported and discussed in some economic systems [48]. From the phase flipping mechanism we uncovered, we can draw some interesting conclusions for economic networks. Notice that, if several negative economic events occur (p_λ^* is increasing) separated by a time interval $\geq \lambda$ (the characteristic time of system relaxation), the system will absorb the damage and avoid global collapse. If the same negative events occur but are separated by a time interval $\leq \lambda$, catastrophic system failure is possible. This has implications for system recovery. Government economic recovery measures applied within a very short time ($\lesssim \lambda$) probably achieve better results. If distributed during a long time, the economic network would probably absorb the positive “kicks” and no transition to the upper phase would follow. The possible relation between the “untriggered cascades” in our model, and the “flash crash” phenomenon in real-world networks, is discussed in the next subsection.

3.4 Flash crashes

Apart from phase switching, our model predicts another phenomenon: exceptionally large isolated “spikes” in $z(t)$. These events are not fluctuations of ordinary type but, as we find, a distinct phenomenon associated with “untriggered cascades” when the system’s trajectory $(r_\lambda(t), p_\lambda^*(t))$ crosses the relevant spinodal and stays in the

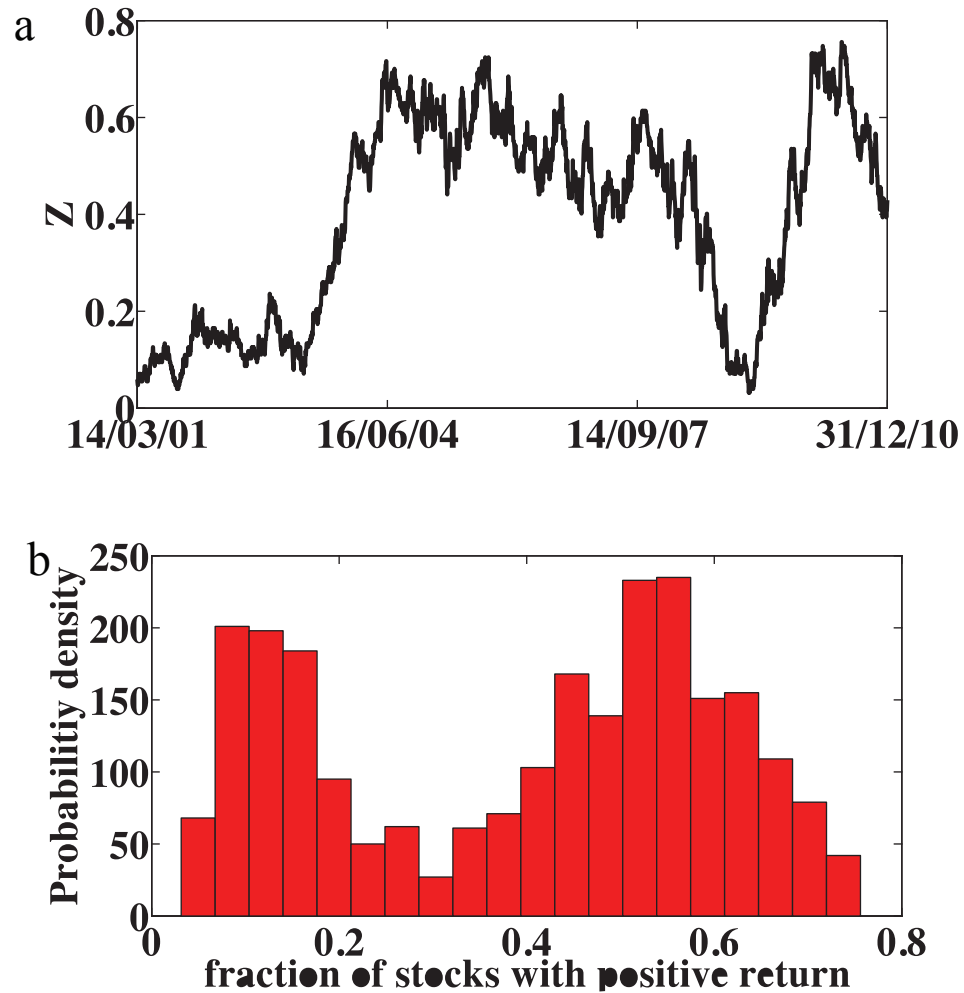


Figure 3.6: **Properties of phase flipping phenomenon in financial data for an undeveloped market.** (a) For the constituents of financial index, the Indian index (BSE200), the fraction of stocks z with positive return as a function of time switches back and forth between the two network modes characterized by high and low network activity. (b) Bimodal form in the pdf of financial data during the last decade.

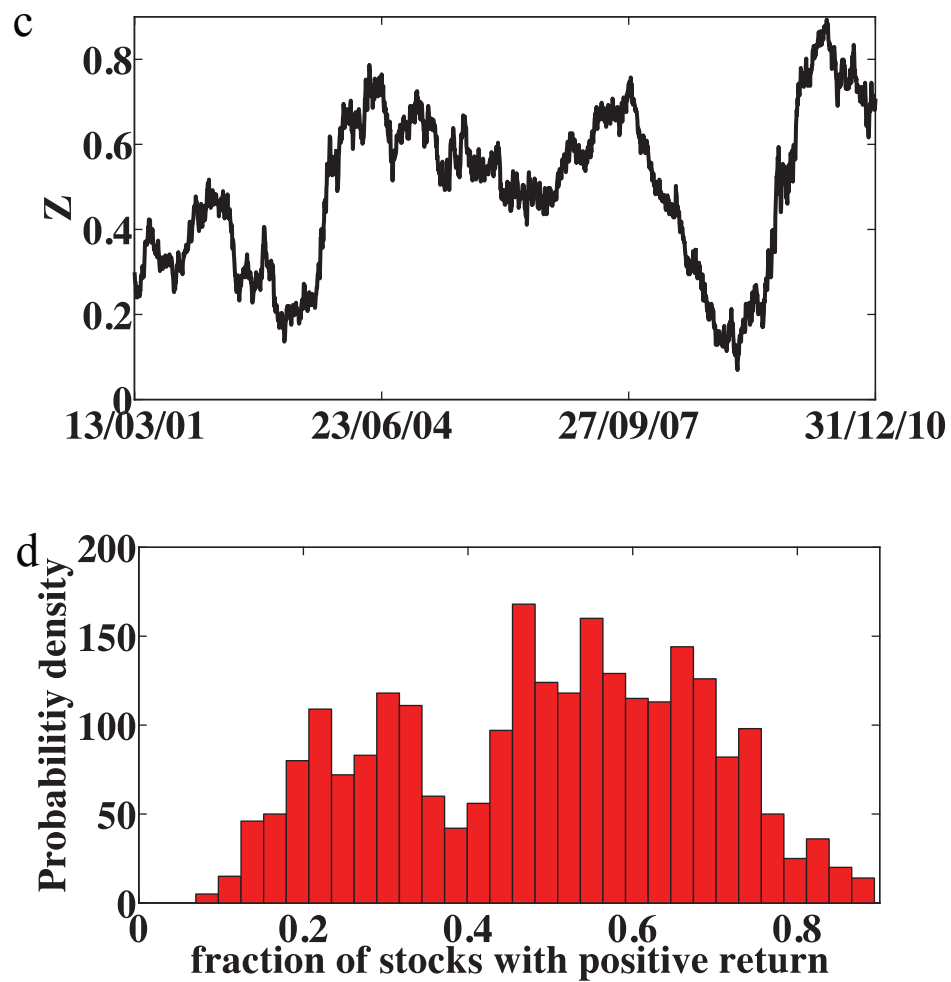


Figure 3.7: **Properties of phase flipping phenomenon in financial data for a developed market.** The same as in Fig 3.6 but for the S&P500 financial index. Ashman's D test validates the significance of bimodality ($D > 2$).

”forbidden region” for a time typically shorter than the relaxation time of the system, and then returns in the hysteresis region. These sharp drops followed by rapid recovery might be related to the phenomenon of ”flash crashes” observed in real dynamical networks. A notable example from economic networks is May 6, 2010 Flash Crash of the US stock markets (see Fig. 3.8a). That day, stock markets in the US reported a large and rapid loss in the market index value, followed by a rapid recovery. Figure 3.8 shows a single sharp drop from Fig. 3.1 (the green circle denoted as ”F”), enlarged to see the structure of the event. The system’s trajectory $(r_\lambda(t), p_\lambda^*(t))$ was approaching the ”right” spinodal (decreasing the value of z below 0.6), and crossed it at the moment marked by a red arrow. That moment was followed by a rapid drop and recovery that lasted only a few timesteps, then followed by a slower recovery as the system’s trajectory returned to the hysteresis region and slowly left the vicinity of the spinodal.

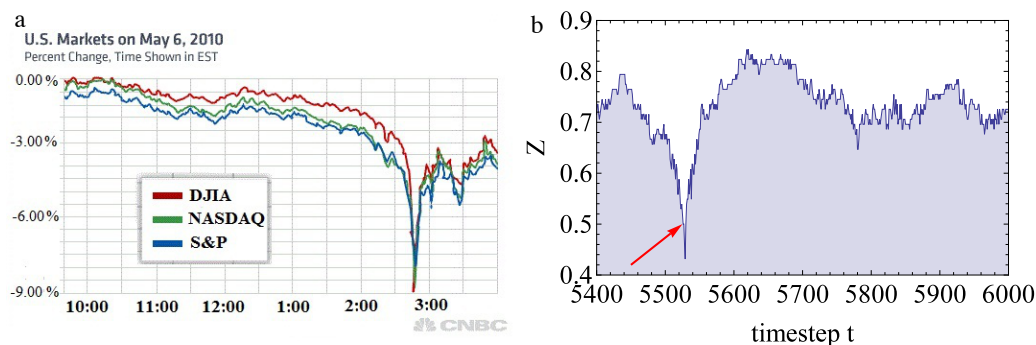


Figure 3.8: **Flash crash.** (a) The infamous flash crash of the US financial market on 6 May 2010. The market index value dropped rapidly, followed by an equally rapid recovery. Source: CNBC. (b) Isolated sharp drop associated with an avoided transition, in our model.

Chapter 4

Phase diagrams of FRS processes in interdependent networks

4.1 Interdependent networks

As already noted, most real networks are not isolated structures but interact with other network structures. As a result, much research has been focused recently on the dynamics of interdependent [17, 21, 49–54] and multilayer [12, 55, 56] networks. Recent studies on network repair [22, 24, 58] have shown the importance of recovery of nodes as a process which leads to reverse transitions, hysteresis effects, and such phenomena as spontaneous recovery [22, 25].

4.2 FRS process in interdependent networks

The cardiovascular and nervous systems in the human body are examples of two dynamically interacting physiological networks [59]. Diseases often result from complex pathological conditions that involve a dynamical interaction with positive or negative feedback between different functional subsystems in the body. Similarly, in the global economy there is a hierarchy of clustered and tightly connected countries, often

grouped geographically, that are further interconnected to one large global interacting economic and financial network [60–62]. To understand the behavior of these systems using network science, we develop a model of interacting networks with nodes that can recover from failure and we examine the resulting phase diagram. We present our method and the results in detail for the simplest case of $n = 2$ interacting networks, which can be easily generalized to any number of interacting networks.

Our model of a generic system consisting of interacting dynamical networks captures the important events found in real-world interacting networks, i.e., node failure [29, 70–72], systemic damage propagation [73], and node recovery [22, 25, 74].

We first introduce the model, describing the details of the dynamical processes. We present the mean field solution of the model and a rather complex phase diagrams that we obtain. Knowing the phase diagram allows us to study a fundamental problem of optimal repairing of damaged interconnected systems, which we do in Chapter 5. In the final chapter (Chapter 6) we apply our model to a selected real system, and we give a full methodology for measuring model parameters.

In our model we first describe the structure of the system and then describe the rules governing the dynamic behavior of the processes occurring within the system.

4.3 Model

The structure of our system for the $n = 2$ case is modeled as follows. We start with two isolated networks, network A and network B, and for simplicity we assume that both networks have the same number of nodes N and the same degree distribution $f(k)$ (these assumptions can be relaxed, but the results stay qualitatively similar). We assume that within each network the nodes are randomly connected. Now, to allow networks A and B to interact, we introduce interdependency links that connect nodes across the two networks [21]. This can be achieved in different ways, and we use a simple one-to-one dependency: each node in network A is dependent on exactly

one node in network B, and vice versa. The pairs of nodes of both networks are chosen randomly.

The dynamic behavior of our system is governed by two categories of event—failure and recovery—and we assume that every node is in either a failed or an active state. Node failure can result from internal failure or from the spread of damage from neighbor nodes in either the same network or the interdependent network. We thus assume that there are three ways a node can fail. The first way is the internally induced failure, when a node’s internal integrity has been compromised, e.g., an organ in the body can fail due to a malfunction within the organ or a company can fail due to bad management. The second type of failure is externally induced failure through failure propagation due to connections with failed nodes within the node’s own network. Finally, there is a failure induced through the dependency link as a result of being dependent on a failed node from another (opposite) network. Apart of these three types of failures, we assume the existence of associated simple recovery processes for every type of failure. We specify quantitatively each of these processes below.

4.3.1 Model rules

For internal failures (I), we assume that in both networks any node can fail due to internal problems, independent of other nodes. For each node in network A we assume that there is probability $p_A dt$ that the node will fail internally during any time period dt . The equivalent parameter in network B is p_B .

Every node in network A and network B is connected by links to nearby nodes in its own network. These nodes constitute the node’s neighborhood. The number of links a node has within the network indicates its *degree* or *connectivity*, denoted by k . If a large number of nodes in a node’s neighborhood have failed, i.e., if the neighborhood is substantially damaged, we assume that the probability that the node itself will fail is increased. This is modelled by external failures (E). As in previous

chapters (and also Refs. [22] and [75]), we use a threshold rule to define a *substantially damaged* neighborhood, which is a neighborhood containing $\leq m$ active nodes, where m is a fixed integer threshold. If node j has $> m$ active neighbors during time dt , we consider its neighborhood to be “healthy” and there is no risk of external failure. On the other hand, if j has $\leq m$ active neighbors during time dt , there is a probability $r_A dt$ (for network A) or $r_B dt$ (for network B) that node j will externally fail. For certain systems it is more appropriate to define a fractional threshold $0 \leq m_{frac} \leq 1$ as in [25]. That is, the minimum number of active nodes as a requirement for a “healthy” neighborhood is replaced by a minimum *fraction* of active nodes in the neighborhood. In the example of random regular network that we consider below, both are equivalent and related by $m = k m_{frac}$.

In the case of two interdependent networks (A and B), we assume that each node in the first network is dependent on a node in the second network via an interdependent link, and vice versa. We assume that if one node in the pair fails there is a finite (but not 100%) probability, $r_d dt$, that during time dt the other node in the pair will fail as well (dependency failure - type D). This represents the probability that the damage will spread through the interdependency link.

We also assume that there is a reversal process, a recovery from each of these three types of failure. A node recovers from an *internal* failure after a time period $\tau \neq 0$, it recovers from an *external* failure after time τ' , and from a *dependency* failure after time τ'' . In simulations, and without loss of generality, we use $\tau = 100$, and for simplicity we set $\tau' = \tau'' = 1$ to take into account the assumption that real-world systems usually require a longer time period to recover from internal problems (physical faults) then from a lack of environmental support. Changing the numerical values however, does not introduce any qualitative difference.

For the node activity notation, we assume that every node is in one of two states: active or failed. A node is considered active in the observed moment, if it is not experiencing internal (I), external (E), or dependency (D) failure.

Parameters r_A and r_B are introduced because they describe how easily the damage is spread through the network. When $r = 0$ there is no damage spread between the nodes, and when $r = 1$ there is perfect damage conduction. Assuming that external failures occur with certainty would mean fixing r to be equal to 1. In the case of a single network with recovery it has been shown (Chapter 3, also [22]) that many important phenomena (e.g., spontaneous recovery) are lost when $r = 1$. The most interesting parts of the phase diagram are in fact where r is far from 1.

4.4 Mean field theory

We characterize this system by studying the order parameters chosen naturally as the fraction of active nodes in network A and network B, z_A and z_B , respectively. To simplify the calculation, however, we first concentrate on the complementary and equally intuitive fraction of failed nodes a_A and a_B , in networks A and B respectively ($a_A = 1 - z_A$, $a_B = 1 - z_B$).

Using the mean field theory presented in Appendix A, we obtain two coupled equations that connect a_A and a_B , which the system must satisfy in the equilibrium

$$a_A = p_A^* + r_d a_B (1 - p_A^*) + \sum_k f(k) F(k, a_A) [r_A - p_A^* r_A - r_A r_d a_B + p_A^* r_A r_d a_B] \quad (4.1)$$

$$a_B = p_B^* + r_d a_A (1 - p_B^*) + \sum_k f(k) F(k, a_B) [r_B - p_B^* r_B - r_B r_d a_A + p_B^* r_B r_d a_A] \quad (4.2)$$

Here $F(k, x) = \sum_{j=0}^m \binom{k}{j} x^{k-j} (1-x)^j$, and we have also introduced simplifying parameters $p_A^* \equiv 1 - e^{-p_A \tau}$ and $p_B^* \equiv 1 - e^{-p_B \tau}$ to make the equations more elegant and to reduce the number of parameters by replacing p_A , p_B , and τ that appear as a product. We find that the parameters p_A^* and p_B^* are very convenient to work with because they correspond to the fraction of internally failed nodes in network A and network B, respectively.

Despite the seeming complexity of Eqs. (4.1) and (4.2), note that there are only two unknown variables, a_A and a_B , and that all other parameters are fixed. These

two equations define two curves in the (a_A, a_B) plane.

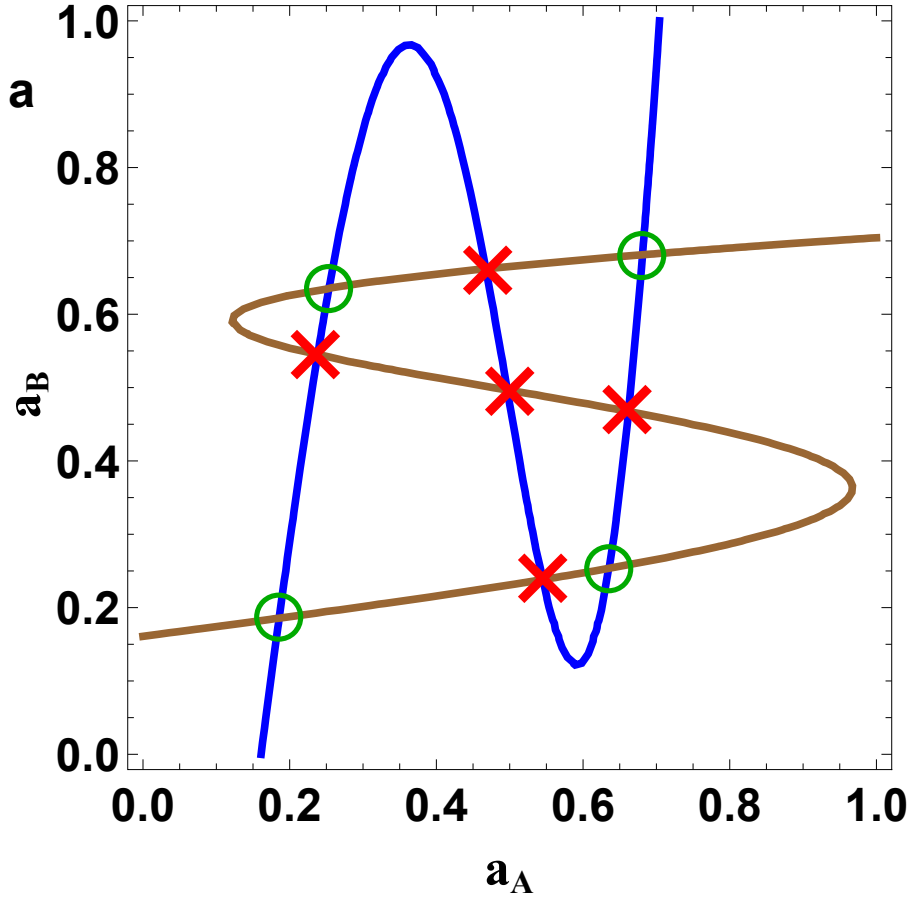


Figure 4.1: **Graphical representations of the mean field equations.** The blue and brown curves represent Eq. (4.1) and Eq. (4.2), respectively, for $p_A^* = p_B^* = 0.16$, $r_A = r_B = 0.60$ and $r_d = 0.15$, in a system with two interdependent networks ($k = 16$, $m = 8$). There are nine intersections, representing mathematical solutions for network activities a_A and a_B . Four of them are stable solutions (green circles) representing physical states that we also observe in our simulations, and five are unstable solutions (red crosses).

Figure 4.1 shows a graphical representation of the curves for a random regular [13] network (in which all the nodes have the same degree) with degree of $k = 16$ and threshold $m = 8$, for the symmetric parameter values $p_A^* = p_B^* = 0.16$, $r_A = r_B = 0.60$, and $r_d = 0.15$. The size of each network is $N = 2 \times 10^4$. The blue curve is a graphical

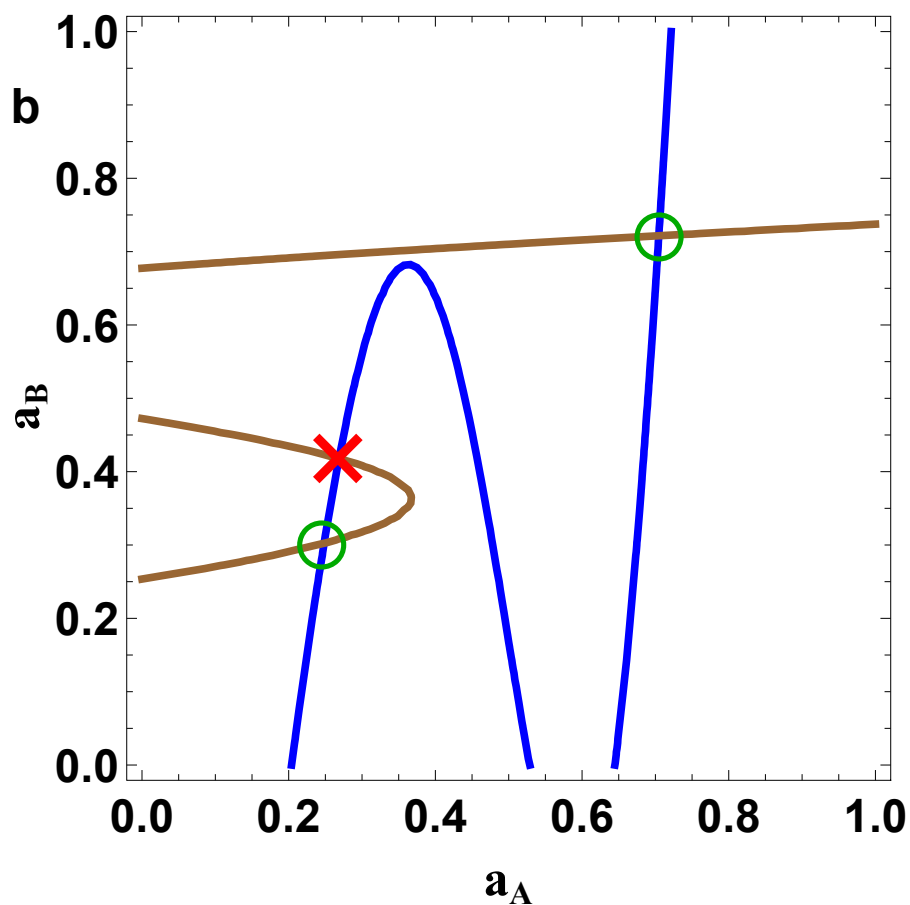


Figure 4.2: **Graphical representations of the mean field equations.** Example for $p_A^* = 0.20$, $p_B^* = 0.24$, $r_A = r_B = 0.60$ and $r_d = 0.15$. Here we obtain two stable solutions and one unstable solution. The two stable solutions correspond to 11 state (both networks are at high activity) and 22 state (both networks are at low activity).

representation of Eq. (4.1), and the brown curve is defined by Eq. (4.2). The curves, like two “ropes,” create a “knot” that can have up to nine intersections, representing mathematical solutions of the system of equations. Not all of these solutions represent observable and stable physical states, however. To see that, observe one of the curves in Fig. 4.1, for example the blue curve described by Eq. (4.1). If we increase damage done to network B (i.e. we increase a_B) and keep everything else constant, some damage will undoubtedly spread to network A. Thus we expect that when a_B is increased, a_A must also increase (it would be very unusual if one network improves its activity as a result of damaging the other network). We conclude that the parts of the blue and brown curve that produce physical solutions are only those where a_A and a_B increase together or decrease together along the curve. This elimination leaves only four states in Fig. 4.1 that are stable (green circles), while the other five states are unstable (red crosses), for this particular choice of parameters. In simulated finite networks, when the network system evolves according to the rules of the model, at $t = 0$ we have a freedom to set initial conditions for the activities. Systems initially prepared to have a pair of values (a_A, a_B) corresponding to an unstable solution of Eq. (1) and (2) will be disturbed by a small fluctuation of a_A or a_B due to the system dynamics, and the values of a_A or a_B will rapidly change until one of the stable states is reached. Systems that are initially prepared to have values of a_A or a_B corresponding to a stable solution will fluctuate around these values, until perhaps a large finite fluctuation occurs and the system “jumps” to another stable state. Generally, for any choice of parameters, we have between one and four stable (physical) states. Figure 4.2 shows the scenario for the same network system when $p_A^* = 0.20$, $p_B^* = 0.24$, $r_A = r_B = 0.60$, and $r_d = 0.15$. In this case we have two stable states and one unstable state.

In subsection 4.4.1 (“Additional phase diagrams”), we show diagrams for $z_A = 1 - a_A$ for a range of different values of p_A^* and all other parameters fixed. This mean field theory calculation agrees well with the states that we observe in our simulations,

as we will demonstrate below.

The four stable solutions found above correspond to the following four scenarios: “11” or “up-up”, when there is high activity in both network A and network B; “12” or “up-down” when there is high activity in network A and low activity in network B; “21” or “down-up” when there is low activity in network A and high activity in network B; and “22” or “down-down”, when there is low activity in both network A and network B.

Depending on the parameters, we obtain between one and four stable states. Each of the states exists in a certain volume of the multi-dimensional space of parameters. Results of the mean field theory calculation for a particular set of parameters are presented in Fig. 4.3-4.6 as a phase diagram with four layers. The figures show the regions in which each of the four states exist in the (p_A^*, p_B^*) parametric sub-space, when other parameters are fixed at values $r_A = r_B = 0.60$ and $r_d = 0.15$, with k and m remaining the same as before.

For example, in Fig. 4.3 the green area indicates the region where the 11 state exists. This state (phase) is bounded with a smooth boundary of three colors. If the boundary is crossed (by increasing p_A^* and p_B^*), the system makes a transition to state 12 (if the orange line is crossed), state 22 (if the blue line is crossed), or state 21 (if the purple line is crossed). The arrows indicate transitions. In Fig. 4.3 there are two triple points (black points) that mark the change in the transition type and where three different states can exist. The blue area in Fig. 4.4 indicates the 22 state. This layer of the phase diagram has two triple points as well, and three possible transitions ($22 \rightarrow 12$, $22 \rightarrow 11$, and $22 \rightarrow 21$).

Figures 4.5 and 4.6 show the regions of state 21 (purple) and state 12 (orange), respectively. Each has two different transitions and one critical point. For example, there are two possible ways out of state 21 (Fig. 4.5): by a transition to the 11 (green arrow) state or the 22 (blue arrow) state. Note that the different state regions (Figs. 4.3, 4.4, 4.5, and 4.6) are not disjoint sets but there is an overlap, resulting in

2-fold, 3-fold, or even 4-fold hysteresis regions.

The state in which the system is found depends on the initial conditions or the system’s past. There are a total of 10 different transitions ($11 \rightarrow 12$, $11 \rightarrow 22$, $11 \rightarrow 21$, $12 \rightarrow 11$, $12 \rightarrow 22$, $21 \rightarrow 11$, $21 \rightarrow 22$, $22 \rightarrow 12$, $22 \rightarrow 21$ and $22 \rightarrow 11$) that connect different layers of the phase diagram (states 11, 12, 21, and 22), much like elevators connecting different floors. Transitions $12 \rightarrow 21$ and $21 \rightarrow 12$ are the only missing (“forbidden”) combinations. Although regions 12 and 21 do overlap, there is no direct transition connecting these two states. These transitions would correspond to the unusual combination in which one network recovers (transitions to a higher activity) and simultaneously the other network fails. Thus a transition from state 12 to state 21 requires the use of an intermediate state (11 or 22). A more detailed discussion of the absence of these two transitions can be found in subsection 4.4.2, *Forbidden Transitions*. The set of all allowed and forbidden transitions is presented in Fig. 4.7. The total phase diagram (all four layers on top of each other) is presented in Fig. 4.8. Here, colored lines represent the boundaries of four states, with each color corresponding to the boundary of one state, e.g., the green line is a boundary of the 11 state. Rich critical phenomena with discontinuous hybrid phase transitions and second order transitions have been recently discovered in multiplex networks. Particularly, Baxter et al. [57] introduced weak bootstrap percolation and weak pruning percolation in multiplex networks, which have potential applications in infrastructure recovery and information security, and can even provide a way to diagnose missing layers in a multiplex network.

We next can examine the activity profile for various cross-sections in the phase diagram. In Figure 4.8 we choose two representative cross sections (dashed straight lines) to measure activity $z_A = 1 - a_A$ as p_A^* and p_B^* change. The black dashed line is defined by the equation $p_B^* = 0.1 + 4/3p_A^*$ and the red dashed line by $p_B^* = 0.4 - p_A^*$. Figure 4.9a shows the activity measured in simulations of network A as we move along the black dashed line, changing both p_A^* and p_B^* and preserving the relation

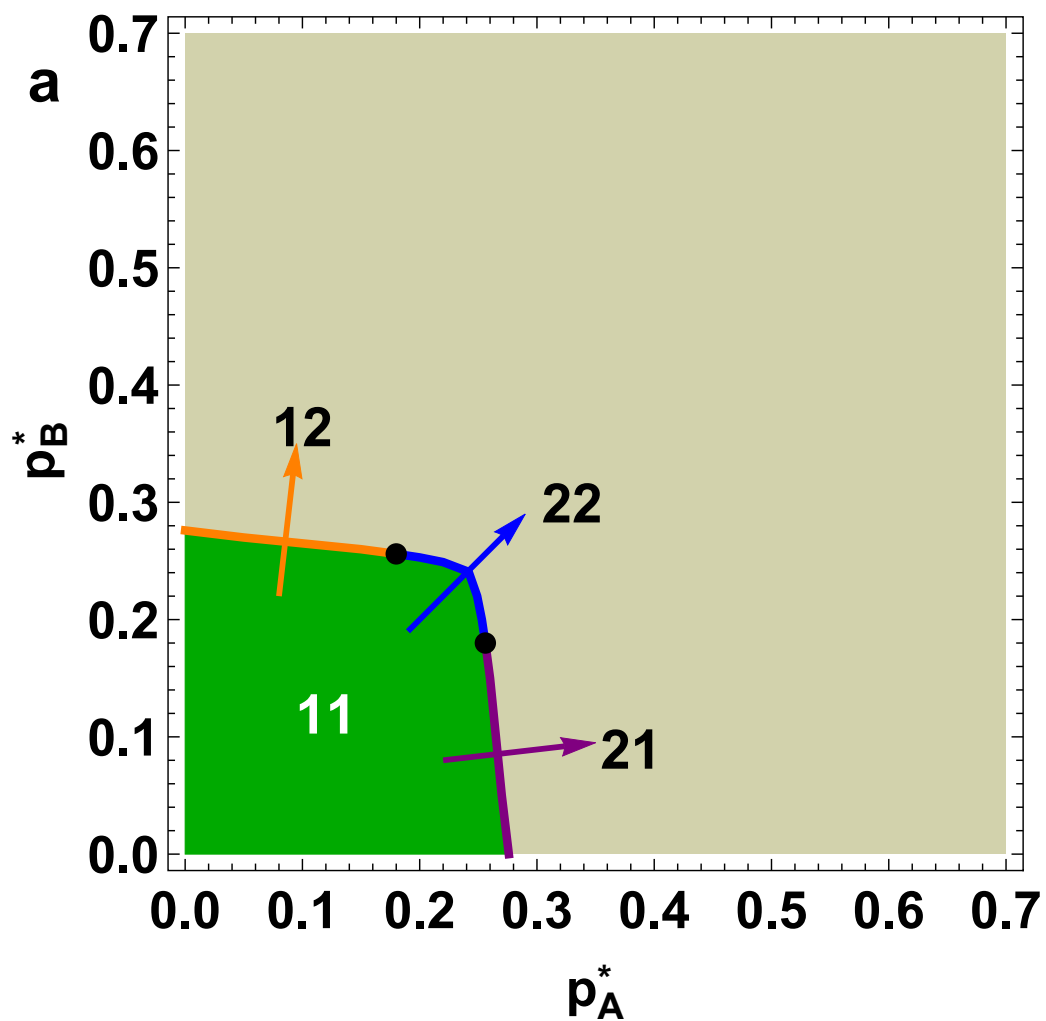


Figure 4.3: **First layer of the phase diagram with corresponding transitions.** Region of 11 state, in green. Possible transitions are $11 \rightarrow 12$ (orange line), $11 \rightarrow 22$ (blue line) and $11 \rightarrow 21$ (purple line). This layer of the phase diagram has two triple points, marked as black points.

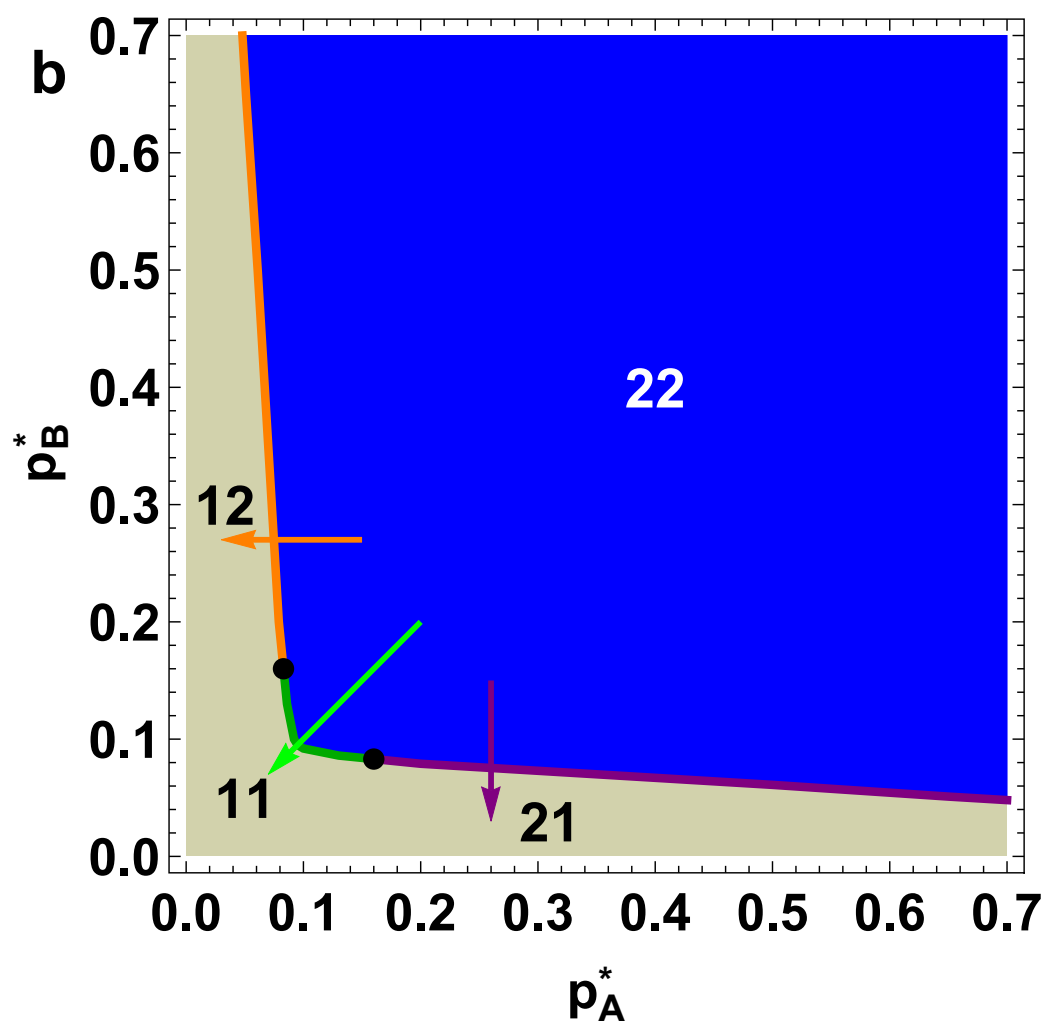


Figure 4.4: Second layer of the phase diagram with corresponding transitions. Region of 22 state (blue), with two triple points and three transitions.

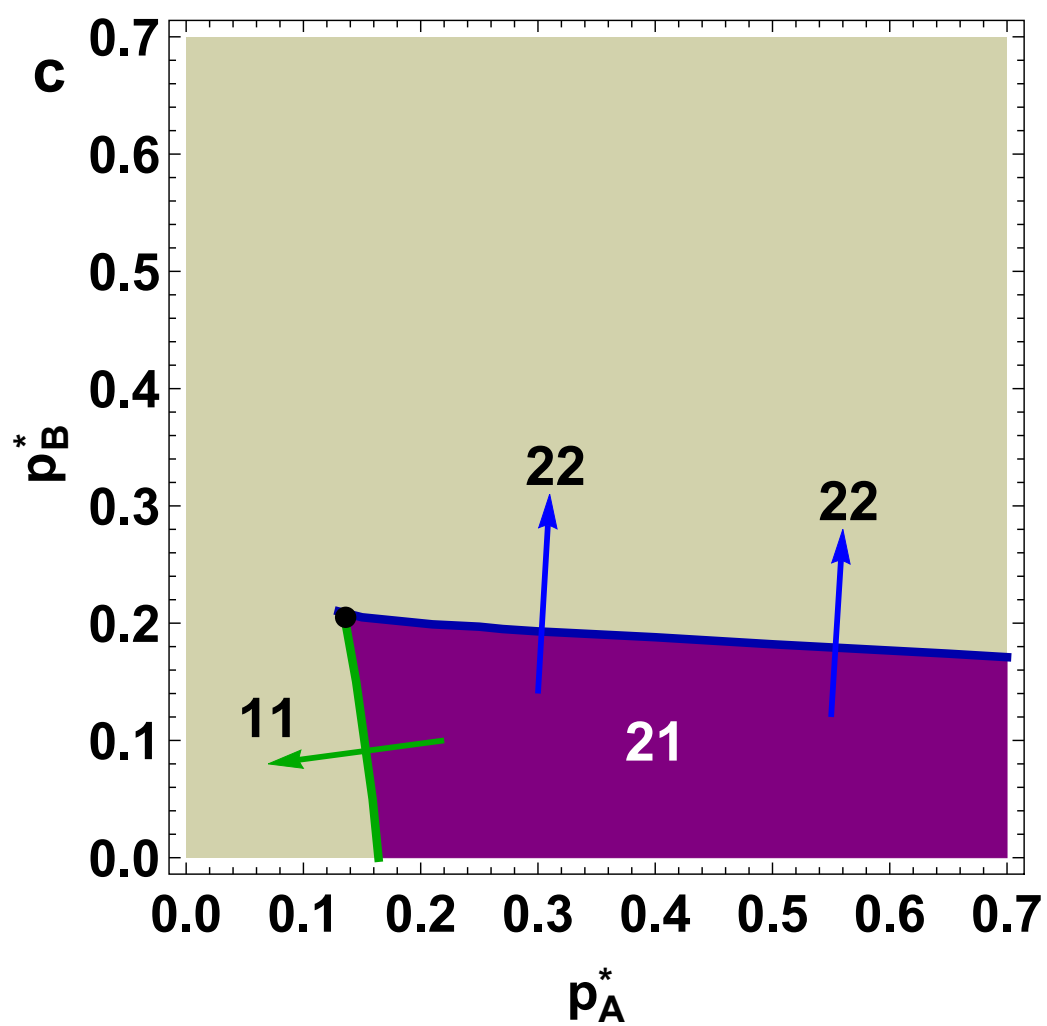


Figure 4.5: Third layer of the phase diagram with corresponding transitions. Region of 21 state (purple), with two transition lines (to 11 and 22 state) that merge in a critical point.

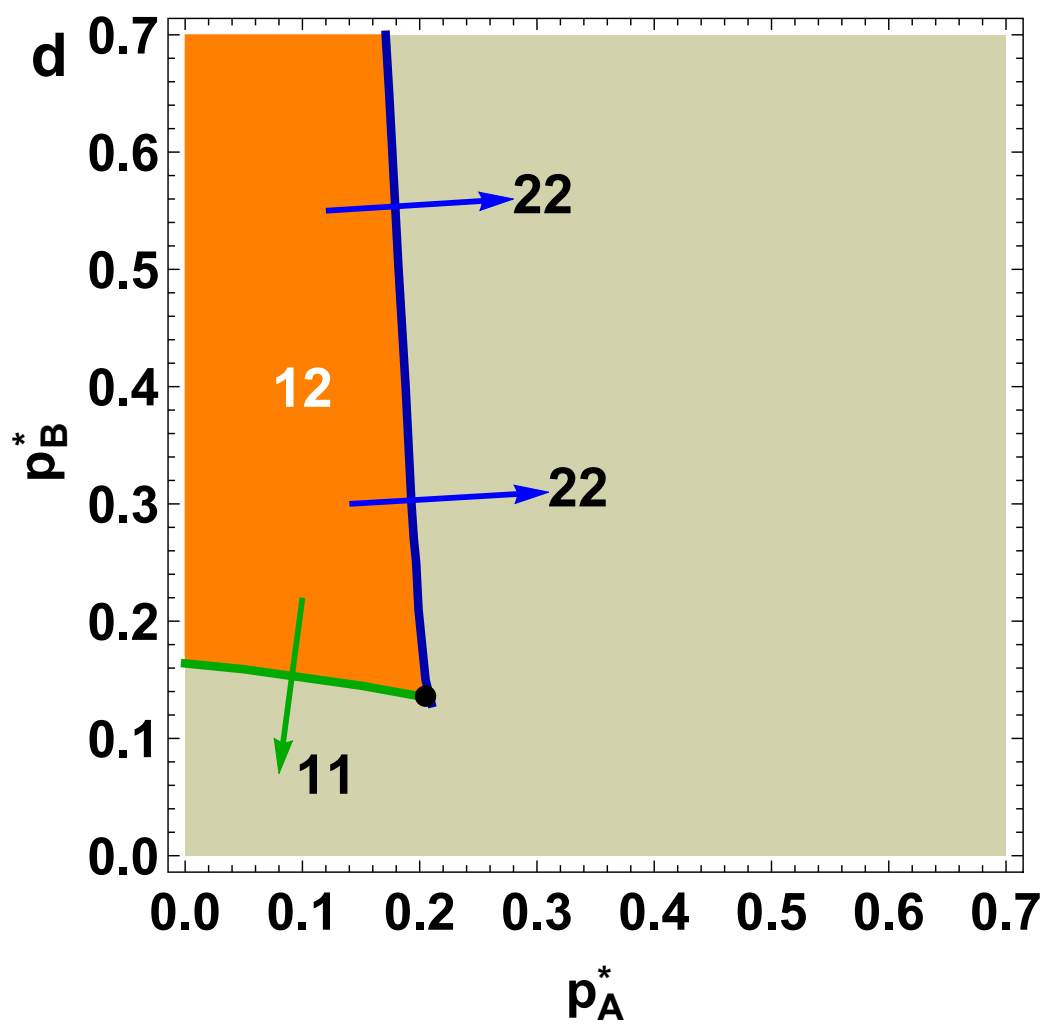


Figure 4.6: Fourth layer of the phase diagram with corresponding transitions. Region of 12 state (orange), with two transition lines (to 11 and 22 state) that merge in a critical point.

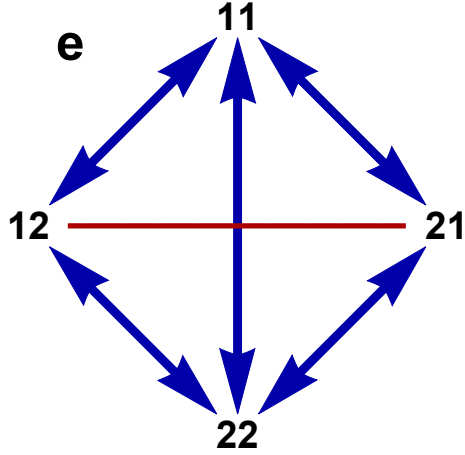


Figure 4.7: Illustration showing states (11, 12, 21 and 22) with allowed (blue arrows) and “forbidden” (red line) transitions.

$p_B^* = 0.1 + 4/3p_A^*$. We perform simulations for various initial conditions and find (Fig. 4.9a) three different states denoted by green, orange and blue colors, which we identify as 11, 12, and 22 states, respectively. We find four different transitions: $11 \rightarrow 12$, $12 \rightarrow 22$, $12 \rightarrow 11$, and $22 \rightarrow 12$. The solid lines show the mean field theory (MFT) prediction [Eqs. (4.1) and (4.2)] for the activity of network A. The good agreement shows that the mean field theory correctly captures all the properties of the system. We note that qualitative agreement between the MFT and the simulations is better for higher values of k , because for higher k the fluctuations are smaller, which improves the accuracy of the MFT. Figure 4.9.b shows the activity when moving along the red dashed line. Here we obtain four states and six different transitions.

The phase diagram of a system of $n = 2$ interacting networks (Fig. 4.8) is much richer than the phase diagram of a single network with damage and recovery [22]. The analytical results we presented here for $n = 2$ can be generalized to n interacting networks in any topological configuration, although as n increases they become increasingly difficult to visualize. In general, a system with n interacting networks can have up to 2^n physical states.

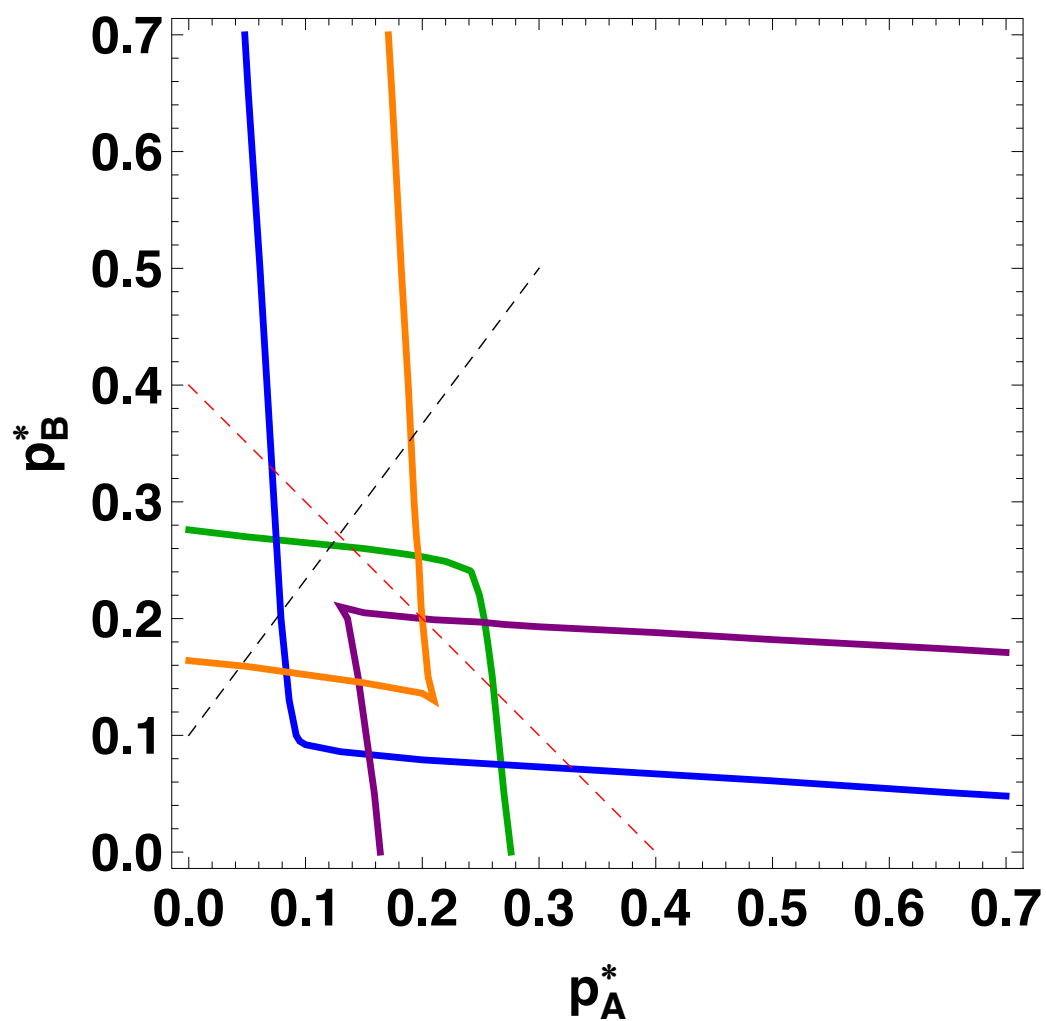


Figure 4.8: **Total phase diagram, with all four layers.** Solid lines represent the borders of region 11 (green), 22 (blue), 12 (orange) and 21 (purple). Dashed lines represent cross-sections where we calculate the activity profile, shown in Figure 4.9. Note that there is a small central “window” where all four states are possible.

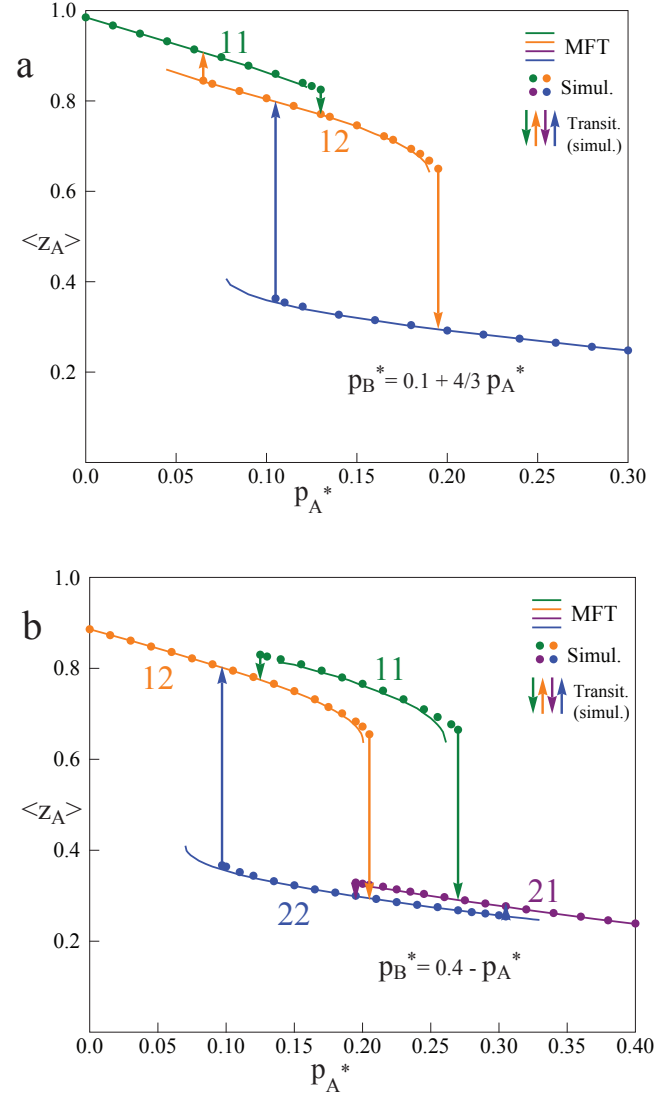


Figure 4.9: **States, transitions and hysteresis loops for two activity profiles.**

a) Activity z_A of network A, as measured in simulations (dots) and predicted by mean field theory (solid lines), along the cross section defined by the black dashed line in Fig 4.8. Parameters p_A^* and p_B^* are changed, preserving the relation $p_B^* = 0.1 + 4/3 p_A^*$. Transitions are denoted by arrows. **b)** Same for the cross section defined by $p_B^* = 0.4 - p_A^*$ (red dashed line in Fig. 4.8). Here we obtain 4 states and 6 different transitions, giving rise to more complex hysteresis loops. Network parameters in all cases are ($k=16$, $m=8$).

4.4.1 Additional phase diagrams

Figure 4.10a shows the collection of stable solutions (solid blue lines) and unstable solutions (dashed red lines) for the activity $z_A = 1 - a_A$ of network A, with parameter values as used in Fig. 4.1, but for a range of different values of p_A^* . The solid black line indicates $p_A^* = 0.16$, the value of p_A^* used in Fig 4.1. Green circles in this figure correspond to the stable states found in Fig 4.1, and red crosses correspond to the unstable solutions for z_A from Fig. 4.1. Figure 4.10b shows an analogous phase diagram for the parameters with values as in Fig 4.2, again for a range of p_A^* .

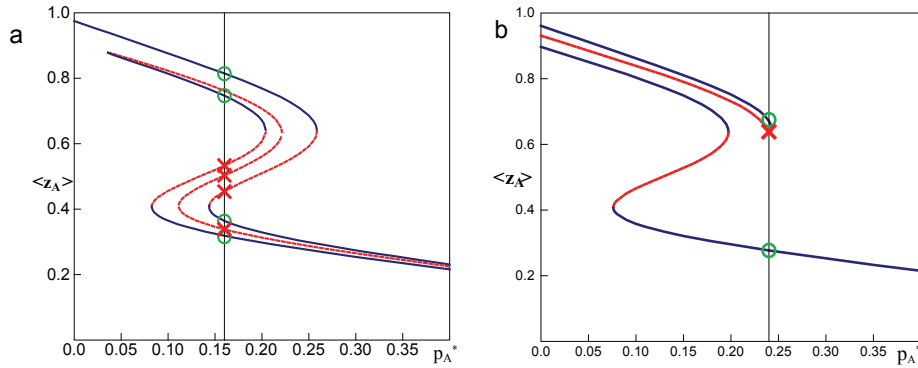


Figure 4.10: **Activity of network A versus internal failure rate.** **a)** Activity $z_A = 1 - a_A$ obtained by solving Eq. (4.1) and (4.2), for a range of p_A^* values, in a system of two interdependent networks ($k = 16$, $m = 8$). Blue lines correspond to stable physical states and red dotted lines represent unstable solutions. In Fig. 4.10a the same parameters as in Fig. 4.1 are used, except p_A^* which is not fixed but varied. When $p_A^* = 0.16$ (vertical black line) the corresponding values on the blue solid lines (green circles) match the graphical solutions in Fig 4.1 (also green circles). **b)** An analogous relationship holds between figures 4.2 and 4.10b, in which case two stable states exist.

4.4.2 Forbidden transitions

Transition lines for $12 \rightarrow 21$ and $21 \rightarrow 12$ do not appear in our phase diagram, and it is quite easy to understand why. Let us assume that the transition line for $12 \rightarrow 21$ does exist. To obtain that transition, the idea would be to simultaneously increase p_A^* and decrease p_B^* (i.e., increase the damage in one part of the system, and decrease in another part). Suppose we are in phase 12 and infinitesimally close to the supposed transition line. Considering the local geometry of this line, we may be able to observe its angle with respect to the p_A^* axis. If a transition occurs when increasing p_A^* and decreasing p_B^* , the tangent on the supposed line would have an angle of $\theta \in [0, \frac{\pi}{2}]$. From here it follows that by increasing p_A^* only, while keeping p_B^* constant, we would also make a transition (cross the transition line). The only other possibility would be that we were moving *along* the transition line, but this is easy to disprove because it would imply that the transition does not depend on p_A^* . If increasing p_A^* only, causes a transition, the transition must end in state 22, not 21. This is because if we only increase p_A^* , we increase damage to both network A (directly) and network B (indirectly, through the interdependent links).

Chapter 5

Optimal repairing strategies in interdependent networks

5.1 The problem of optimal repair

Knowing and understanding the phase diagram of interacting networks enable us to answer some fundamental and practical questions. A partially or completely collapsed system of $n \geq 2$ interacting networks in which some of them are in the low activity state is a scenario common in medicine, e.g., when diseases or traumas affect the human body and a few organs are simultaneously damaged and need to be treated, and the interaction between the organs is critical. It is also common in economics, when two or more coupled sectors of the economy [61] experience simultaneous problems, or when a few geographical clusters of countries experience economic difficulties. The practical question that arises is: What is the most efficient strategy to repair such a system? Many approaches are possible if resources are unlimited, but this is usually not the case and we would like to minimize the resources that we spend in the repairing process.

For simplicity, consider two interacting networks, both damaged (low activity). Is repairing both networks simultaneously the more efficient approach, or repairing

them one after the other? What is the minimum amount of repair needed to make the system fully functional again? In other words, what is the minimum number of nodes we need to repair in order to bring the system to the functional 11 (“up-up”) state, and how do we allocate repairs between the two networks? An optimal repairing strategy is essential when resources needed for repairing are limited or very expensive, when the time to repair the system is limited, or when the damage is still progressing through the system, threatening further collapse, and a quick and efficient intervention is needed.

5.2 Solution

We show that this problem is equivalent to finding the minimum Manhattan distance between the point in the phase diagram where the damaged system is currently situated, and the recovery transition lines to the 11 region. The Manhattan distance between two points is defined as the sum of absolute horizontal and vertical components of the vector connecting the points, with defined vertical and horizontal directions. It is a driving distance between two points in a rectangular grid of streets and avenues. In our phase diagram, it is equal to $|\Delta p_A^*| + |\Delta p_B^*|$. It turns out that two triple points of the phase diagram play a very important role in this fundamental problem. We find that these special points have a direct practical meaning and are not just a topological or thermodynamic curiosity.

To show this, we start by making some simplifying but reasonable assumptions. First, we assume that only internal failures can be repaired by human hands, since these failures are physical faults in nodes (any external and dependency failures and recoveries are “environmental,” and are a spontaneous recognition of the changing neighborhood of a node). We mentioned above that the parameters p_A^* and p_B^* correspond to fractions of internally failed nodes in networks A and B, respectively. This implies that the number of internally failed nodes repaired in, say, network A, is di-

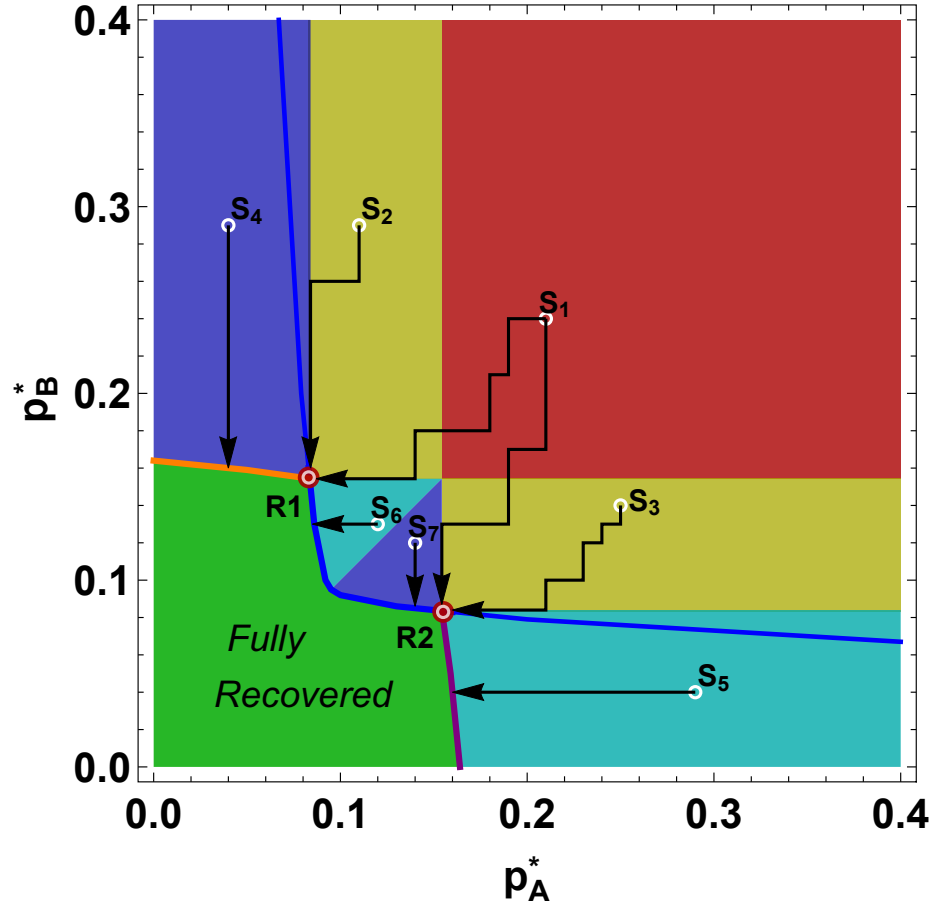


Figure 5.1: **Optimal repairing strategies.** The optimal repairing procedure (least expensive in terms of the number of individual node repairs) depends on the initial condition of the collapsed system. The total cost of repair is $|\Delta p_A^*| + |\Delta p_B^*|$ and the problem of optimal repairing translates into finding the minimal Manhattan distance from the point (in the phase diagram) where the collapsed system is initially situated (S_i) to the nearest border of the green region where it becomes fully functional. For a system having the initial condition within the red section (e.g. point S_1), there are two solutions: it is equally optimal to reach any of the two triple points R1 and R2 by decreasing p_A^* and p_B^* . For the systems starting in the yellow regions, it is optimal to reach only one triple point, R1, for the sector containing point S_2 , or R2 for the sector containing point S_3 . Starting in the dark blue regions it is optimal to decrease p_B^* only, i.e., repairing *only* network B. Similarly, in the light blue regions it is optimal to decrease p_A^* only. Triple points play a crucial role when both networks are initially significantly damaged (red and yellow regions).

rectly proportional to the change of p_A^* . Hence repairing nodes in networks A and B means decreasing p_A^* or p_B^* . We also assume that these repairs are done fast enough that there is only a small probability that the newly repaired nodes will internally fail again before the repair process is completed. The total number of repaired nodes is therefore $N_{\text{rep}} = N(|\Delta p_A^*| + |\Delta p_B^*|)$, and it is proportional to the Manhattan distance between the starting and final point in the phase diagram.

Figure 5.1 shows the solution to the minimization problem, and a detailed discussion is provided in the next section. The different colors in Fig. 5.1 correspond to the different optimal repair strategies, which depend on the failure state of the system. If the system is initially at point S_1 , both networks are in a low activity state, i.e., they are non-functional. Our goal is to decrease p_A^* and p_B^* and arrive to the region where the system is fully recovered (the green region) by performing a minimal number of repairs, i.e. minimal N_{rep} . We find that for any point in the red region there are actually two closest points in the green region, at an equal Manhattan distance away from the red region point. These two points are the triple points R1 and R2 shown in Fig. 5.1, which also correspond to the triple points in Fig. 4.4. Although R1 may be closer to point A than R2 by Euclidian distance, the Manhattan distance is the same. Thus two equally good repairing strategies are available. One involves allocating more node repairs to network A, and the other allocating more repairs to network B. For the yellow regions (points S_2 and S_3), the closest points by Manhattan distance are R1 (for point S_2) or R2 (for point S_3). Here only one triple point represents the optimal solution. Note that the path samples in Fig. 5.1 are “zig-zag” in shape (to highlight that we are minimizing $|\Delta p_A^*| + |\Delta p_B^*|$), but even when a diagonal path (direct straight line) to a triple point is used, the Manhattan distance is the same. For the dark blue regions (points S_4 and S_7), the optimal strategy is to decrease p_B^* only, until the system is recovered. Similarly, for the light blue regions (points S_5 and S_6), the optimal strategy is to decrease only p_A^* .

5.3 Optimizing the Manhattan distance

The optimal strategies shown in different colors in Fig. 5.1 are derived from the geometrical reasoning shown in Fig. 5.2. To optimize repairing we need to minimize $N_{\text{rep}} = N(|\Delta p_A^*| + |\Delta p_B^*|)$. Figure 5.2 shows a plot of a series of curves consisting of points at identical Manhattan distances from point S_1 (equidistant curves). They produce a “diamond” shape, and the minimal Manhattan distance between point S_1 and the green region translates into the task of “fitting” the diamond so that it just touches the green region and its center is at S_1 . The diamond in Fig. 5.2a touches the green region at two points—triple points, which are the solution to the minimisation problem. Figure 5.2b shows the solution for point S_6 in the light blue region. Here the solution suggests a different strategy—decreasing only p_A^* .

5.4 Maintaining the functionality

In this subsection we do additional considerations of the functionality after the initial “awaking” of the system due to the positive shock, in which triple points play major role. Notice that after the initial successful repair (targeted repairing of individual nodes), described in the previous subsection, if the repair not sustained, will lead the system to relax back to point S_1 of Figure 5.1. Thus, we conclude that after the initial positive “shock”, during which the system is awoken, it is still necessary for the system to remain within the region limited by the green line in Figure 4.8. If point S_1 is situated within the region limited by this line (which is much broader than the green region in Figure 5.1 - for this choice of numerical parameters it is about four times larger by area), then no additional intervention is needed. However, if initial point S_1 is outside of that region, then a subsequent constant repair is needed to keep the system within the green region of Figure 4.8. Best strategy for this repair is sketched in Figure 5.3: for systems initially within the red region of Figure 5.3

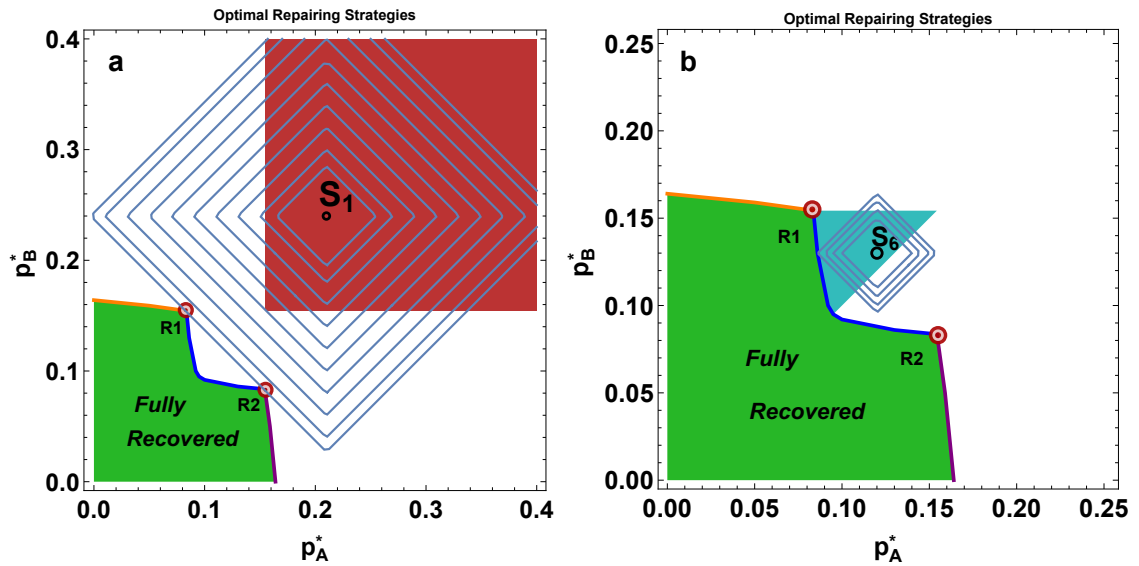


Figure 5.2: **Minimum Manhattan distance problem, in two examples.** **a** Finding the minimum Manhattan distance between point S_1 in the red sector and the green region where the system is fully functional. Equidistant curves are plotted in gray and form a “diamond” shape. The largest “diamond” barely touching the green region and having its center at point S_1 , suggests there are two equally optimal solutions to the minimization problem - points R1 and R2. **b** The same geometrical construction for point S_6 in the light blue region, suggests a unique solution: decreasing p_A^* .

additional repair should bring the system to point T; otherwise if in the blue region repair should simply decrease p_A^* (for the "right" blue region) or p_B^* (for the "upper" blue region).

Therefore, our conclusion is that, in order to truly repair the system, the optimal repairing procedure should consist of two steps: a) initial shock that will "awake" the network (bring it to the green region of Figure 5.1, and then b) if needed, increasing the repair rate to keep the system within the boundaries of green line of Figure 4.8. Step b) is not needed if initial filed state S1 is already within the green line region in Figure 5.1.

5.5 Conclusion

From our optimal repairing strategy analysis we find that the order of repair (the specific path taken between the initial point and final point) does not affect the final result. Minimizing the Manhattan distance only determines the optimal destination point. Therefore, there is actually a set of paths corresponding to equally optimal repairing processes. However, if we value early partial results during the repair process (for example, if we appreciate to have one of the networks repaired as quickly as possible), the definition of "optimal" may be further restricted, and it may be optimal to choose those paths from the set of optimal paths, that allow the quick recovery of subsystems, i.e., individual networks.

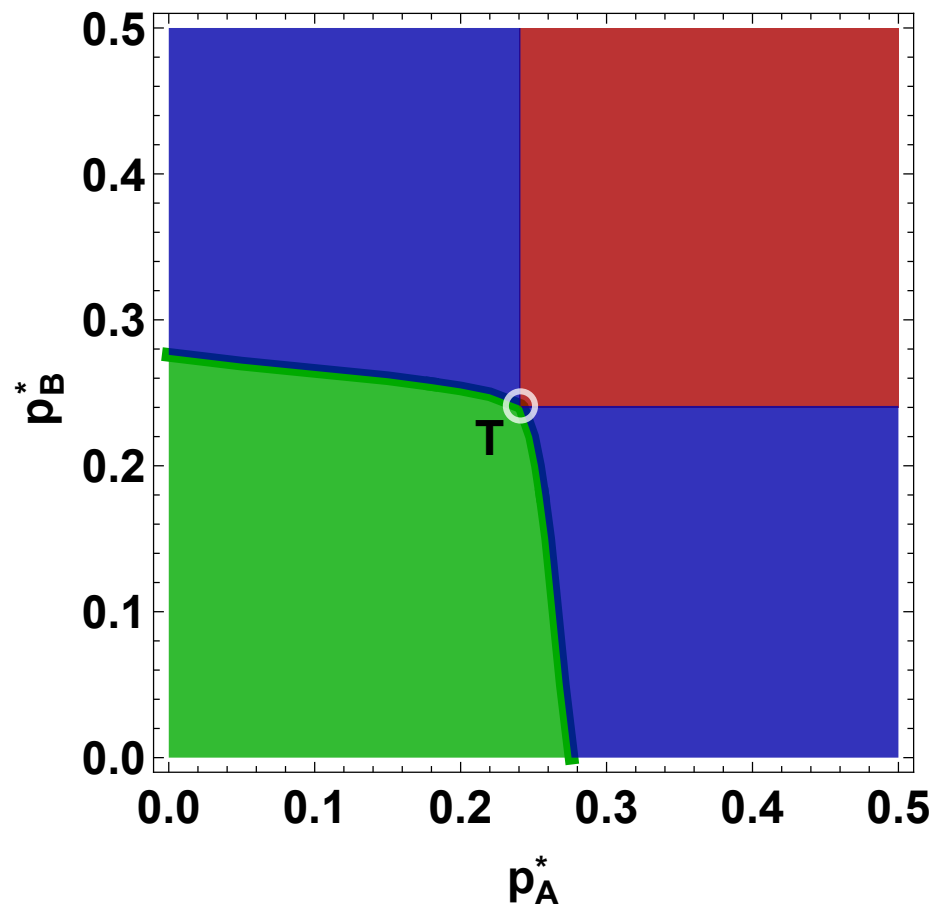


Figure 5.3: **Subsequent maintenance.** Depending on the the initial state, additional repairing support should be provided to the system to be functional after it has beed awaked with a positive shock discused in Figure 5.1. Optimal strategy for the red region is bringing the system to point T, and for blue regions it is decreasing p_A^* only (for the "right" blue region) or p_B^* only (for the "upper" blue region).

Chapter 6

Dynamics of real interdependent networks

6.1 Finite size phenomena

In relatively small networks ($N \approx 10\text{--}1000$) fluctuations are very large. Thus, in small network systems exhibiting multistability it is possible to observe phase flipping [22, 25, 76] between different states. Figure 6.1 shows the fraction of active nodes for both networks, in time, for a symmetric choice of parameters, $p_A^* = p_B^* = 0.21$, $r_A = r_B = 0.60$, and $r_d = 0.15$, when each network has only $N = 100$ nodes. Large fluctuations cause the system to jump between the different states allowed for this set of parameters. Note that interdependent links cause the two networks to have partially dependent and correlated dynamics. Very often a transition in one network triggers a transition in the other. In Figure 6.1 we can identify examples of all four global states: 22, 11, 21 and 12. For example, at time $t \approx 400$ both networks are in the high activity state (11), while at $t \approx 620$ network A is in the low activity and network B in the high activity state (21).

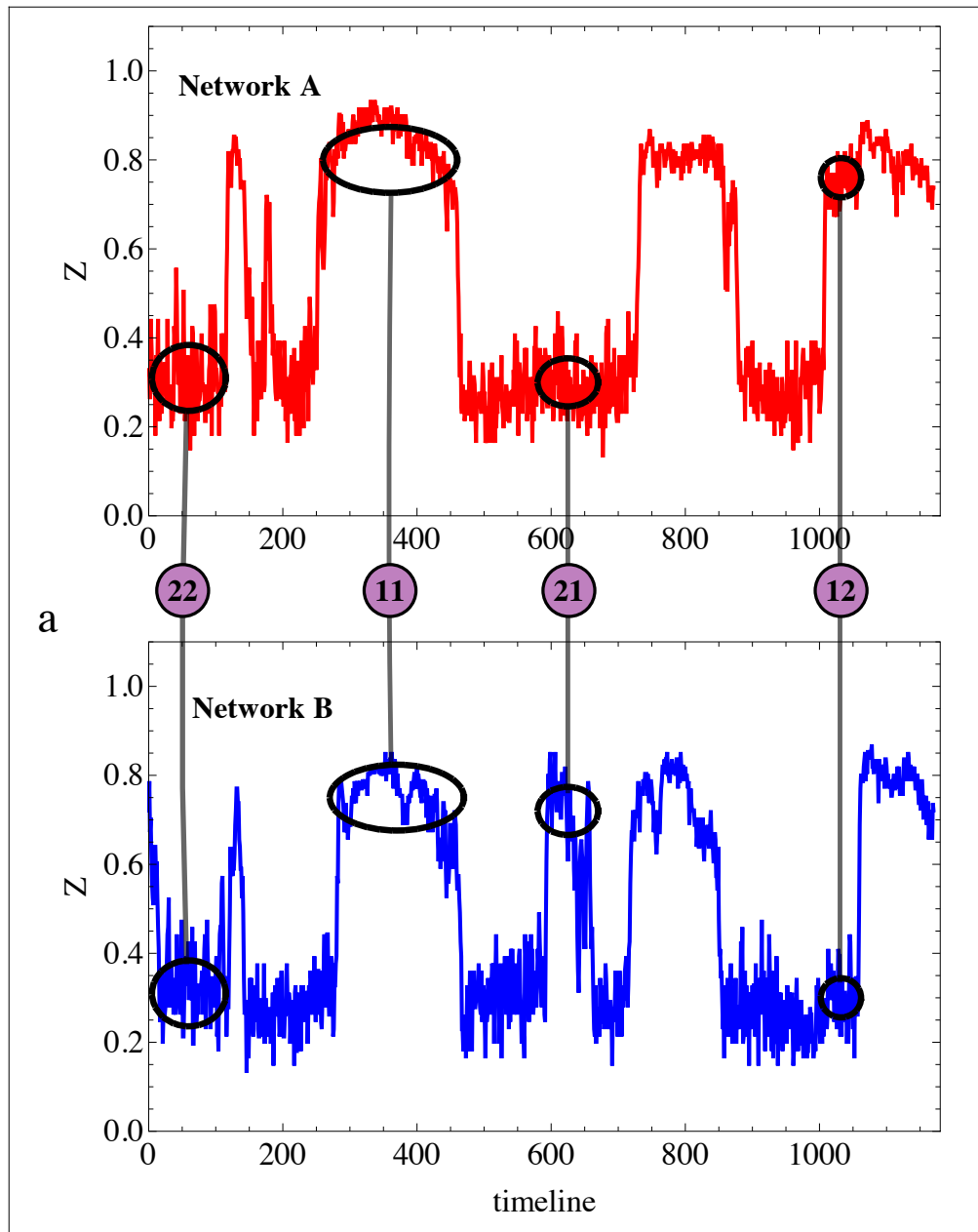


Figure 6.1: **Collective dynamics in simulated interacting networks.** Simulation of the networks' dynamics, activity versus time, for $N = 100$ and failure parameters $p_A^* = p_B^* = 0.21$, $r_A = r_B = 0.60$, $r_d = 0.15$, shows the switching of the system between four different states. We can easily identify four collective states - 11, 22, 12, and 21.

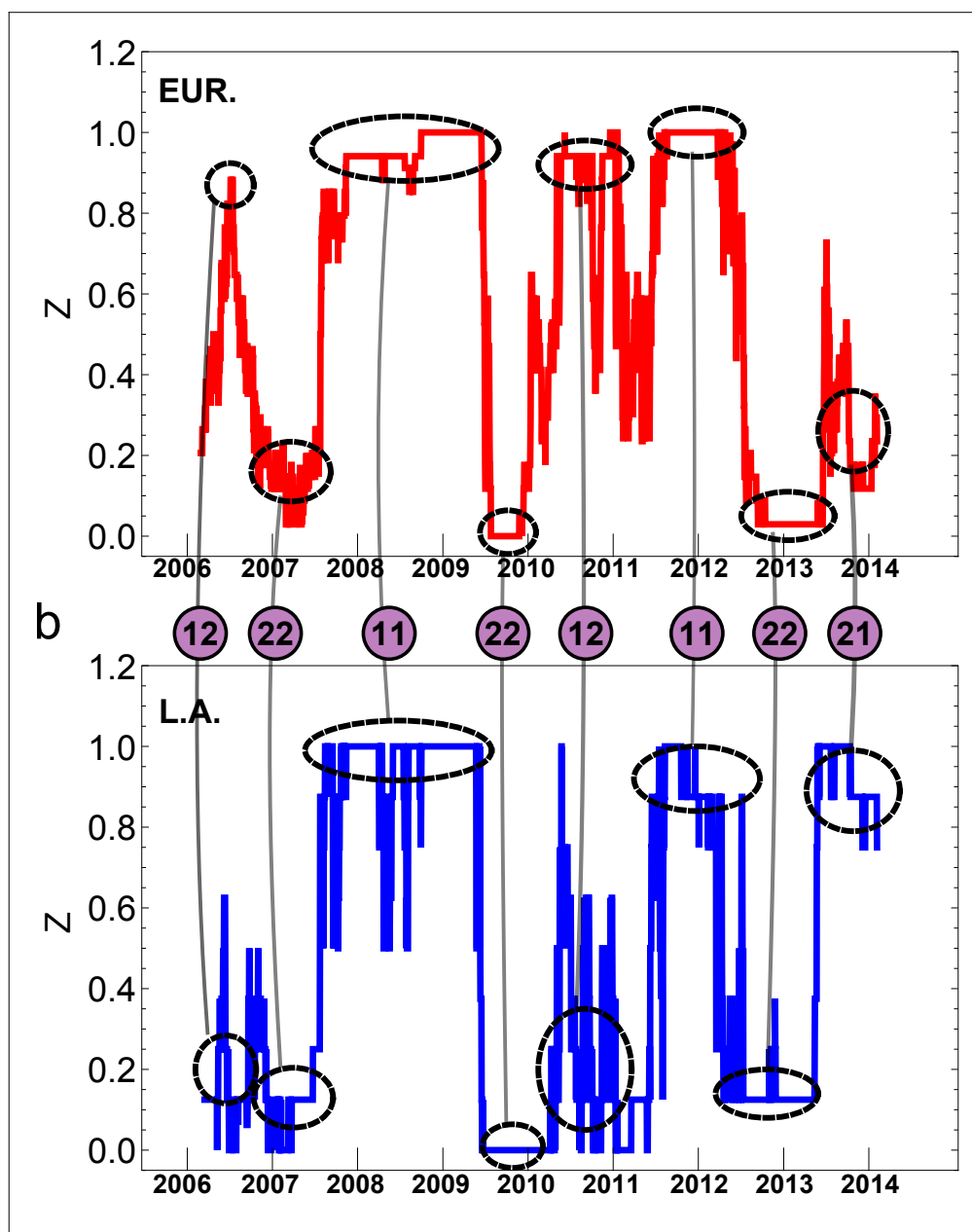


Figure 6.2: **Collective dynamics in real interacting networks.** Dynamics of two CDS geographical networks consisting of 17 European and 8 Latin American countries, showing very similar behavior: individual networks switching between well defined high activity and low activity states, as well as correlated collective behavior of the two networks in interaction. We identify collective states 11, 22, 12 and 21 and mark them with connected black ovals. Note that since the CDS value grows with risk, a higher activity in a CDS network corresponds to bad economic news.

6.2 Empirical example: Credit default swap networks

Because many real-world interacting network systems have a small number of nodes, in those systems we can potentially uncover dynamics similar to what we observe in our model networks. As an example of a real system, we investigate the interacting sovereign 5-year CDS (*5-year credit default swap*) system, consisting of 25 European Union and Latin American countries (see Appendix B for the full list of countries) that began to issue the CDSs from 2005. We divide countries into two groups on a geographical basis: 8 countries belong to the Latin American group, and 17 belong to the EU group. Sovereign CDSs are financial instruments, for which the value reflects the probability that the reference country will default on its debts. Each country has a CDS value assigned, and this value changes in time reflecting the economic news about this country and the perceived risk of default, which results in a time series that we can observe. CDSs are highly sensitive to important economic news, positive or negative. There is also a significant contagion and influence between the countries, especially between those with strong economic ties, which is reflected in the correlation between their CDSs. These characteristics make the CDS signals a candidate for modeling using our interacting network approach.

We can draw a parallel between the CDS system and our model network if we assume that each country (with its associated CDS signal) can be represented as a node, which has connections (links) to other countries within its own geographical region, as well as ties with countries from another continent. In this case, we might expect that random and independent bad (or good) economic news appearing in any given country have behavior similar to random internal processes in nodes in our artificial model (random internal failures/recoveries). When economic problems in one country propagate to a neighboring country within the same geographical region, the process resembles the external failures in our artificial model, while interaction

between countries from different continents may be modelled by the interdependent links from our network model. For the CDS network system we also suppose that the fractional definition for the threshold (m_{frac}) is somewhat more natural than the absolute definition, as it is less dependent on the country size or its importance, i.e., the number of links a country has to other countries.

We study the international CDS system during the period between June 2005, the earliest date when CDSs traded for all countries, and February 2014. We apply the network model to it as follows. We represent each country with one node that can have two states: active or failed. Because the raw CDS values are continuous by nature, and our model uses binary node states (up or down), we perform a trend mapping procedure to form a binary signal (0 or 1) for each country. In particular, for each time t , we consider the interval $[t - 252, t]$ of 252 business days (the usual number of business days in a year). If the CDS value of a country has a net increase during that period, we consider the node of the country to be active at t (state = 1). If it does not, it is inactive (state = 0). Having individual binary signals for each country, we can calculate the average activity $0 \leq z(t) \leq 1$ for both EU and Latin American networks. The resulting time series for EU and LA activities are shown in Figure 6.2. First, we note that the two geographical networks spend most of time having either a significantly high activity or significantly low activity (i.e., there is an indication for two well-defined single-network states). We confirm this by measuring the frequency distribution of network activities, Figs. 6.3a and 6.3b, which exhibit a strong bimodality in z . The CDS network system in Fig. 6.2 shows rapid transitions between the high and low activity states, much like the artificial network system in Fig. 6.1. Figure 6.4 shows the calculated correlations between binary signals of pairs of individual nodes. The correlation matrix reveals two strongly correlated blocks, which we identify as Latin American block (numbers 1-8) and EU block (numbers 9-25).

In Fig. 6.2 we also observe that the two networks sometimes make transitions

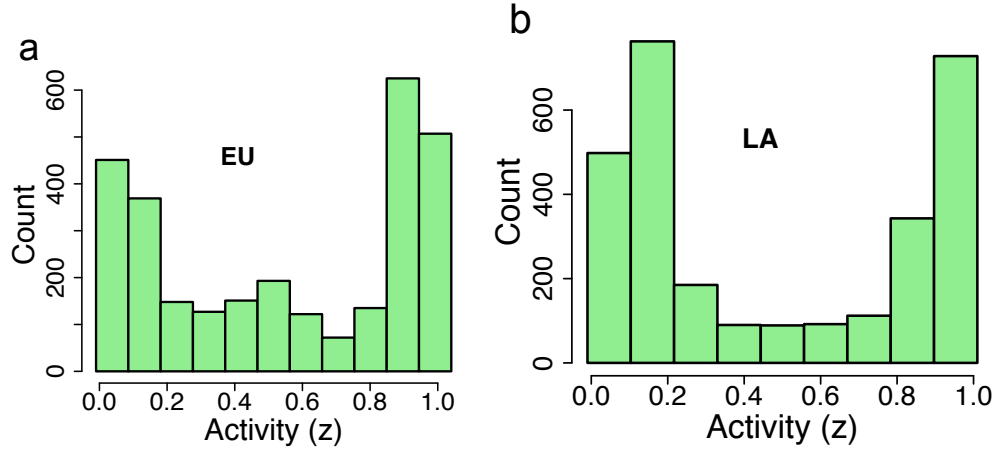


Figure 6.3: **Density plots for the activity of real networks.** **a** Activity density plot for the EU network reveals bimodality, an indication of the existence of two states. **b** Same for the LA network.

simultaneously, but not always. This behavior also resembles the behavior observed in the artificial networks in Fig. 6.1.

Finally, we find that it is possible to estimate numerical values for all the model parameters of this real system (internal p_{EU}^* , p_{LA}^* , external $m_{\text{frac,EU}}$, $m_{\text{frac,LA}}$, r_{EU} , r_{LA} , interdependent r_d) from the data. The basic idea is that for each parameter we identify an *observation experiment* in which this particular parameter dominates, enabling us to effectively isolate individual parameters from the noise of many others. For example, when both networks (EU and LA) are in the high activity phase, most of the failures are in fact internal failures. This allows us to almost directly estimate p_{EU}^* and p_{LA}^* from Fig. 6.2, by observing $p_{\text{EU}}^* = 1 - \langle z_{\text{EU}} \rangle$ and $p_{\text{LA}}^* = 1 - \langle z_{\text{LA}} \rangle$. External failures are most significant when a network is in a low activity state. Interdependent parameter r_d can be estimated by studying the correlation between $z_{\text{EU}}(t)$ and $z_{\text{LA}}(t)$, as this is an increasing function of r_d . Threshold parameters $m_{\text{frac,EU}}$ and $m_{\text{frac,LA}}$ can be estimated by exploiting the fact that they most significantly determine the fraction of time that each network spends in the high, or low, activity states. We describe in detail our procedures for numerically estimating these model parameters

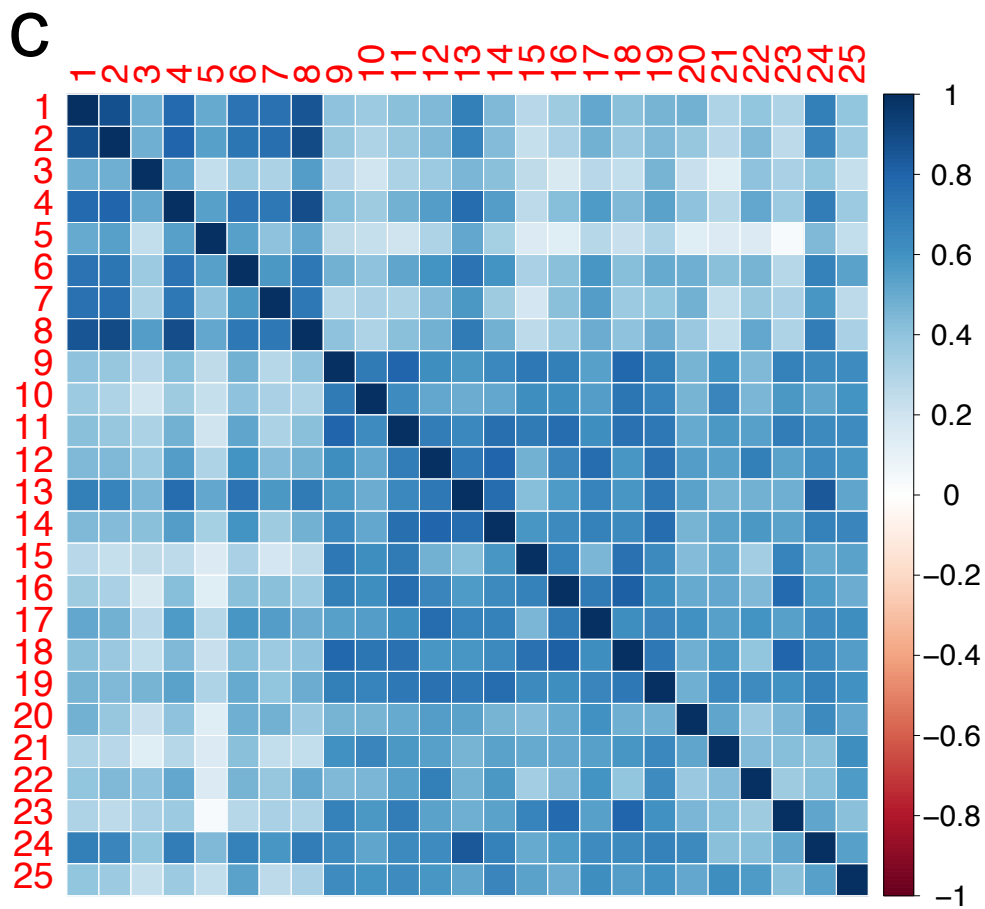


Figure 6.4: **Correlation between individual CDS signals.** Correlation matrix of binary CDS signals with the EU (1-8) and LA (9-25) block. Separation into blocks reinforces our initial decision to sort the countries by geographic location.

in section 6.5. Our dynamical network model also independently predicts that the typical fluctuation size of $z(t)$ is not uniform for all values of z , but has a spike around $z \approx \frac{1}{2}$. We observe this phenomenon in both our simulations and the real network dynamics (section 6.6).

6.3 Applying the model to the CDS network: Outline

There are two steps in applying our model to the system of binary CDS signals: 1) *building the network* (choosing the rules for connecting the nodes), and 2) *estimating model parameters* (for internal failures: p_A^* , p_B^* , for external failures: $m_{frac,A}$, $m_{frac,B}$, r_A , r_B , and for the interdependent interaction: r_d) which are the core of our model. We first make reasonable assumptions to model the structure of the links. We then show that we are capable of estimating – based on the real records – all of the model parameters, by analyzing the situations in which one of these parameters dominates the dynamics of the system.

6.4 Building the CDS network

Because the CDS system is a symbolic network, we have a certain freedom in modelling the links connecting the countries. First, we make few assumptions. We assume that LA and EU countries are each represented by a network, one with $N_{LA} = 8$ nodes and the other with $N_{EU} = 17$ nodes. We make a simplifying assumption that both have the same average degree $\langle k \rangle$, which we do not fix: we vary it and investigate how it affects the estimates of dynamics parameters. We assume a probabilistic rule for the links: the probability that there is a link between two nodes within the same

network is *proportional to the correlation coefficient* between the nodes taken from the correlation matrix in Fig. 6.4. Because the total number of links per network is fixed to $\langle k \rangle \frac{N}{2}$, and the links are probabilistic, this results in many possible physical realizations for each network. We run simulations for a large sample of such network realizations, with the same parameters, and average over the ensemble. During each simulation, the links do not change. For the interdependent links we assume that every node in both the LA and EU networks has at least one interdependent link, but some nodes can have more than one (because $N_{LA} \neq N_{EU}$ it is not possible to have one-to-one interdependency). Here we also apply the probabilistic rule: the probability that there is an interdependent link between a node in EU and a node in LA is proportional to the associated matrix element in the correlation matrix in Fig. 6.4. There is a degree of freedom for the total number (L) of interdependent links between the two networks: we do not fix this value but investigate how various quantities depend on the range of reasonable values of L .

6.5 Measuring and estimating model parameters

We find that it is possible to estimate from the data all the model parameters (internal p_{EU}^* , p_{LA}^* , external $m_{\text{frac},EU}$, $m_{\text{frac},LA}$, r_{EU} , r_{LA} , interdependent r_d), using quite simple and reasonable arguments. For each parameter, we identify an *observation experiment*, a part of the dynamics, or a phenomenon, in which this particular parameter dominates. This method enables us to effectively isolate individual parameters from the noise of many others. Below we outline our procedure.

6.5.1 Estimating internal parameters (p_{EU}^* , p_{LA}^*): observing high activity states

When both networks (EU and LA) are in the high activity phase, most of the failures are in fact *internal failures*. In Fig. 6.1 for example, only about 3% of the failures observed during the high activity are external failures, because there is a small chance for having a critically damaged neighborhood when z is very high. The contribution from interdependent failures when both networks have high activity is also rather small (of the order of $(1 - z)r_d$, where both $(1 - z)$ and r_d are small). This allows us to almost directly estimate p_{EU}^* and p_{LA}^* from the real records, because with only internal failures present we know that $\langle z \rangle = 1 - p^*$, so $p_{\text{EU}}^* = 1 - \langle z_{\text{EU}} \rangle$ and $p_{\text{LA}}^* = 1 - \langle z_{\text{LA}} \rangle$. By measuring the average $\langle z_{\text{EU}} \rangle$ and $\langle z_{\text{LA}} \rangle$ for the times when both networks are highly active (such as when $z_{\text{EU}} > 1/2$ and $z_{\text{LA}} > 1/2$ - an example of a time interval with that condition is colored in red in Fig 6.5), we get estimates $p_{\text{EU}}^* = 0.07 \pm 0.01$ and $p_{\text{LA}}^* = 0.11 \pm 0.02$.

6.5.2 Alternative measurement of the internal parameters: micro-dynamics

Alternatively, by observing the network on the micro level, i.e. observing the dynamics of individual nodes, it is also possible to measure the average internal time of recovery, τ_{EU} and τ_{LA} , the crude failure rates p_{EU} and p_{LA} , and to verify the previously measured p_{EU}^* and p_{LA}^* in an alternative way. Figure 6.6 shows an example of the Columbia signal (red) for a fraction of time between November 2006 and March 2007, when the activity of both LA and EU networks was in the upper half ($z_{\text{EU}} > 1/2$, $z_{\text{LA}} > 1/2$). By measuring *how long* a country (node) stays in the

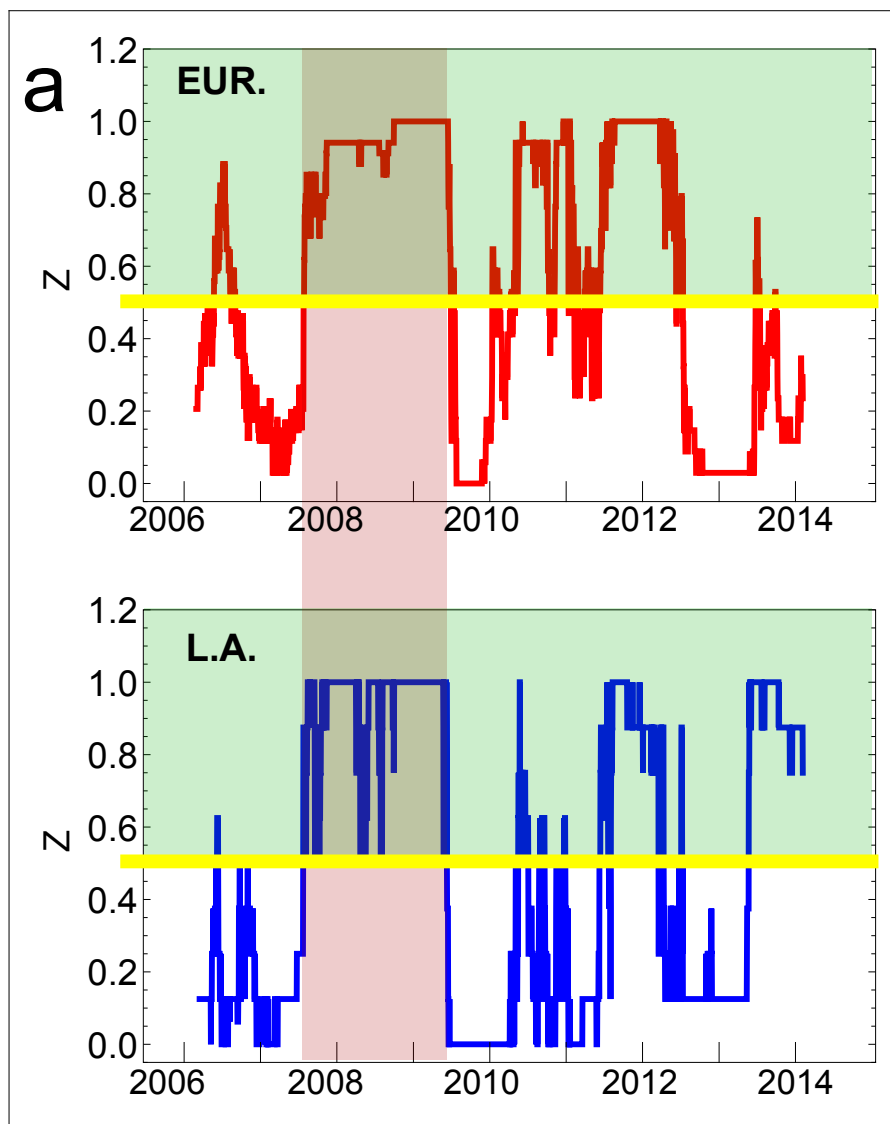


Figure 6.5: **Quantifying the CDS network and estimating model parameters.** Estimating p_A^* and p_B^* by observing intervals in which both networks have high activity ($z \geq \frac{1}{2}$). The region of interest (above $z = \frac{1}{2}$, yellow line) is colored in green, with an example interval in red.

0 state each time it fails under these conditions, and measuring *how often* it fails, we can estimate its mean recovery time and the crude failure rate. We find the average values for the EU countries to be $\tau_{\text{EU}} = 13 \pm 2$, $p_{\text{EU}} = (3.0 \pm 0.5) * 10^{-3}$ and $p_{\text{EU}}^* = 0.07 \pm 0.01$ (same as before). For LA countries we find the average values of $\tau_{\text{LA}} = 9 \pm 1$, $p_{\text{LA}} = (7.6 \pm 0.8) * 10^{-3}$ and $p_{\text{LA}}^* = 0.11 \pm 0.02$ (same as before). Note that because for any nonlinear function f and random variable x , the expectation $E(f(x)) \neq f(E(x))$, we have $\langle p^* \rangle \neq 1 - \exp(-\langle p \rangle \langle \tau \rangle)$.

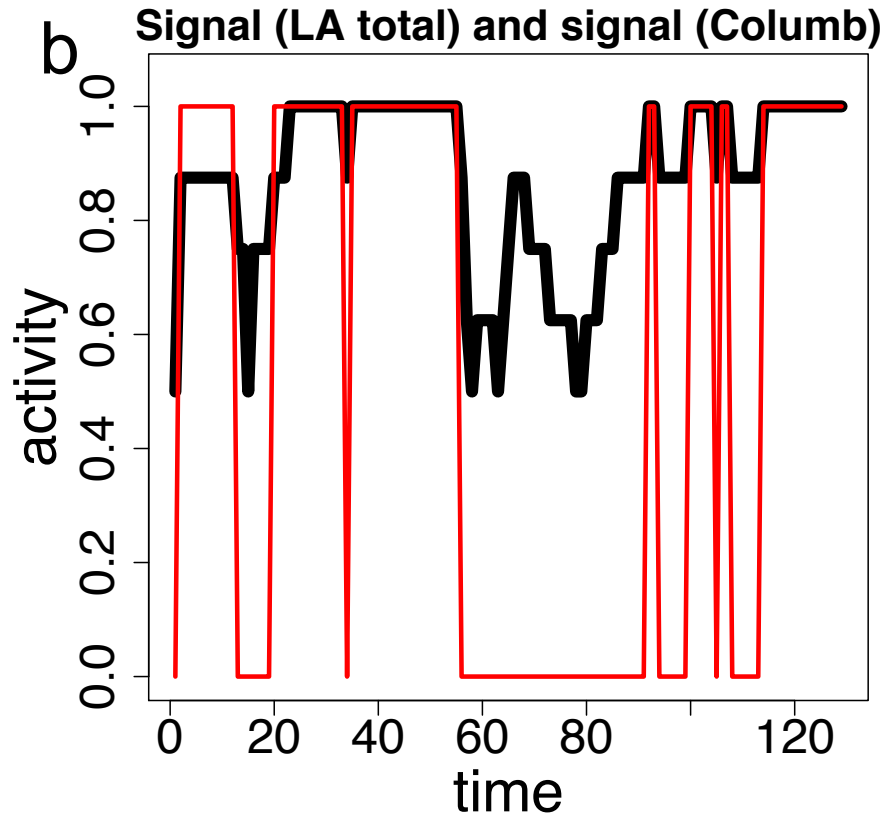


Figure 6.6: **Alternative method of estimation of the internal failure rate.** Dynamics of an individual binary signal (Columbia), when the LA network is in the high activity state ($z_{\text{LA}} \geq \frac{1}{2}$).

6.5.3 Estimating the external parameters r_{EU} and r_{LA} : observing low activity states

When both networks are in the low activity state (low values of z for EU and LA), external failures dominate. Internal failures are present all the time, but they are known as we have already estimated the internal failure parameters. To get a first estimate of r_{EU} and r_{LA} , we will neglect the interdependent failures temporarily, which are also present but much weaker than external failures, and assume that the networks are weakly coupled (when we later estimate the value of r_d , we will get a small correction for the values of r_{EU} and r_{LA}). Also, luckily, for low values of z , and if m_{frac} has a reasonable value (not too close to 0, and not too close to 1, which is always satisfied by requiring the existence of two states per network - values of m_{frac} too close to 0 or 1 lead to single states), nearly every node has a critically damaged neighborhood, so the dependence on m_{frac} vanishes and in this case the value of $\langle z \rangle$ is almost independent on the threshold m_{frac} . Indeed, our simulations confirm that the positions of the network stable states (which in the thermodynamic limit coincide with $\langle z_{\text{low}} \rangle$ and $\langle z_{\text{high}} \rangle$) do not depend much on m_{frac} . The parameter m_{frac} however strongly determines the amount of time a network spends in the upper state, as opposed to the lower state, but it has little influence on the position of those states. Because of the structure of function $F(1 - z; m_{\text{frac}}) \approx \theta(1 - z - m_{\text{frac}})$ in Eq. (1) and (2), which behaves similarly to the Heaviside step function θ , the influence of m_{frac} on the dynamics is strongest when $1 - z(t)$ is close to m_{frac} . However this is rare when the system is in the low or high activity states where it spends most of its time; medium values of z are usually achieved when the system makes a transition which lasts shortly and does not contribute much to $\langle z \rangle$. Appreciating these simplifications, the equation that connects the average fraction of failed nodes with the internal and external parameters becomes $1 - \langle z_i \rangle = p_i^* + r_i - p_i^* r_i$ (where $i = \{\text{EU}, \text{LA}\}$), with r_i as

the only unknown. By measuring $\langle z_i \rangle$ in the low states ($z_{\text{EU}} < 1/2$ & $z_{\text{LA}} < 1/2$) and already knowing p_i^* , we obtain estimates $r_{\text{EU}} = 0.81 \pm 0.03$ and $r_{\text{LA}} = 0.88 \pm 0.03$.

6.5.4 Estimating the thresholds $m_{\text{frac,EU}}$ and $m_{\text{frac,LA}}$: visiting times

If we picture the two states per network (low and high) as a double well, then the parameter m_{frac} through the function $F(z; m_{\text{frac}})$ controls the position and the shape of the potential barrier between the wells, and m_{frac} dominates in determining the total fraction of time that each network spends in the upper, or lower, state. Higher values of m_{frac} lead to the network spending more time in the low activity state, and vice versa. This is another useful observation, which allows us to estimate the values of $m_{\text{frac,EU}}$ and $m_{\text{frac,LA}}$ from the real data. In Figure 6.2, both networks spend approximately half of their time in the high activity state or $z \geq 1/2$ (precisely, EU - 53%, LA - 47%). By simulating decoupled ($r_d = 0$) EU and LA networks using previously measured parameters ($p_{\text{EU}}^*, p_{\text{LA}}^*, \tau_{\text{EU}}, \tau_{\text{LA}}, r_{\text{EU}}, r_{\text{LA}}$), and requiring that the networks spend roughly 50% of time in each state, we are able to get first estimates for the thresholds. We find that they slightly depend on the choice of $\langle k \rangle$, ranging from $m_{\text{frac,EU}} = 0.57 \pm 0.02$ and $m_{\text{frac,LA}} = 0.50 \pm 0.02$ for $\langle k \rangle = 3$, to $m_{\text{frac,EU}} = 0.59 \pm 0.02$ and $m_{\text{frac,LA}} = 0.50 \pm 0.02$ for $\langle k \rangle = 7$ ($\langle k \rangle$ is limited by the number of nodes in the smaller network to a maximum of 7). Later, after we estimate r_d , we will get small corrections for $m_{\text{frac,EU}}$ and $m_{\text{frac,LA}}$ by simulating the networks with a nonzero value of r_d .

6.5.5 Estimating r_d : correlation between networks EU and LA

The parameter r_d represents the interaction strength of the interdependent nodes in the two networks. If r_d were zero, the two networks would have perfectly independent dynamics. On the other extreme, if $r_d = 1$ we would expect the two networks to have extremely correlated dynamics. Thus, studying the correlation between $z_{\text{EU}}(t)$ and $z_{\text{LA}}(t)$ represents a natural way for estimating the interaction parameter r_d . The correlation between the two real signals in Fig. 6.2 has the value of 0.61. The idea for measuring r_d is straightforward: By simulating an artificial interacting network system, using our estimated numerical values for all other parameters (p_{EU}^* , p_{LA}^* , r_{EU} , r_{LA} , etc.), we can determine which value of r_d yields the target correlation of ≈ 0.61 between the two network activity signals. We find that the value of r_d that achieves this is affected somewhat by the structure of the network. Table 6.1, Column #6 shows the values of r_d that we obtain for a range of values of $\langle k \rangle$ (average degree) and $L = 30$ interdependent links. Thus our estimate for r_d is in the range 0.10–0.16, and it is higher for smaller $\langle k \rangle$. A possible explanation is that for small values of $\langle k \rangle$, nodes have fewer neighbors, intensifying the fluctuations in the rate of external failures (we confirmed this in simulations), which increases the noise of $z(t)$ for each network. This noise component intrinsic to each network lowers the correlation between the two network signals, and a higher value of r_d is needed to compensate. Finally, by varying the total number of interdependent links L between 30 and 70, we find that the optimal r_d is only slightly affected by the value of L (as long as every node has at least one interdependent link): high values of L lower the estimate for r_d by approximately 0.01. If we relax the constraint that each node has at least one interdependent link and allow for nodes without interdependent links, this increases the estimate for r_d ; some nodes are not engaged in the interaction with the other

network, which weakens the interaction between the two networks, and a higher r_d is needed to compensate. In this case an *effective* r_d (a product of r_d and the fraction of nodes having at least one interdependent link) is approximately invariant with respect to L .

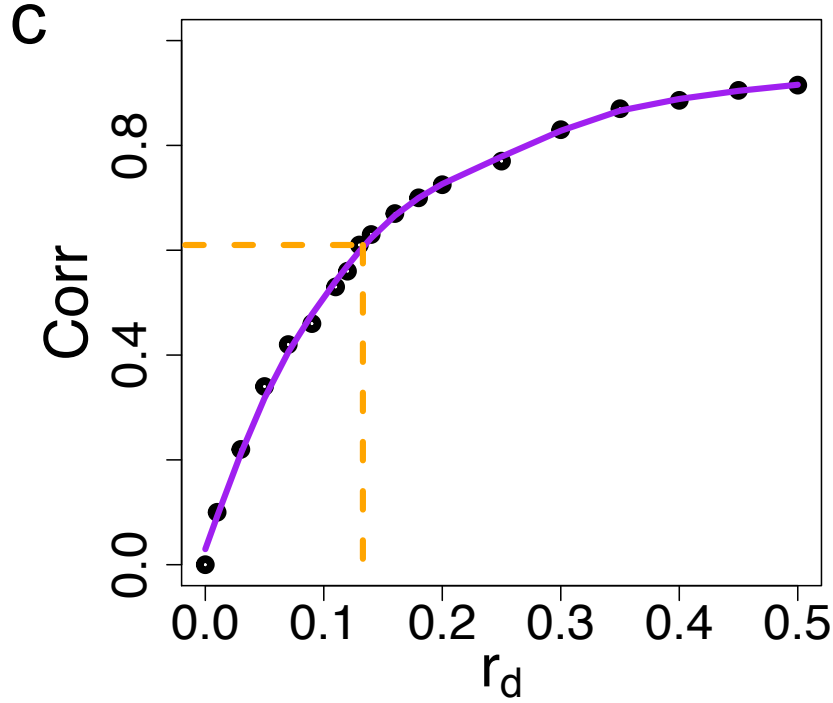


Figure 6.7: **Estimating the numerical value of interdependency parameter.** Matching the value of r_d for $Corr = 0.61$: correlation between the signals of two artificial networks with $N_A = N_{EU} = 17$ and $N_B = N_{LA} = 8$ nodes, for different values of r_d , with other parameters fixed to the values from $\langle k \rangle = 5$ row in Table 6.1.

Once we have estimated r_d , we can correct our initial estimates for r_{EU} and r_{LA} in the estimation method #3 above, where we had initially neglected the contribution from interdependent failures. Simulating the dynamics with a nonzero r_d also gives a correction to our initial estimates for $m_{frac,EU}$ and $m_{frac,LA}$. Corrections for all

parameters are quite small, and the final values of r_{EU} , r_{LA} , $m_{frac,EU}$ and $m_{frac,LA}$ are shown in Table 6.1, which also shows that the estimates slightly depend on $\langle k \rangle$. Figure 6.7 presents an example of an actual measurement of the correlation between the two artificial network signals as a function of r_d , using numerical values from Table 1 for $\langle k \rangle = 5$ and $L = 30$. The dashed orange line indicates the correlation target value of 0.61.

The estimate of r_d and the corrections to other parameters complete our estimation for the model parameters using the real CDS records. Figure 6.8a shows a typical outcome of the artificial network simulation using numerical values from Table 6.1, for the $\langle k \rangle = 5$ row. Figures 6.8b-c show the frequency distribution histograms of the signals simulated with the $\langle k \rangle = 5$ row data, but with much longer simulation time for better statistics.

$\langle k \rangle$	$m_{frac,EU}$	$m_{frac,LA}$	r_{EU}	r_{LA}	r_d
3	0.55	0.43-0.49	0.78	0.87	0.16
4	0.55	0.43-0.49	0.79	0.87	0.14
5	0.57	0.43-0.49	0.79	0.87	0.13
6	0.57	0.43-0.49	0.79	0.87	0.11
7	0.57	0.43-0.49	0.79	0.87	0.10

Table 6.1: **Numerical estimates for the model parameters.** Using the "isolation method" we find limits on the numerical values of the model parameters. These observation experiments allow us to gauge the strength of various effects in real world systems. Here we confirm experimental accessibility of all of the model parameters. Note that values for r_d are rather small - this is expected as discussed in the text.

6.6 Similarity in fluctuation size structure

Our dynamical network model predicts that the typical fluctuation size of $z(t)$ is not uniform for all values of z . Supplementary Figures 6.9a and 6.9b show the average squared fluctuation $\langle [z(t) - z(t-1)]^2 \rangle$ of the activity signal as a function of z , for artificial networks A and B ($N_A = 17$, $N_B = 8$, for the parameters from Table 6.1, row $\langle k \rangle = 5$). The average fluctuation size shows a spike around $z \approx \frac{1}{2}$. This is a reminiscent of a critical phenomenon, since $z \approx \frac{1}{2}$ is the critical value of z below which the system is attracted to the lower single-network state, and above which it is attracted to the higher state. This behavior is best visualized by imagining a double well, where the single-network states (z_{low} and z_{high}) correspond to two wells, separated by a barrier where the top of the barrier corresponds to $z \approx \frac{1}{2}$. This is especially clear in simulations with large networks ($N > 10000$) where, depending on the initial condition, the system relaxes to either the higher state (if the initial z is above the critical value), or to the lower state (if the initial z is below the critical value). We analyze the two real CDS networks (EU and LA) and find that they also show a strong spike in average fluctuation size as a function of z (Fig. 6.9c-d), with the maximum at approximately the same position as in their artificial network counterparts ($z \approx \frac{1}{2}$).

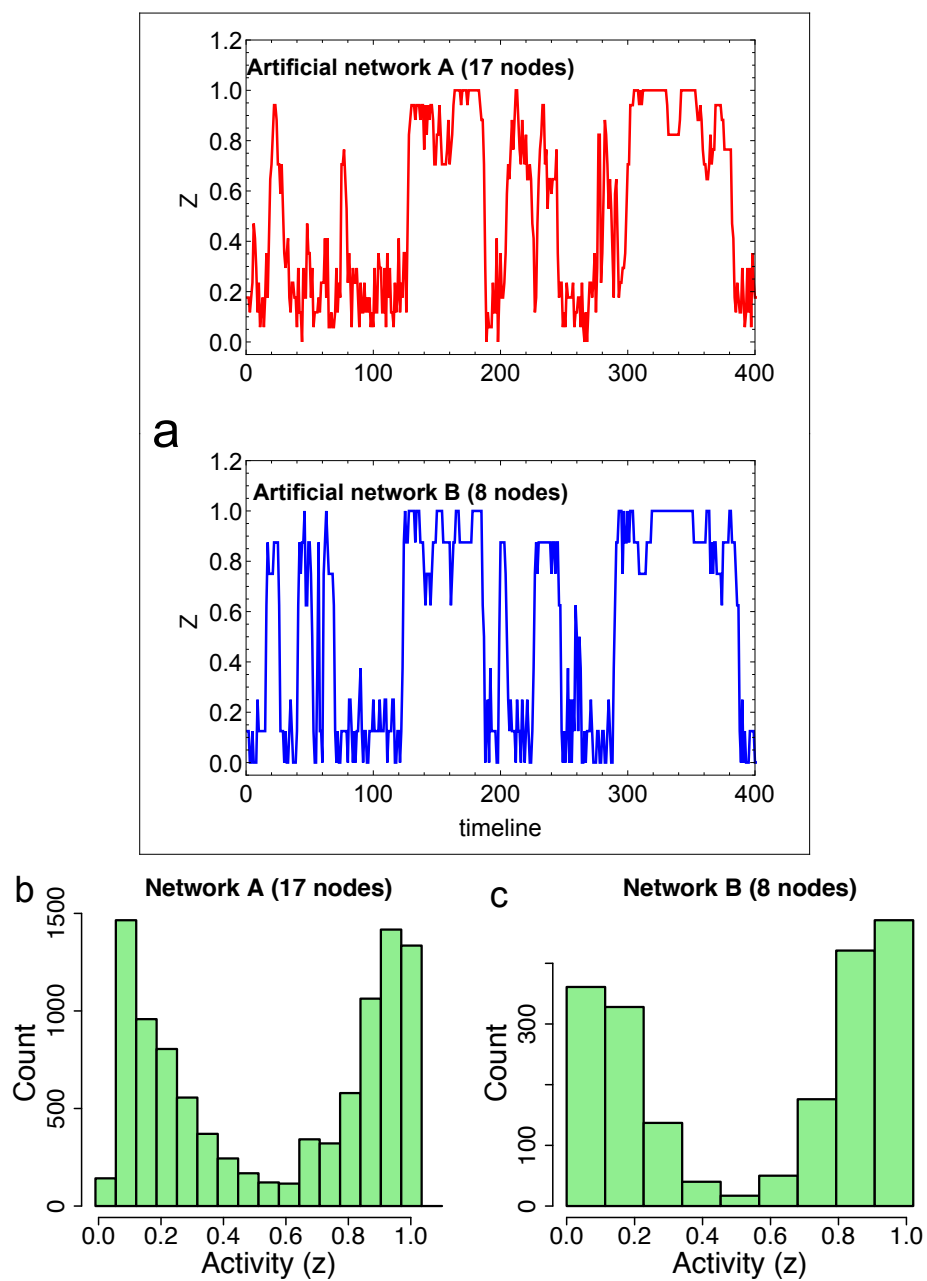


Figure 6.8: **Analysis of network dynamics.** **a** Two model (artificial) networks: Typical time evolution of activity. **b–c** Activity density plot for two model networks reveals bimodality.

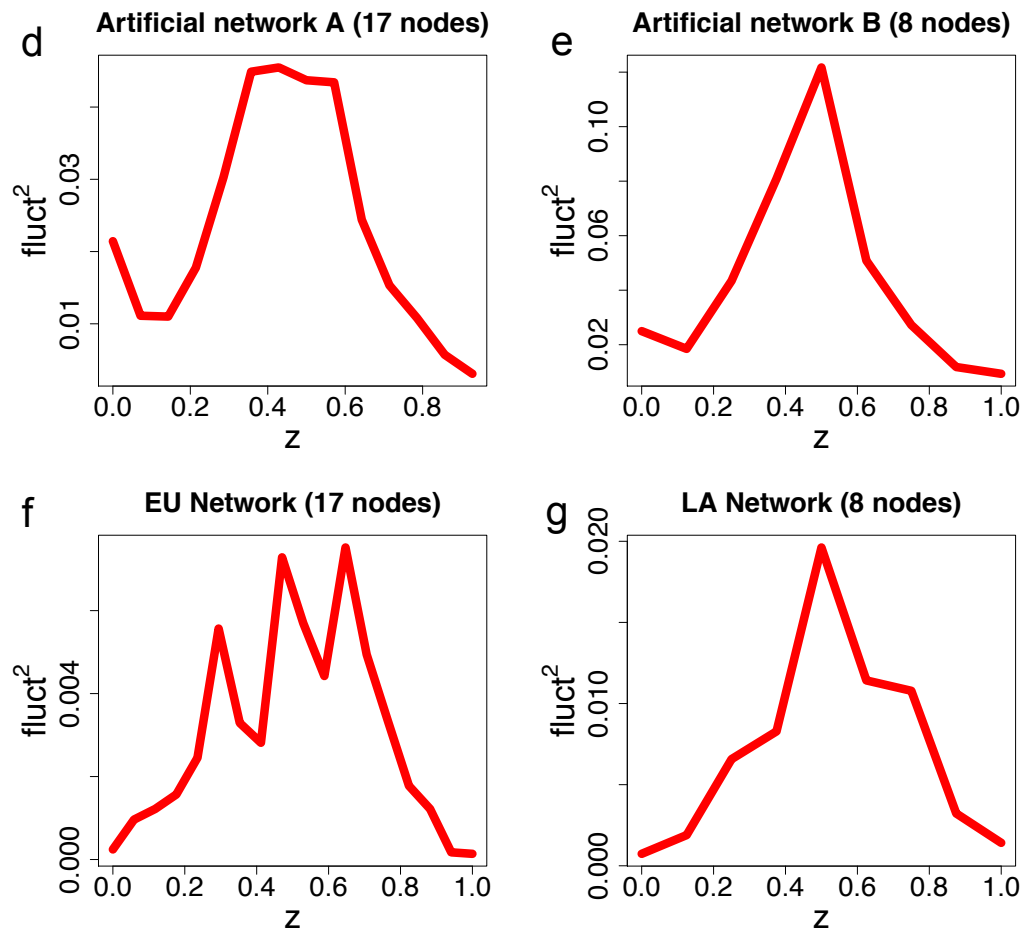


Figure 6.9: **Correlation structure.** **a–b** Fluctuation size peaks around $z \approx 0.5$ for model networks A (**d**) and B (**e**). A very similar pattern is found in real networks, EU (**c**) and LA (**d**).

Appendices

Appendix A

Mean field theory solution for the FRS process in interacting networks

Mean field theory.

Fractions a_A and a_B denote the fraction of nodes that are failed due to any of the three types of failures: internal (I), external (E), or dependency failure (D). We denote the probabilities that a node at a time of observation experiences a failure of I, E, or D type as $P(I)$, $P(E)$, and $P(D)$, respectively. As a first approximation, we assume that these failures are mutually independent events. Considering network A first, we write an expression for the probability $a_{A,k}$ that a node of degree k in network A is failed. The node can fail due to I, E, or D events or to a combination of them.

Using the inclusion-exclusion principle for independent events, we write

$$a_{A,k} = P(I) + P(E) + P(D) - P(I)P(E) - P(I)P(D) - P(E)P(D) + P(I)P(E)P(D). \quad (\text{A.1})$$

Next, we separately calculate $P(I)$, $P(E)$, and $P(D)$.

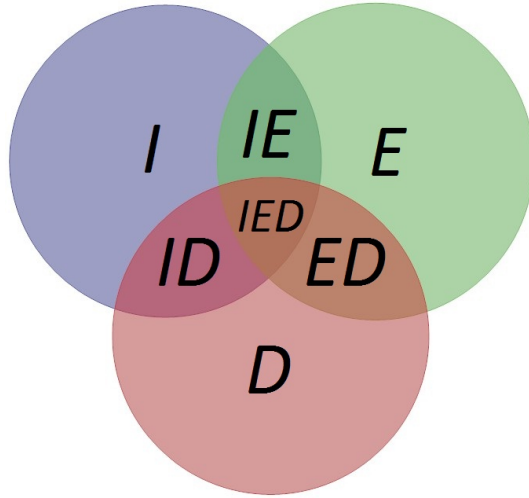


Figure A.1: Inclusion-exclusion principle.

Calculating $P(I)$, the probability that a randomly chosen node is internally failed at the time of observation.

$P(I)$ is also the average fraction of internally-failed nodes in a network, since internal failures are independent events. This is a Poisson process on individual nodes [22, 77], and therefore $P(I) = e^{-p_A \tau}$. Since parameters p_A and τ come in this expression as a product, we can replace them with a single parameter, $p_A^* \equiv e^{-p_A \tau}$, which is bounded and also has the property $0 \leq p_A^* \leq 1$, and so $P(I) = p_A^*$ for network A.

Calculating $P(E)$, the probability that a randomly chosen node with degree k has externally failed.

Focusing once again on network A, without a loss of generality, we let $F(k)$ be the probability that a node of degree k in network A is located in a critically damaged neighborhood (where fewer than $m + 1$ nodes are active). By definition, the time-averaged fraction of failed nodes (for any reason) in network A is $0 \leq a_A \leq 1$. In a mean-field approximation, this is also the average probability that a randomly chosen node in that network has failed. Using combinatorics, we obtain $F(k, a_A) =$

$\sum_{j=0}^m \binom{k}{j} a_A^{k-j} (1 - a_A)^j$ [22]. The probability that a node of degree k in network A has externally failed is then $P(E) = r_A F(k, a_A)$. An analogous result is valid for network B.

Calculating P(D), the probability that a node has failed due to the failure of its dependent counterpart node in the other network.

For network A, this probability is equal to the product of parameter r_d and the probability that a counterpart node in B has failed: $P(D) = r_d a_B$. In network B by analogy this probability is equal to $r_d a_A$.

Writing Eq. (A.1) for both networks and inserting the results for P(I), P(E), and P(D) after summing over all k (and noting $a_A = \sum_k f(k) a_{A,k}$ and $a_B = \sum_k f(k) a_{B,k}$), we get a system of two coupled equations that describes the system of networks,

$$a_A = p_A^* + r_d a_B (1 - p_A^*) + \sum_k f(k) F(a_A) [r_A - p_A^* r_A - r_A r_d a_B + p_A^* r_A r_d a_B] \quad \text{A.2}$$

$$a_B = p_B^* + r_d a_A (1 - p_B^*) + \sum_k f(k) F(a_B) [r_B - p_B^* r_B - r_B r_d a_A + p_B^* r_B r_d a_A] \quad \text{A.3}$$

Appendix B

Credit default swaps (CDS)

In Chapter 6 we have analyzed 5-year sovereign debt CDSs for a set of European countries: France, Germany, Italy, Spain, Portugal, Belgium, Austria, Denmark, Sweden, Greece, Ukraine, Hungary, Poland, Croatia, Slovenia, Romania, Bulgaria, and Slovakia. This is the set of European countries that had a sovereign debt CDS in 2005. The set of Latin American countries we analyze consists of Brazil, Colombia, Argentina, Mexico, Venezuela, Chile, Peru, and Panama. A CDS is typically used to transfer the credit exposure of fixed income products from one party to another. The buyer of the CDS is then obligated to make periodic payments to the seller of the CDS until the swap contract matures. In return, the seller of the CDS agrees to compensate (pay off) the seller who holds this third party debt if this (third party) defaults on the issued debt.

A CDS is, in effect, an insurance against non-payment of a debt owed by a third party. The buyer of a CDS does not have to hold the debt of the third party but can speculate on the possibility that the third party will indeed default, and the buyer can purchase the CDS for this speculative purpose. CDSs were developed in the 1990s and, given their simple structure and flexible conditions, they are now a major part of the credit derivative activity in the OTC market used to hedge credit risk. One of the most important aspects of a CDS is the definition of the “credit event” that

triggers the CDS. These events include bankruptcy, obligation acceleration, obligation default, failure to pay, repudiation (moratorium), and restructuring. In the case of the sovereign bond market, the last three are typically included in the contracts. CDSs are used by investors to hedge exposure to a fixed income instrument, to speculate on likelihood of a third party (reference asset) default, or to invest in foreign country credit without currency exposure.

Bibliography

- [1] Erdős, P. & Renyi, A. On Random Graphs. I. *Publicationes Mathematicae* **6**, 290–297 (1959).
- [2] Newman, M. E. J. *Networks: An Introduction* (Oxford University Press, New York, 2010).
- [3] Tang, Y. Y., Rothbart, M. K. & Posner, M. I. Neural correlates of establishing, maintaining, and switching brain states. *Cell Trends in Cognitive Sciences* **16**, 330–337 (2012).
- [4] Berndt, A., Yizhar, O., Gunaydin, L. A P. Hegemann1 & Deisseroth, K. Bi-stable neural state switches. *Nature Neuroscience* **12**, 229–234 (2009).
- [5] Garlaschelli, D., Caldarelli, G. & Pietronero, L. Universal scaling relations in food webs. *Nature* **423**, 165–168 (2003).
- [6] Vespignani, A. Modeling dynamical processes in complex socio-technical systems. *Nature Phys.* **8**, 32–39 (2012).
- [7] X. Huang and I. Vodenska and S. Havlin and H. E. Stanley. Modeling dynamical processes in complex socio-technical systems. *Scientific Reports* **3**, 1219 (2013).
- [8] Faloutsos, M., Faloutsos, P. & Faloutsos, C. On power-law relationships of the Internet topology. *Comput. Commun. Rev.* **29**, 251–262 (1999).

- [9] Adamic, L. & Huberman, B. A. Internet: Growth dynamics of the World-Wide Web. *Nature* **401**, 131–131 (1999).
- [10] Cohen, R., Erez, K., ben-Avraham, D. & Havlin, S. Resilience of the Internet to random breakdowns *Phys. Rev. Lett.* **85**, 4626–4628 (2000).
- [11] Newman, M. E. J. The structure and function of complex networks. *SIAM Rev.* **45**, 167–256 (2003).
- [12] S. Boccaletti *et al.*, “The structure and dynamics of multilayer networks”, *Phys. Rep* 544, 1 (2014).
- [13] R. Cohen and S. Havlin, “Complex Networks: Structure, Robustness, and Function”, Cambridge University Press, Cambridge, (2010).
- [14] Romualdo Pastor-Satorras and Alessandro Vespignani: Immunization of complex networks. *Phys. Rev. E* 65, 036104, (2002)
- [15] Albert, R., Jeong, H. & A. L. Barabási. Error and attack tolerance of complex networks. *ibid.* **406**, 378–382 (2000).
- [16] Gao, J., Buldyrev, S. V., Havlin, S. & Stanley, H. E. Robustness of a network of networks. *Phys. Rev. Lett.* **107**, 195701 (2011).
- [17] Gao, J., Buldyrev, S. V., Stanley, H. E. & Havlin, S. Networks formed from interdependent networks. *Nature Physics* **8**, 40–48 (2012).
- [18] Buldyrev, S. V. *et al.* Catastrophic cascade of failures in interdependent networks. *Nature* **464**, 1025–1028 (2010).
- [19] Shao, J., Buldyrev, S. V., Havlin, S. & Stanley, H. E. Cascade of failures in coupled network systems with multiple support-dependence relations. *Phys. Rev. E* **83**, 036116 (2011).

- [20] Vespignani, A. The fragility of interdependency. *Nature* **464**, 984–985 (2010).
- [21] S. V. Buldyrev, R. Parshani, G. Paul, H. E. Stanley, and S. Havlin, “Catastrophic Cascade of Failures in Interdependent Networks”, *Nature* **464**, 1025–1028 (2010).
- [22] A. Majdandzic *et al.*, “Spontaneous recovery in dynamical networks”, *Nature Phys.*, **10**, 34-38 (2014).
- [23] A. Majdandzic *et al.*, “Multiple Tipping Points and Optimal Repairing in Interacting Networks”, Accepted in *Nature Communications* (2016).
- [24] B. Podobnik *et al.*, “Predicting Lifetime of Dynamical Networks Experiencing Persistent Random Attacks”, *Sci. Rep* **5**, 14286 (2015).
- [25] B. Podobnik *et al.*, “ Network risk and forecasting power in phase-flipping dynamical networks”, *Phys Rev E* **89**, 042807 (2014).
- [26] Watts, D. J. & Strogatz, S. H. Collective dynamics of ‘small-world’ networks. *Nature* **393**, 440–442 (1998).
- [27] Barabási, A. -L. & Albert, R. Emergence of scaling in random networks. *Science* **286**, 509–512 (1999).
- [28] Albert, R. & Barabási, A. -L. Statistical mechanics of complex networks. *Rev. Mod. Phys.* **74**, 47–97 (2002).
- [29] Schneider, C. M., Moreira A. A., Andrade J. S. Jr, Havlin S. & Herrmann H. J. Mitigation of malicious attacks on networks, *Proceedings of the National Academy of Sciences USA* **108**, 3838–3841 (2011).
- [30] Milo, R. *et al.* Network motifs: Simple building blocks of complex networks. *Science* **298**, 824–827 (2002).

- [31] Schlapfer, M. & Shapiro J. L. Modeling Failure Propagation in Large-Scale Engineering Networks, in *Complex Sciences: Proceedings of First International Conference/Shanghai*, edited by J. Zhou (Springer, New York, 2009)
- [32] Krapivsky, P. L., Redner S. & Leyraz F. Connectivity of growing random networks, *Phys. Rev. Lett.* **85**, 4629–4632 (2000).
- [33] Parshani, R. Buldyrev, S. V. & Havlin, S. Critical effect of dependency groups on the function of networks *Proc. Natl. Acad. Sci. USA* **108**, 1007–1010 (2011).
- [34] Parshani, R. *et al.* Inter-similarity between coupled networks. *Europhys. Lett.* **92** 68002 (2010).
- [35] Angeli, D., Ferrell, J. E. Jr., & Sontag, E. D. Detection of multistability, bifurcations, and hysteresis in a large class of biological positive-feedback systems. *PNAS* **17**, 1822 (2004).
- [36] Das, J. *et al.* Digital signaling and hysteresis characterize Ras activation in lymphoid cells. *Cell* **136**, 337 (2009)
- [37] Watts, D. J. A simple model of global cascades on random networks. *PNAS* **99**, 5766–5771 (2002).
- [38] Bak, P., Chen, K. & Tang, C. A forest-fire model and some thoughts on turbulence. *Phys. Lett. A* **147**, 297 (1990).
- [39] Drossel, B. & Schwabl, F. Forest-fire model with immune trees. *Physica A* **199**, 183 (1993).
- [40] Gleeson J. P. & Cahalane D.J. An analytical approach to cascades on random networks. Proc. SPIE 6601, *Noise and Stochastics in Complex Systems and Finance*, 66010W (2007).

- [41] Dorogovtsev, S. N. & Goltsev, A. V. Critical phenomena in complex networks, *Review of Modern Physics* **80**, 1275–1335 (2008).
- [42] Stanley, H. E. *Introduction to Phase Transitions and Critical Phenomena* (Oxford University Press, Oxford, 1971).
- [43] Kesselring, T. A., Franzese, F., Buldyrev, S. V., Herrmann, H. J. & Stanley, H. E. Nanoscale dynamics of phase flipping in water near its hypothesized liquid-liquid critical point. *Scientific Reports* **2**, 474 (2012).
- [44] Kesselring, T. A., *et al.* Finite-Size Scaling Investigation of the Liquid-Liquid Critical Point in ST2 Water and its Stability with Respect to Crystallization. *J. Chem. Phys.* **138**, 244506 (2013).
- [45] Menck, P. J., Heitzig, J., Marwan, N. & Kurths, J. How basin stability complements the linear-stability paradigm. *Nature Physics* **9**, 89-92 (2013).
- [46] Barunik, J. & Vosvrda, M. Can a stochastic cusp catastrophe model explain stock market crashes? *Journal of Economic Dynamics & Control* **33**, 1824–1836 (2009).
- [47] Kenett, D. Y. *et al.* Index cohesive force analysis reveals that the US market became prone to systemic collapses since 2002. *PLoS ONE* **6**, e19378 (2011).
- [48] Blanchard, O. J. & Summers, L. H. Hysteresis and the European Unemployment Problem. *NBER Macroeconomics Annual* **1**, 15–90 (1986).
- [49] G. D’Agostino, A. Scala (Eds.), *Networks of Networks: The Last Frontier of Complexity*. Springer, (2014).
- [50] F. Radicchi and A. Arenas, “Abrupt transition in the structural formation of interconnected networks”, *Nature Phys.* **9**, 717-720 (2013).

- [51] A. Vespignani, “Complex networks: The fragility of interdependency”, *Nature* **464** (7291): 984-985 (2010).
- [52] J. F. Donges, H. C. H Schultz, N. Marwan, Y. Zou and J Kurths, “Investigating the topology of interacting networks”, *Eur. Phys. J. B* **84**, 635–651, (2011).
- [53] S. D. S. Reis *et al.*, “Avoiding catastrophic failure in correlated networks of networks”, *Nature Phys.*, **10**, 762-767 (2014).
- [54] A. Bashan *et al.*, “The extreme vulnerability of interdependent spatially embedded networks”, *Nature Phys.*, **9**, 667-672 (2013).
- [55] M. Kivela, A. Arenas, M. Barthelemy, J. P. Gleeson, Y. Moreno, M. A. Porter, “Multilayer networks”, *Journal of Complex Networks* **2**, 203–271 (2014).
- [56] G. Bianconi, “Multilayer networks: Dangerous liaisons?”, *Nature Phys.*, **10**, 712-714 (2014).
- [57] G. J. Baxter, S. N. Dorogovtsev, J.F.F. Mendes, D. Cellai, “Weak percolation on multiplex networks”, *Phys Rev E* **89**, 042801 (2014).
- [58] C. Liu *et al.*, “Modeling of self-healing against cascading overload failures in complex networks”, *Euro Phys. Lett.* **107** 68003 (2014).
- [59] A. Bashan *et al.*, “Network physiology reveals relations between network topology and physiological function”, *Nat. Commun.* **3**, 702 (2012).
- [60] G. Caldarelli, A. Chessa, F. Pammolli, A. Gabriell and M. Puliga, “Reconstructing a credit network”, *Nature Phys.* **9**, 125–126 (2013).
- [61] C. Curme *et al.*, “Emergence of statistically validated financial intraday lead-lag relationships”, *Quantitative Finance* **15**, Iss. 8, (2015)
- [62] X. Huang, I. Vodenska, S. Havlin, H.E. Stanley, “Cascading failures in bi-partite graphs: model for systemic risk propagation”, *Sci. Rep* **3**, 1219 (2013).

- [63] R. Albert, A.L. Barabasi, “Statistical mechanics of complex networks”, *Rev. Mod. Phys* **74**, 47-97 (2002).
- [64] S. N. Dorogovtsev, A. V. Goltsev and J.F.F. Mendes, “Critical phenomena in complex networks” *Rev. Mod. Phys.* **80**, 1275-1335 (2008).
- [65] L. D. Valdez, P. A. Macri, H. E. Stanley and L. A. Braunstein, “Triple point in correlated interdependent networks”, *Phys. Rev. E* **88**, 050803(R) (2013).
- [66] S. Wieland and A. Nunes, “Asymmetric coevolutionary voter dynamics”, *Phys. Rev. E* **88**, 062809 (2013).
- [67] L. D. Valdez, P. A. Macri and L A Braunstein, “A triple point induced by targeted autonomization on interdependent scale-free networks”, *J. Phys. A: Mathematical And Theoretical*, **47** 055002, (2014).
- [68] A. Vespignani, “Modeling dynamical processes in complex socio-technical systems”, *Nature Phys.*, **8**, 32-39 (2012).
- [69] B. Buca and T. Prosen, “Exactly Solvable Counting Statistics in Open Weakly Coupled Interacting Spin Systems”, *Phys. Rev. Lett.*, **112**, 067201 (2014).
- [70] R. Albert, H. Jeong, and A. L, Barabási, “Error and attack tolerance of complex networks”, *Nature* **406**, 378-382 (2000).
- [71] R. Parshani *et al.*, “Interdependent Networks: Reducing the Coupling Strength Leads to a Change from a First to Second Order Percolation Transition”, *Phys. Rev. Lett.* **105(4)**, 048701 (2010).
- [72] I. Simonsen, L. Buzna, K. Peters, S. Bornholdt, and D. Helbing, “Transient Dynamics Increasing Network Vulnerability to Cascading Failures”, *Phys. Rev. Lett.* **100**, 218701 (2008).

- [73] L. Buzna, K. Peters, D. Helbing, “Modelling the dynamics of disaster spreading in networks”, *Physica A: Statistical Mechanics and its Applications* **363** (1), 132–140
- [74] M. Stippinger, J. Kertész, “Enhancing resilience of interdependent networks by healing”, *Physica A*, **416**, 481-487 (2014).
- [75] D. J. Watts, “A simple model of global cascades on random networks”, *Proc. Natl Acad. Sci.* **99**, 5766-5771 (2002).
- [76] T. A. Kesselring, G. Franzese, S.V. Buldyrev, H.J. Herrmann and H. E. Stanley, “Nanoscale Dynamics of Phase Flipping in Water near its Hypothesized Liquid-Liquid Critical Point”, *Sci. Rep* **2**, 474 (2012).
- [77] T.L. Saaty, “ Elements of queueing theory: with applications.”, McGraw-Hill, (1961).
- [78] May, R. M. Thresholds and breakpoints in ecosystems with a multiplicity of stable states. *Nature* 269, 471-477 (1977)
- [79] Balaji, S., Madan Babu, M., Iyer, L., Luscombe, N. Aravind, L. Principles of combinatorial regulation in the transcriptional regulatory network of yeast. *J. Mol. Biol.* 360, 213-227 (2006)

Curriculum Vitae

Antonio Majdandzic

Boston University, Department of Physics / Nomura Securities
548 W 50th street C1FW
New York, NY 10019 USA

E-mail: antem@bu.edu

EDUCATION

- 2016, Ph.D. Physics, Boston University, Boston, MA, USA

Advisor: H. Eugene Adviser

Thesis: *Recovery Processes and Dynamics in Single and Interdependent Networks*

- 2011, M.A. Physics, University of Zagreb, Zagreb, Croatia

Advisor: Boris Podobnik

Thesis: *Statistical Physics of Nonstandard Interactions*

RESEARCH AND TEACHING EXPERIENCE

- Sep '11 – Present, Research assistant, Boston Univ. Research in statistical physics of complex networks and econophysics. Devising optimal strategies in dynamical processes on networks. Dynamical phenomena in small networks, recovery processes, critical phenomena and phase transitions.

- Jan '12 – May '12, Teaching assistant, Boston Univ. Courses: General Physics, Principles of Physics.
- Jan '12 – Oct '15, Grader, Boston Univ. Courses: Electromagnetism, Mathematical Methods of Physics, Statistical Physics, Econophysics, Networks.

AWARDS

- Bronze medal, International Physics Olympiad, South Korea (2004)
- Bronze medal, International Physics Olympiad, Spain (2005)
- Croatian National Physics Olympiad, first place (winner, among circa 1000 contestants), four consecutive years (2002, 2003, 2004, 2005)
- Croatian National Mathematics Olympiad (2004), third prize (top 0.3%)
- Coat of Arms of the City of Zadar, highest civilian award in Zadar county, Croatia

WORKING EXPERIENCE

- Oct '15 – Present, Associate, Nomura Securities. Quantitative trading support for interest rate trading desks (treasuries, inflation protected securities, interest rate derivatives), electronic trading.

INTERNSHIPS

- Jun '15 – Aug '15, Summer Associate, Barclays, New York. Automatic trading strategies of VIX (volatility index) futures.

COMPUTER SKILLS

- C++ R Mathematica Excel Fortran L^AT_EX
- VBA Python Financial business softwares SQL

PUBLICATIONS

1. **A. Majdandzic**, B. Podobnik, S.V. Buldyrev, D. Kenett, S. Havlin, and H.E. Stanley, *Spontaneous recovery in dynamical networks*, Nature Physics, 10, 34 (2014).
2. **A. Majdandzic**, L. Braunstein, C. Curme, I. Vodenska, S. Levy-Carciente, H. E. Stanley and S. Havlin. *Multiple tipping points and optimal repairing in interacting networks*. (<http://arxiv.org/abs/1502.00244> , accepted in *Nature Communications*).
3. B Podobnik, **A. Majdandzic**, C. Curme, Z. Qiao, W.X. Zhou, H.E. Stanley, B. Li, *Network risk and forecasting power in phase-flipping dynamical networks*, Physical Review E 89 (4), 042807.
4. A. Siber and **A. Majdandzic** (2009). *Spontaneous curvature as a regulator of the size of virus capsids*, Physical Review E 80 (2), 021910.
5. B. Podobnik, T. Lipic, D. Horvatic, **A. Majdandzic**, S. Bishop, H.E. Stanley. *Predicting Lifetime of Dynamical Networks Experiencing Persistent Random Attacks*, arXiv preprint arXiv:1407.0952.

REVIEWING ACTIVITIES

- Physica A
- PLOS ONE

PROFESSIONAL COLLABORATION

- Raiffeisen Mandatory and Voluntary Pension Funds, Croatia. Training in risk modeling, research collaboration, analysis of equities, portfolios and fixed income securities (2010).

LANGUAGES SKILLS

- English (fluent)
- Croatian (fluent, native)
- South Slavic Languages (fluent)

LEADERSHIP

Principal mentor, preparation of gifted students for Physics competitions,
Zagreb 5th Mathematical Gymnasium, Croatia **2007 – 2009**

- Mentor of 20 gifted students, two of them becoming Croatia's national champions in Physics

HOBBIES

- **Sports:** Tennis, swimming, squash, soccer, basketball, beach volleyball, ping-pong
- **Reading:** History, geography, medicine
- Acting and drama, travelling, fitness, chess